Title
Biomedical System for Monitoring Pressure Ulcer Development

Author
Wang, Frank Tinghwa

Publication Date
2013

Peer reviewed|Thesis/dissertation

UNIVERSITY OF CALIFORNIA

Los Angeles

Biomedical System for Monitoring Pressure Ulcer Development

A dissertation submitted in partial satisfaction

of the requirements for the degree

Doctor of Philosophy in Electrical Engineering

by

Frank Tinghwa Wang

2013

ABSTRACT OF THE DISSERTATION

Biomedical System for Monitoring Pressure Ulcer Development

by

Frank Tinghwa Wang

Doctor of Philosophy in Electrical Engineering

University of California, Los Angeles, 2013

Professor William Kaiser, Co-chair

Professor Mau-Chung Frank Chang, Co-chair

Pressure ulcers (PU) are one of the leading health concerns among patients living in long-term care facilities and are a common occurrence in hospitals. In the United States alone, over 2.5 million patients will suffer from pressure ulcers each year, and over 60,000 patients will die due to pressure ulcer related complications. The cost to treat pressure ulcers including hospitalization costs is also prohibitively expensive; just in the United States alone it is estimated that $9.2-15.6 Billion dollars are spent annually on pressure ulcer treatments. [NPU01]

Pressures ulcers are often preventable if the symptoms are detected early enough, yet the monitoring of skin integrity and pressure ulcer has always relied on a direct visual inspection, which has been shown to be unreliable especially for patients with darkly pigmented skin. As such, there is an urgent need for a handheld medical device to detect and monitor the early symptoms of pressure ulcer development.

Research conducted at the UCLA School of Nursing has shown a relationship between the presence of sub-epidermal moisture (SEM) and the formation of pressure ulcers. Prior research also has shown that this sub-epidermal moisture can be directly interrogated by

measuring the dielectric properties of the tissue. This led to the design of a biomedical system for the monitoring of pressure ulcer development. This system, called the SEM Scanner, is a smart compact capacitive sensing wireless handheld system which measures SEM as a mean to detect and monitor early symptoms of pressure ulcer development. The wireless handheld unit incorporates an array of bio-compliant flexible Kapton electrodes which are excited to measure and scan the SEM in a programmable and multiplexed manner. The SEM Scanner is also wireless enabled, allowing the patient data to be wirelessly uploaded through a gateway, to a remote server, where patients skin integrity can be tracked and monitored over time.

The efficacy of this system was verified through three IRB-approved clinical trials. Combined, over 100 patients participated in these trials. In one trial, the SEM scanner was able to classify the onset of PU 1.5 days prior to the visual detection of pressure ulcer symptoms in almost 70% of those patients who ended up developing a PU.

This research will have a direct impact on improving healthcare as the SEM Scanner is currently in contract manufacturing, targeting a market release in Q3 of 2013. The SEM Scanner has already received CE certification for sale in the European Union, and is currently awaiting FDA 510(k) clearance for sale in the United States.

In the design of this SEM Scanner, fundamental research was conducted on determining the most efficient electrode geometry to interrogate the moisture present in the subepidermal layer of the skin. Research was also conducted in how to maximize yield for manufacturing. In particular, an end of line calibration protocol was developed to ensure that despite manufacturing tolerances, each device will perform within the target specification.

Expanding upon the success of the SEM Scanner, a next generation device was designed to provide spatial imaging of SEM. This device, called the SEM Imager utilizes a novel electrode array to maximize the spatial resolution. Instead of using concentric rings as used on the SEM scanner, the SEM Imager uses an array of hexagon pads, where each

pad can be programmatically reconfigured for different electrode geometries. With this architecture, the electrode geometry is not limited to concentric rings, but can be of any arbitrary shape. The SEM Imager has been shown to positively image areas of tissue with higher moisture content in a healthy subject trial.

Both the SEM Scanner and SEM Imager will have a major, tangible impact in healthcare. The SEM Scanner, as a product, will be used in hospitals and nursing homes, providing clinicians with an evidence-based method of detecting and quantifying pressure ulcers. The SEM Imager, with its general purpose distributed architecture, provides researchers a new way of visualizing tissue health. This broadly-applicable system will allow researchers to develop new methods to characterize various health challenges that the global population currently faces today.

The dissertation of Frank Tinghwa Wang is approved.

Majid Sarrafzadeh

Barbara Bates-Jensen

Mau-Chung Frank Chang, Committee Co-chair

William Kaiser, Committee Co-chair

University of California, Los Angeles

2013

To my parents who helped kindle my curiosity in electronics as a kid.

TABLE OF CONTENTS

List of Figures

List of Tables

ACKNOWLEDGMENTS

I'd like to acknowledge the generous support from Bruin Biometrics for this research and also for them bringing the SEM Scanner onto the market. With their support, the research was able to be commercialized allowing our work to positively impact healthcare outcomes on a global scale.

I also like to thank my labmates Yeung Lam, Bijan Mapar and Alireza Merhnia for their help in running the clinical trials, and also providing key insights for the design of the SEM Imager architecture. I'd also like to thank Chunyu Ching for her support and statistical guidance in analyzing the clinical data.

VITA

2006	B.S. (Electrical Engineering and Computer Science) University of California, Berkeley.
2009	M.S. (Electrical Engineering) University of California Los Angeles.

RELATED PUBLICATIONS AND PATENTS

A Wireless Biomedical Instrument for Evidence-Based Detection of Pressure Ulcers Wireless Health Conference, 2011.

A Wireless Biomedical Instrument for Evidence-Based Tissue Wound Characterization Wireless Health Conference, 2010

Apparatus, Systems, and Methods for Tissue Oximetry and Perfusion Imaging Patent Pending #61/434,014, Filed Jan 19, 2011

SEM Scanner Sensing Apparatus, System and Methodology for Early Detection of Ulcers Patent Pending #61/332,755, Filed May 8, 2009, #61/453,852, Filed March 17, 2011.

CHAPTER 1

Introduction

Millions of people, from the frail elderly population to immobile hospitalized patients, develop pressure ulcers of varying severity each year. It is a global healthcare issue that can affect anyone, regardless of the person's ethnicity, age and gender. If a person is unfortunate to be inflicted with a pressure ulcer, it causes them untold amount of stress and pain. Late stage pressure ulcers, such as those with an open wound are also notoriously hard to heal. Typically, hope of fully recovering from the pressure ulcer is quite dim. Instead the treatment plan for these open wounds usually shifts from healing the wound, to preventing the worsening progression of the pressure ulcer. Complications from the pressure ulcer also increases the mortality rate for the patient.

The treatment of pressure ulcers and its associated complications also account for a large portion of the societies' healthcare costs. In the United States alone, it is estimated that $9.2-15 Billion dollars are spent each year on pressure ulcer treatment. [NPU01]

Fortunately, pressure ulcers are often preventable. If the early symptoms of pressure ulcers are detected, steps can be taken to prevent the wound from developing into a full-blown pressure ulcers. Typically the treatment revolves around relieving the pressure on the damaged tissue and maintaing the cleanliness of the wound which allows for the tissue to heal on its own.

The key step IN preventing pressure ulcers is the early detection of its symptoms. Currently, the only way to detect the onset of a pressure ulcer is by having a trained health care practitioner perform a visual assessment of the skin. However, this visual assessment

is not very effective with patients that have darker skin tones, as their skin tone masks the early visual indications of the pressure ulcer.

Therefore there is an urgent need to develop an evidence-based method for the early detection of pressure ulcers. By having a technology solution, it would work indiscriminately across all patient populations. Its use would be simple enough that an average consumer, such as an adult taking care of their elderly parent, can monitor the patient for signs of this dangerous condition. By shifting the diagnosis away from a subjective visual inspection, pressure ulcers can be quantitatively defined, which allows for easier tracking of the condition.

This Ph.D. thesis deals with the development of such technology. This project is the cumulation of a collaboration between multiple disciplines, from the School of Nursing to the School of Engineering and also industry collaboration.

One of the main goals of this research is to have a direct impact on healthcare, to bring the research out of the laboratory environment into the real world where it can be used to improve patient outcomes. Thanks to industry collaboration, this research is in the process of being commercialized with a targeted release in the third quarter of 2013. This thesis will also dive into the fascinating journey of turning a biomedical research into an actual commercial product that will be used in hospitals and nursing homes worldwide. Throughout this journey there was a diverse range of challenges that needed to be overcome, such as regulatory approvals, performing clinical trials to issues relating to the mass manufacturing of the device, and I'm thankful that as a Ph.D. student I was able to be part of it.

This thesis is organized starting with a brief description of what pressure ulcers are, how they are formed, and what treatment options are available if they are detected early enough. Ultrasound, which is a competing technology in imaging pressure ulcer is briefly discussed. The next chapter is a discussion of skin physiology, in particular the biophysical properties that will be exploited by this technological solution. Chapter 4 talks about the

techniques to measure the biophysical property, with a focus on measuring capacitance as a direct mean of measuring that biophysical property. Chapter 5 walks through the design process in designing the electrodes, and the complications with manufacturing a kapton-based electrode. In Chapter 6, the entire SEM Scanner system is described in detail, where it was then used for clinical trials, which is discussed in Chapter 7. With the positive results from the clinical trial, a contract manufacturer was selected to help commercialize the device. Chapter 8 talks about design decisions and manufacturing issues that arose from going from a research project to a commercial device.

In performing the clinical trials, limitations in the SEM Scanner were discovered, and new needs were identified. Chapter 9 will dive into the inner workings of the electrode and extrapolate the SEM Scanner design from a single point measurement system to an imager. This was achieved by a distributed electrode architecture that allows the formation of any electrode geometry, with spatial scanning capability to form an image of the sub-epidermal moisture within tissue.

Lastly, the thesis is concluded with alternative applications of this technology.

CHAPTER 2

Pressure Ulcers

2.1 Impact

Over 2.5M patients in the United States each year will develop a pressure ulcer which are commonly known as bedsores. Patients of all ages, gender and ethnicity are all susceptible to pressure ulcers, however pressure ulcers are particularly prevalent among patients living in intensive care units and in long-term care facilities. Patients living in acute-care facilities have a reported incidence rate ranging from 0.4% to 38%, while patients living in long-term care facilities have a reported incidence rate between 2.2% to 23.9% [NPU01]. The high incidence rate at these facilities can be mainly attributed to the patient's lack of mobility, resulting in a prolong period of time where pressure was applied to the tissue which resulted in tissue damage.

Patients who suffer from pressure ulcers also have a higher mortality rate compared to those without, due to pressure ulcer related complications. Nearly 70% of patients who develop a stage 3 or 4 pressure ulcer will die within 6 months [Bro03]. Pressure ulcers are also very costly to treat; a single treatment for pressure ulcer at an acute care facility costs $43,180 [B 09]. It is estimated that in 2008 for the United States alone, $9.2 to 15.6 Billion dollars were spent on pressure ulcer treatments.

2.2 Formation of Pressure Ulcers

Pressure ulcer forms when pressure is applied to a bony prominence. The pressure restricts blood flow to the skin and the underlying tissue. Without an adequate blood flow, oxygen and other nutrients cannot be delivered to the tissue. As a result, the skin and the underlying tissues become damaged and may die. Shear force and friction can also contribute to tissue damage. Friction force occurs when the skin is dragged across a surface such as the friction between the skin and the bed sheet when the patient is moved on the bed. Shear force might occur when the patient slides down from an elevated bed. In that scenario, the tail bone moves down, while the skin over the bone stays in place causing tissue damage. [May12]

2.3 Detection

2.3.1 Visual Inspection

Pressure ulcers are currently detected through a visual inspection of the tissue by trained health care practitioners. The health care practitioners in the United States categorizes the pressure ulcers according to the definitions defined by the National Pressure Ulcer Advisory Panel.

The National Pressure Ulcer Advisory Panel classifies pressures ulcers into 4 stages. The definitions are as follows: [Nat07]

Stage 1: Non-Blanchable Erythema

Intact skin with non-blanchable redness of a localized area usually over a bony prominence. Darkly pigmented skin may not have visible blanching; its color may differ from the surrounding area. The area may be painful, firm, soft, warmer or cooler as compared to adjacent tissue. Category I may be difficult to detect in individuals with dark skin tones. May indicate at risk persons.

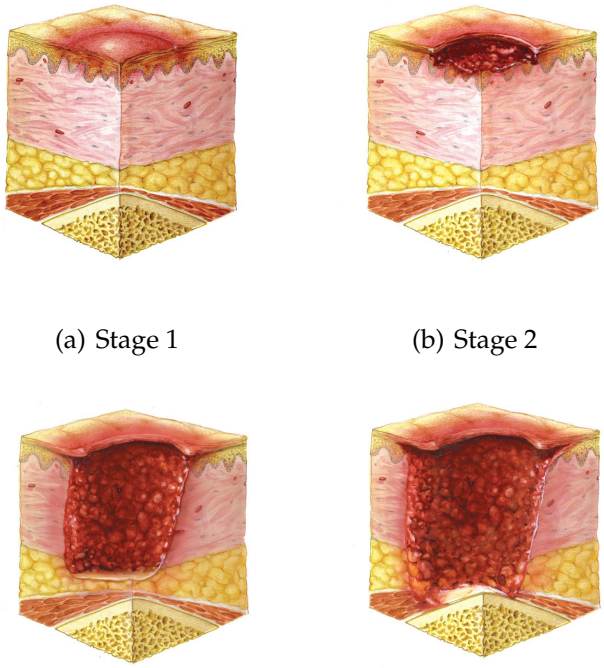

(a) Stage 1 (b) Stage 2

(c) Stage 3 (d) Stage 4

Figure 2.1: The four stages of pressure ulcer progression. [Nat07]

Stage 2: Partial Thickness

Partial thickness loss of dermis presenting as a shallow open ulcer with a red pink wound bed, without slough. May also present as an intact or open/ruptured serum-filled or sero-sanginous filled blister. Presents as a shiny or dry shallow ulcer without slough or bruising. This category should not be used to describe skin tears, tape burns, incontinence associated dermatitis, maceration or excoriation.

Stage 3: Full Thickness Skin Loss

Full thickness tissue loss. Subcutaneous fat may be visible but bone, tendon or muscle are not exposed. Slough may be present but does not obscure the depth of tissue loss. May include undermining and tunneling. The depth of

a Category/Stage III pressure ulcer varies by anatomical location. The bridge of the nose, ear, occiput and malleolus do not have (adipose) subcutaneous tissue and Category/Stage III ulcers can be shallow. In contrast, areas of significant adiposity can develop extremely deep Category/Stage III pressure ulcers. Bone/tendon is not visible or directly palpable.

Stage 4: Full Thickness Tissue Loss

Full thickness tissue loss with exposed bone, tendon or muscle. Slough or eschar may be present. Often includes undermining and tunneling. The depth of a Category/Stage IV pressure ulcer varies by anatomical location. The bridge of the nose, ear, occiput and malleolus do not have (adipose) subcutaneous tissue and these ulcers can be shallow. Category/Stage IV ulcers can extend into muscle and/or supporting structures (e.g., fascia, tendon or joint capsule) making osteomyelitis or osteitis likely to occur. Exposed bone/muscle is visible or directly palpable.

2.3.2 Ultrasound

Ultrasound can visualize the soft tissue all the way up to the bone. It is able to image tissue damage associated with early stages of pressure ulcer, including sub-epidermal, dermal, and subcutaneous edema. Episcan Dermal Ultrasound Scanner is an ultrasound imager targeted for imaging the skin. Using a high frequency ultrasound at 50MHz, the ultrasound imaging system can achieve resolution as small as 40 microns, and a tissue penetration depth of 2 to 3 cm [Int06].

One of the downside to the system is the cost and size. The Episcan system costs $8000 and is a very bulky system. The system needs to be carted into the patient room in order to perform the scan. Also a trained technician is required to interpret the result. This is one of the motivation for the SEM Scanner, in that the device is portable and with easy to

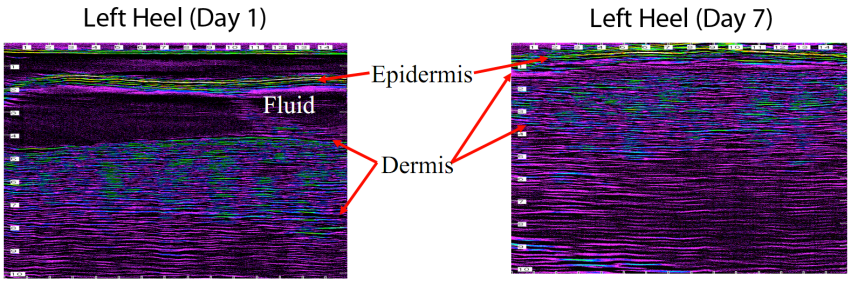

Figure 2.2: Ultrasound imaging of the healing process from a pressure ulcer on the heel. [Int06]

interpret results.

2.4 Prevention and Treatment

The current accepted method of preventing pressure ulcers from forming is by turning and repositioning the bed-ridden patient every few hours. If the patient is at a high risk of developing pressure ulcers, the patient might need to be repositioned as often as every 2 hours.

In the case that an early stage pressure ulcer has formed, preventive measures can be taken to prevent the tissue damage from progressing into an open wound, but only if the pre-stage 1 pressure ulcer symptoms were detected early on. Once the symptoms are detected, the first step would be to reposition the patient in a way to relieve pressure to the tissue in question. Additional support cushions can be used to distribute and reduce the pressure on the damaged tissue. For pressure ulcers that develop on the heel, special heel protectors can be used to relieve the pressure on the heel. Stage 1 and Stage 2 pressure ulcers typically heal within several weeks to months, through tissue regeneration.

If the pressure ulcer has advanced to a full-thickness wound (Stage 3 or 4), any dead tissues must first be removed and the wound needs to be periodically cleaned and dressed. Full thickness pressure ulcer are difficult to treat. Full thickness pressure ulcer heals by forming scar tissue and through contraction. If the patient has a compromised immune

system, the wound usually will not completely heal. In this situation, the patient care focus would shift from healing the wound to preventing further damage to the tissue and and managing pain [May12].

CHAPTER 3

Skin Physiology

The electrical properties of biological tissue can be described by electrical conductivity σ and dielectric permittivity ϵ. The conductivity of the tissue depends on the mobility of the ions in the extracellular fluid. Therefore the conductivity of a particular tissue depends on the ratio of extracellular to intracellular volume. The conductivity of the tissue typically remains static and is not greatly influenced by the frequency of the electric field. The permittivity of tissue is related to the polarization of the media. In the presence of a time-varying electric field, the orientation of the dipoles formed by cells and molecules will be time-delayed due to the relaxation process. This will introduce a phase-shift relative to the time-varying electric field. [SA00]

It is known that the dielectric constant of tissue occurs in three steps. The first step, also known as the alpha dispersion occurs at very low frequencies, $f < 100KHz$. In this dispersion range, the dielectric constant is very high, reaching up to 10^6 to 10^7 for frequencies less than 100 KHz. The high dielectric constant is predicted by theories of ionic diffusion in heterogenous media. The models are able to predict the high dielectric constant within an order of magnitude. Relating to the skin, extracellular membrane polarization of large cells contribute to this high dielectric permittivity. The second step is the beta dispersion, which occurs at frequencies between 100KHz and 100MHz. In this region, the dielectric constant is primarily dominated by the capacitive charging and discharging of the cellular membranes. The third step is the gamma dispersion, for frequencies above 100MHz. At this high frequency, the dielectric response is dominated by the water content within the

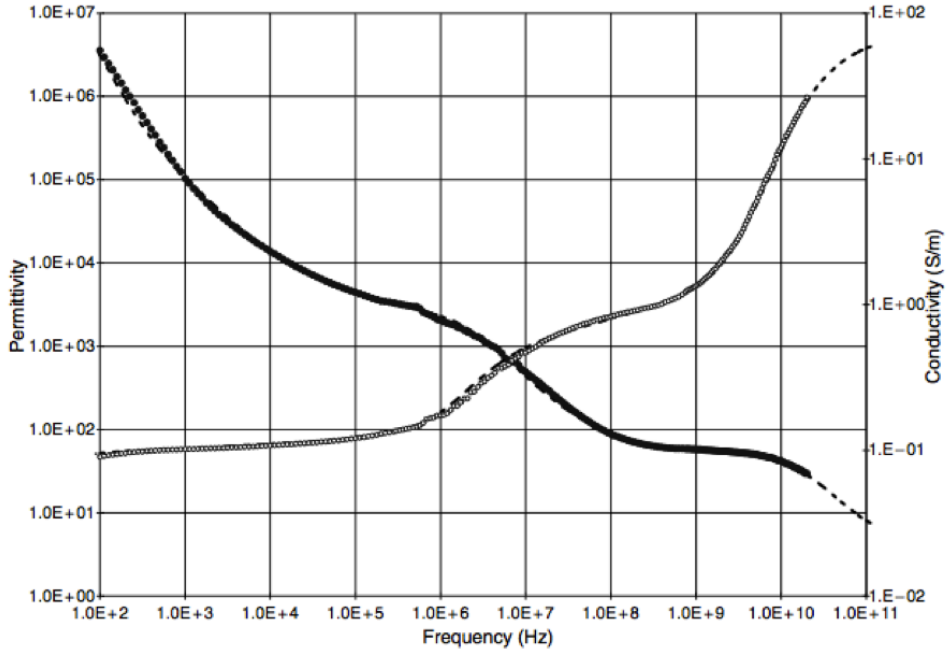

Figure 3.1: Dielectric Spectrum of High Water Content Tissue.

tissue. There is a strong correlation between the dielectric constant and the water content present within the tissue. [Gab96a]

3.1 Two Layer Skin Model

In the two layer model of the skin, as proposed by Lahtinen, the model consists of an upper layer comprising of the stratum corneum, epidermis and dermis, while the lower layer comprises of the subcutaneous fat. The upper layer of the model is represented by having a high dielectric constant, while the lower, fatty layer has low dielectric constant. [LNA97] However this model has several shortcomings. In particular, the stratum corneum consists of dead cells with no fluids. However, the epidermis and dermis layer consists of blood vessels and sweat glands, which is expected to exhibit dielectric behavior associated with high water content tissues. When dry skin was capacitively probed, [Gab96b] no alpha and beta dispersions were observed. This seems to indicate that the dielectric properties

of the stratum corneum layer dominated this measurement. However when the skin was wetted, the dielectric constant exhibited similar behavior to tissues with high water content [Gab97].

As such, the model was revised by Alanen [ALN99] where the upper layer was now defined to consist solely of the stratum corneum and the lower layer defined by the epidermis and dermis. The upper layer was modeled as having a low dielectric constant, due to the lack of water content. The lower layer was defined to have a high dielectric constant, to model the high water content tissues. In the Alanen model, the skin was modeled as a capacitor, where the stratum corneum acts as the dielectric between the probe and the well conducting dermis. However, experiments had shown that only the dielectric constant associated with the stratum corneum can be measured for frequencies below 1MHz. Alanen did note that at lower frequencies, larger probes provide higher measurement accuracy of dielectric constant.

Raicu [RKI00] performed experiments to quantitatively validate the two layer model proposed by Alanen. If the skin is relatively dry, the stratum corneum dominates the measurement due to its low conductivity and low permittivity. The electric field lines almost exclusively concentrates within this layer. However, if the skin was wetted, for example by using a physiological saline, the effective penetration depth of the electric field lines seemed to increase. This effect was hypothesized to be caused by the stratum corneum becoming more conductive. Therefore, with the application of physiological saline, there was the possibility for the electrode to probe into the deeper layers of the skin. However, Gabriel [Gab06] believed that by wetting the skin, the stratum corneum becomes a more homogenous material with the lower epidermis and dermis layer. As such, the skin will exhibit dielectric behavior consistent with high water content tissues.

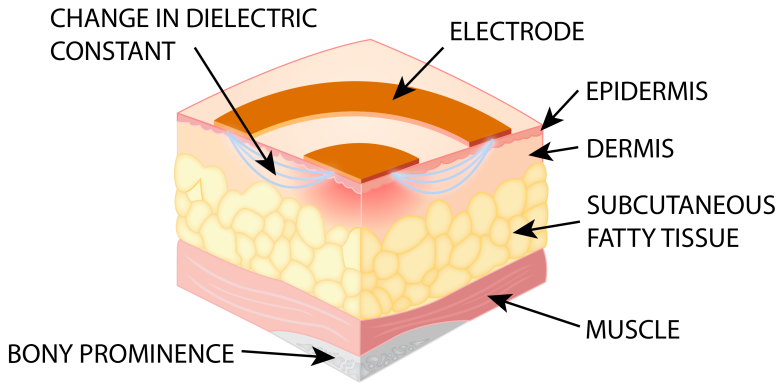

Figure 3.2: Increase in sub-epidermal moisture can be capacitively measured with an electrode.

3.2 Sub-Epidermal Moisture

The sub-epidermal moisture (SEM) is a biophysical measure that assesses the skin barrier as a function of hydration. Sub-epidermal moisture can be measured by using a surface capacitance measurement, and the result is directly related to the amount of moisture in the epidermal layer of the tissue. Bates-Jensen has shown with her studies that SEM can serve as an early indicator of pressure ulcers as shown in Figure 3.2 [BMK07] [BMP08].

Pressure ulcers typically occur where external pressure is continuously applied to a bony prominence. When pressure is applied to such a point, blood flow becomes restricted to the area through the combination of the applied pressure and shear force. When blood flow is restricted to the tissue, the tissue begins to die causing an inflammatory response. This inflammation results in an increase in moisture level within the dermis due to increase blood flow and capillary permeability. The increase in sub-epidermal moisture causes the skin dielectric constant to rise, resulting in a higher surface capacitance measurement. Thus the sub-epidermal moisture level can be interpreted from the skin capacitance measurement. Despite the presence of tissue damage, there might not be any visible indication of damage at the surface of the skin.

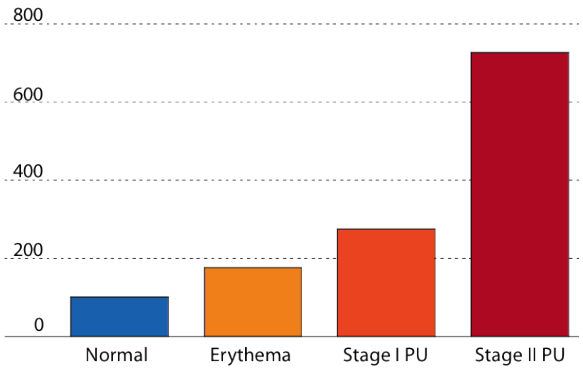

Figure 3.3: Relative capacitance for various stages of pressure ulcer.

CHAPTER 4

Capacitance Measurement Architectures

In the early stages of pressure ulcer development, damage to the tissue causes an inflammatory response. This response is marked by an increase of both the blood flow and capillary permeability around the damaged tissue, resulting in an influx of fluids into the region. Therefore determining the hydration level of the skin can serve as an early indicator for the onset of pressure ulcers. One technique to measure the hydration level of the skin, is through a surface capacitance measurement as shown in papers [ANN04] and [Og07].

Measuring capacitance is quite a mature field in the electronics world, due to its recent widespread use in touchpads, mobile phones and tablet computers. There are multiple techniques to measure capacitance. In prior literature, most experiments for measuring the dielectric properties of tissue have relied on the technique of driving the capacitance with a fixed frequency sine wave through a known resistance and measuring the resulting voltage and phase shift. However, this is not the only method of measuring capacitance. Other methods include measuring the RC time constant, measuring the ratio to a known capacitor either using a capacitive bridge divider or using charge transfer and directly measuring the charge on a capacitor through a relaxation oscillator.

4.1 Relaxation Oscillator

A common technique used to measure capacitance is based on the relaxation oscillator. The simplified system is shown in Figure 4.1.

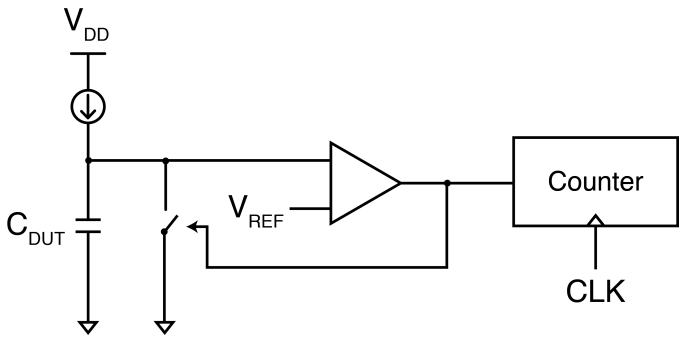

Figure 4.1: General system diagram of a relaxation oscillator.

In this architecture, the capacitor is charged using a constant current source and the time (in counts) for the voltage on the capacitor to surpass V_{th}, as set by a bandgap reference, is measured. The capacitance is linearly proportional to the time required to charge the capacitor to the bandgap reference voltage.

Depending on the capacitance to be measured, and also for the desired resolution, the constant current source can be adjustable through a digital-analog converter. The count required for the capacitor to charge up to the bandgap reference voltage is given by:

$$t = \frac{C_{DUT} V_{BG}}{I_{charge}}$$

Therefore, by increasing the current, the capacitance can be measured in a shorter amount of time, but at the expense of resolution. This is because the delta increase in voltage on the capacitor during each clock cycle will be larger due to the increased current, which may lead the voltage on the capacitor to overshoot the reference voltage by a large amount, which directly affects the capacitance measurement. However if the current is set too small, the acquisition time will increase and will be much more susceptible to noise and to charge leakage.

Capacitance can be calculated from the equation

$$C_{DUT} = \frac{I_{charge}}{V_{BG}} t$$

.

The count stored in the digital counter is directly related to time. To convert count to time

$$t = \frac{1}{f_{clk}} * count$$

Since the measured capacitance using this architecture is the linear addition of both the parasitic capacitance of the electrode and the skin capacitance, to calculate just the skin capacitance, C_{skin} can be solved from the above equation by substituting t with t_{skin}, where

$$t_{skin} = t_{electrode\_with\_skin} - t_{electrode}$$

$t_{electrode\_with\_skin}$ is the time required to charge both the skin and the electrode capacitance to the bandgap reference voltage, while $t_{electrode}$ is the time required just to charge the electrode capacitance to the bandgap reference voltage.

The disadvantage to this architecture is that it measures both the parasitic capacitance and the skin capacitance. The parasitic capacitance includes the capacitance from the PCB board trace, chip-pin capacitance and the inherent capacitance within the electrode. Unfortunately, the parasitic capacitance dominates this measurement, with the skin capacitance only being a fraction of the parasitic capacitance.

4.1.1 Evaluation of Cypress CapSense Evaluation Board

Cypress CapSense is an off-the-shelf commercial solution for measuring capacitance, based on the relaxation oscillator architecture. This chipset's primary market is for touch buttons, and as a result was not designed for high-accuracy capacitance reading. An experiment was performed to asses whether this system can detect a change in moisture in the skin. The skin capacitance on the finger was measured before and after moisturizer was applied to the skin for a period of 30 seconds. Table 4.1 summarizes the findings.

When the current source was programmatically set to be at a lower value, the system was able to detect an average of 4.5% increase in the time required to charge the capaci-

Experiment	I_{DAC} Setting	Count Value Dry	Count Value Moisturized	% Increase
1	250	727	733	0.82%
2	50	3070	3214	4.69%
3	50	3040	3140	3.28%
4	50	3040	3213	5.69%

Table 4.1: Results from Cypress Capsense evaluation board on moisturized vs dry finger.

tance to the threshold value. However, when the current source was programmed to be at the maximum level, the delta change in the count was too small to be significant, as the datasheet stated that the chipset was only accurate to 10 counts.

4.2 Charge Transfer

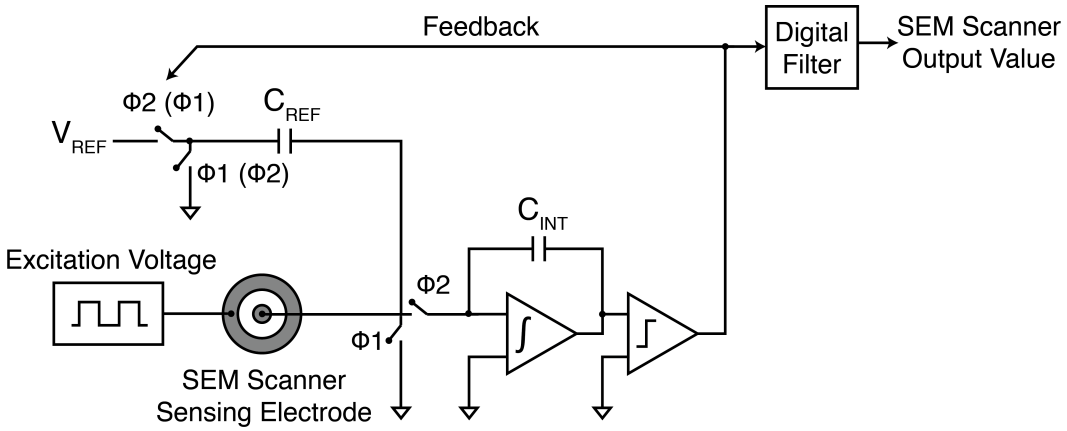

Figure 4.2: General system diagram of a sigma-delta capacitance architecture.

In the sigma-delta capacitance to digital converter, a known excitation voltage is used to excite the unknown capacitance. The capacitance C_{sensor} and C_{ref} is switched periodically between the known V_{exc} and V_{ref}. The charge from C_{sensor} and C_{ref} is dumped into or extracted from the integrating capacitor C_{int} depending on the output of the comparator. The comparator monitors the output of the integrating capacitor to determine whether the

switch for C_{int} is connected to C_{sensor} or C_{ref}. The constant switching from the comparator will result in an output stream of 1's and 0's which is then fed into a digital filter. The output from the digital filter will be the ratio of the C_{sensor} to C_{ref}. One of the benefits of this architecture is that it is immune to parasitic capacitances to ground, and also immune to charge leakage to ground, as the architecture only measures the charge being transferred from one terminal of the electrode to the other. [Bry05]

4.2.1 Evaluation of Analog Devices AD7746 Evaluation Board

Analog Devices has an entire product line dedicated to measuring absolute capacitances called capacitance to digital converters (CDC). This product was mainly designed for use in medical instrumentations. These chip provides calibrated capacitance measurements with resolution in the femtofarad range. The Analog Device AD7746 was selected for evaluation. The AD7746 is a 24-bit CDC with internal temperature compensation. It is factory calibrated to be within +/- 4fF, and can detect a change in capacitance up to +/-4pF. This CDC is designed to measure floating capacitive sensors, where none of the capacitor plates are connected to ground.

For the evaluation of the AD7746, two electrode geometry were fabricated to evaluate the performance of the CDC. The electrodes was fabricated on single-sided Kapton, model F9130. The dimensions are shown in Figure 4.3. A piece of 2-mil thick packaging tape covered the exposed copper, to prevent the electrode from saturating the CDC when in contact with the skin due to low surface resistance of the skin. The electrodes were connected to the AD7746 through a soldered wire connection, with special care taken to isolate the excitation wire from the sensing wire. Parasitic capacitance from the wire was not a big concern as the CDC can tolerate up to 17pF of parasitic capacitance.

Using the charge transfer based architecture, the CDC was able to detect on average a 25% increase in capacitance after the finger has been moistened, for both electrode geometries. The CDC solution proved that it was more sensitive than the relaxation-oscillator

Figure 4.3: Simple capacitive electrodes fabricated on Kapton.

Pad	Body Part	Moisturizer	Dry	Moisturized	% Increase
Square	Finger	Sanitizer	1.65pF	1.80pF	9.09%
Circle	Finger	Sanitizer	1.00pF	1.20pF	20.0%
Square	Heel	Sanitizer	1.48pF	2.12pF	43.24%
Square	Heel	Lotion	1.25pF	1.83pF	46.40%
Square	Heel	Lotion	2.30pF	2.52pF	9.56%

Table 4.2: Measurement results from Analog Devices AD7746 evaluation board for sanitized vs dry finger for both the square and circular electrodes.

based solution, and thus better suited for measuring the skin surface capacitance. During the experiment, it was found that the CDC was extremely sensitive. It was noted that the skin capacitance reading was affected by the rest of the human body from both resistive and capacitive coupling. For example, as the subject moved his hand closer to the ground, the hand formed an increased parasitic capacitance to ground. To minimize this effect, the subject needed to maintain the same posture for both the skin capacitance measurement before and after the application of moisturizer.

4.2.1.1 Verification of Absolute Value

The accuracy of the Analog Devices AD7746 performance was validated against a NIST calibrated Agilent E4980A LCR meter. A total of 40 discrete capacitors (10 each of the following component values: 0.5, 1, 2, 4pF) were tested and compared between the two devices. The mean error of the AD7746 was 0.173%, with a standard deviation of 0.067%.

CHAPTER 5

Electrode Design

Measuring the sub-epidermal moisture requires not only a capacitance measurement system, but also a carefully designed electrode. The geometry of the electrodes affects the measurement penetration depth and also the spatial resolution. The stackup of the electrode is also critical, as it affects the total amount of parasitic capacitance from the electrode. If using the charge-transfer architecture for measuring capacitance, the two terminals on the electrode needs to be electrically isolated from one another while minimizing the insulator's effect on the capacitance measurement sensitivity. In guiding the design of the most optimal electrode geometry for measuring sub-epidermal moisture, various simulations and experiments were performed.

5.1 Electrode Geometry

Prior experiments measuring sub-epidermal moisture were performed at the UCLA School of Nursing [BMK07]. In that experiment, the Delfin Moisture Meter was successfully used to measure the skin surface capacitance. To minimize risk, the starting point for the design of the electrode geometry was based on the Delfin probe as that geometry has been clinically validated to be able to measure sub-epidermal moisture. The Delfin probe used a concentric ring design. The probe dimensions for the Delfin are listed in Table 5.1.

An alternative product to measure skin surface capacitance was the Skicon meter as used in the experiments performed by Alanen et al to measure skin hydration level [ANN04].

	XS	S	M	L
Contact Diameter (mm)	10	20	23	55
Approx Outer (mm)	10	20	23	55
Approx Middle (mm)	6	10	15	40
Approx Inner (mm)	2	4	5	7

Table 5.1: Probe dimension for various Delfin probes.

5.2 FR4 Electrodes

Each of the Delfin meter's electrode geometry was evaluated through experimentation. Each electrode was fabricated on a 2-layer rigid FR4 printed circuit board. The layout of the electrodes are shown in Figure 5.1.

In evaluating the various electrode geometry, all other factors needed to be kept constant. In particular, it was observed that skin capacitance had a linear dependence on the applied pressure. To validate this observation, an experiment was conducted using the Delfin S geometry, which had a 400 mil outer radius. The applied pressure to the electrode on the skin was varied, and the capacitance was then measured. Figure 5.2 confirmed that skin capacitance was linearly proportional to the applied pressure.

The inner volar forearm was selected as the trial site for the evaluation of the electrodes, due to the similarity in tissue structure with the buttocks and the trochanter, which are areas where pressure ulcer typically forms. A resistive pressure sensor was placed on the back of each electrode to monitor the pressure applied to the electrode on the arm.

First, the dry volar forearm was measured using the Delfin XS, S and M electrode geometry. Then the same area was masked off with tape, and lotion was subsequently applied to the area for 30 minutes. After 30 minutes, any residual lotion was removed and measurements were made at the same location, while ensuring that the pressure remained constant across measurements.

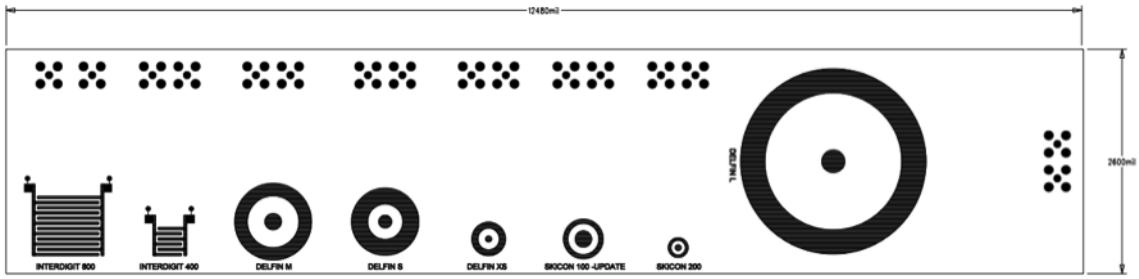

(a) Top

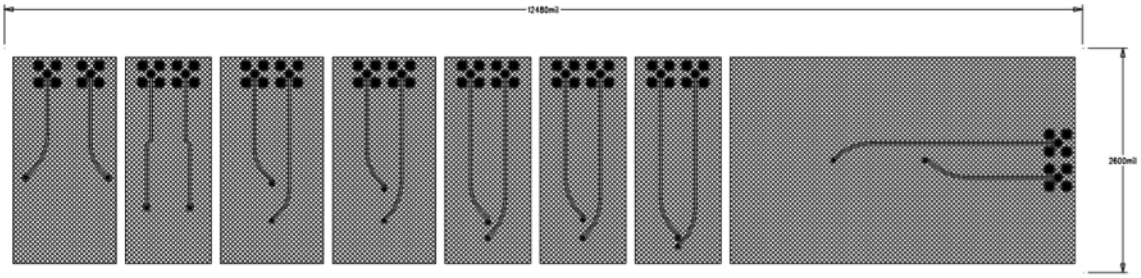

(b) Bottom

Figure 5.1: Various electrode geometry fabricated on FR4 to experimentally test the properties of each electrode.

The result of the experiment shows that the three electrodes have very similar sensitivity, all three detecting an average 25% increase in capacitance due to the increased moisture.

5.3 Kapton Electrodes

Since the electrode will be in direct contact with the patient's skin, the electrode must be made with a bio-inert material. Kapton exhibits this property in addition to being durable and easy to clean. The Kapton used for the sensor is the Pyralux FR material from Dupont. Due to the high cost for Kapton, only the Delfin M and Delfin S electrodes were evaluated. The initial flex stackup is shown in Figure 5.4.

The flex electrodes were evaluated in a similar manner as with the FR4 electrodes. Novalin was applied to the inner volar forearm for a period of 15 minutes. Pressure was

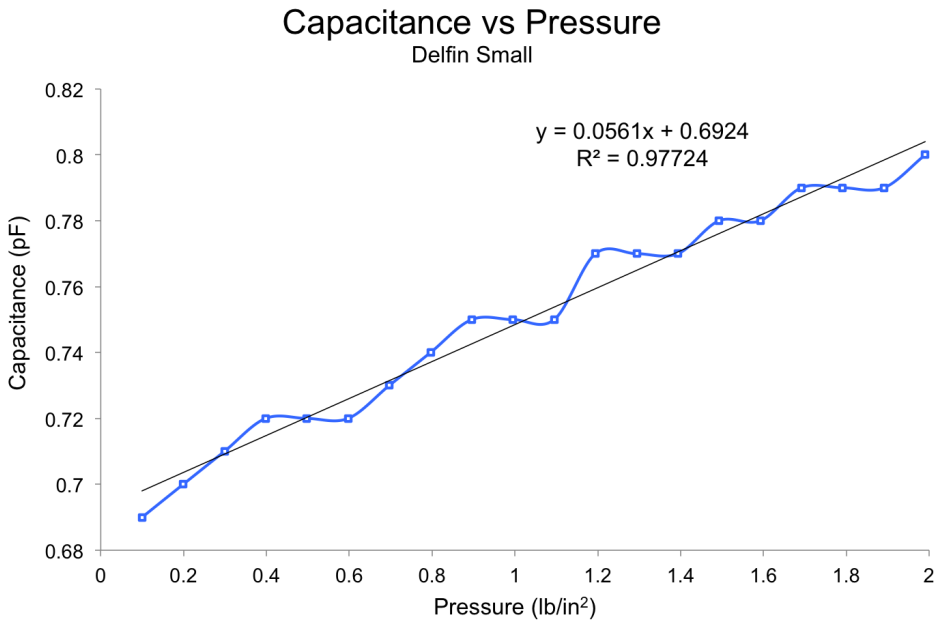

Figure 5.2: Pressure has a linear effect on the capacitance measured.

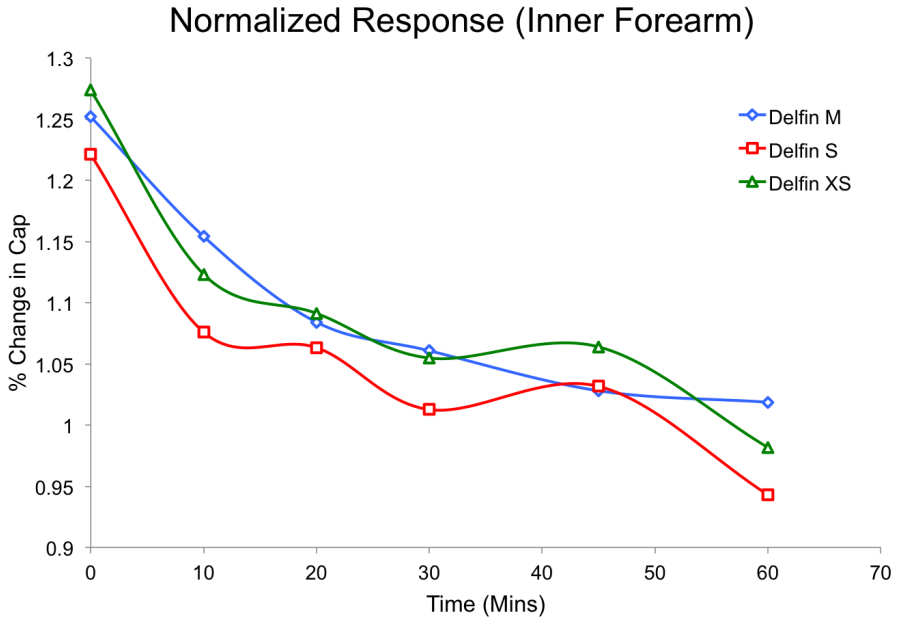

Figure 5.3: Normalized response for various sized circular FR4 electrode on the inner arm.

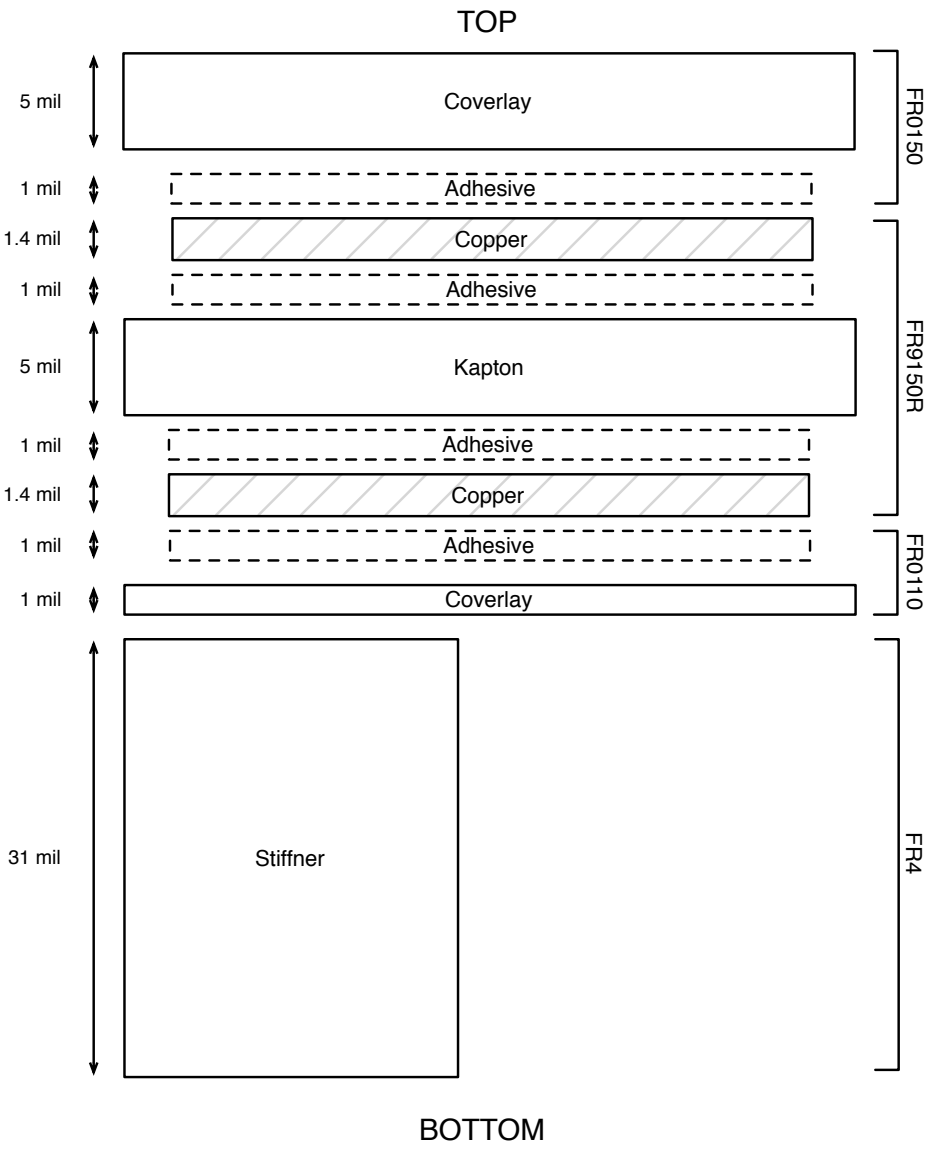

Figure 5.4: Initial flex stackup.

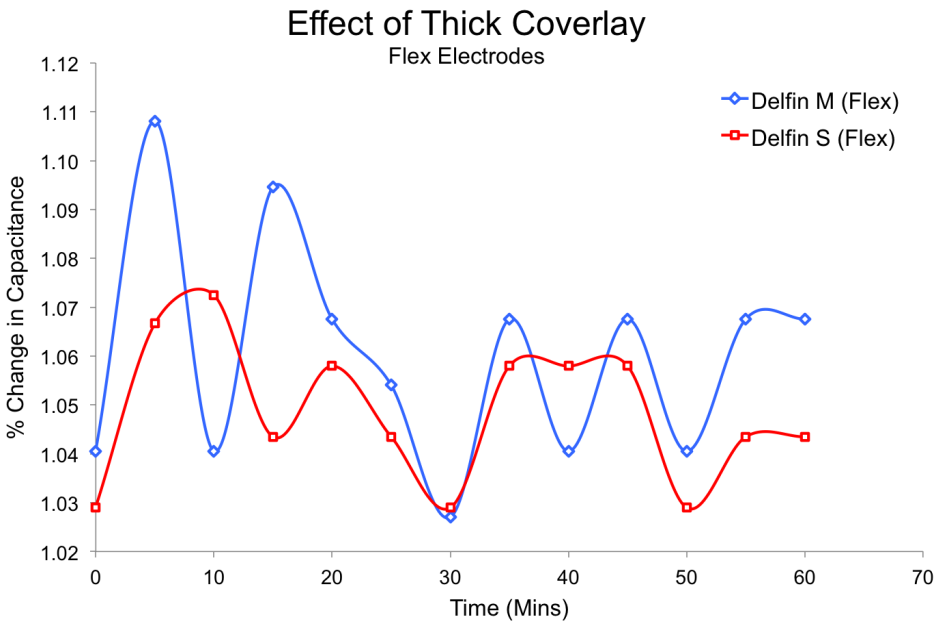

Figure 5.5: Evaluation of flex electrode.

maintained such that the resistive pressure sensor had a resistance of 50kOhms.

Compared to the PCB board sensor, the overall measured skin capacitance was much lower. This was attributed to the thicker coverlay used on the flex (5 mils) compared to the soldermask thickness on the PCB (1 mil). A thick coverlay was selected because of concerns that a thin coverlay will saturate the CDC sensor, as was the case with the PCB electrode. The PCB electrode saturation was remedied by applying a thin layer of tape on top of the electrode, to increase the distance between the surface of the skin and the copper electrode). As a result, the overall percentage change in capacitance was much lower, with the capacitance measurements registering a 6% change instead of the typical 25% change when compared to the PCB electrode.

5.3.1 Effect of Coverlay Thickness

The thickness of the coverlay directly affects the measured capacitance value. For the current design, the coverlay thickness was specified at 5mils. This however resulted in a

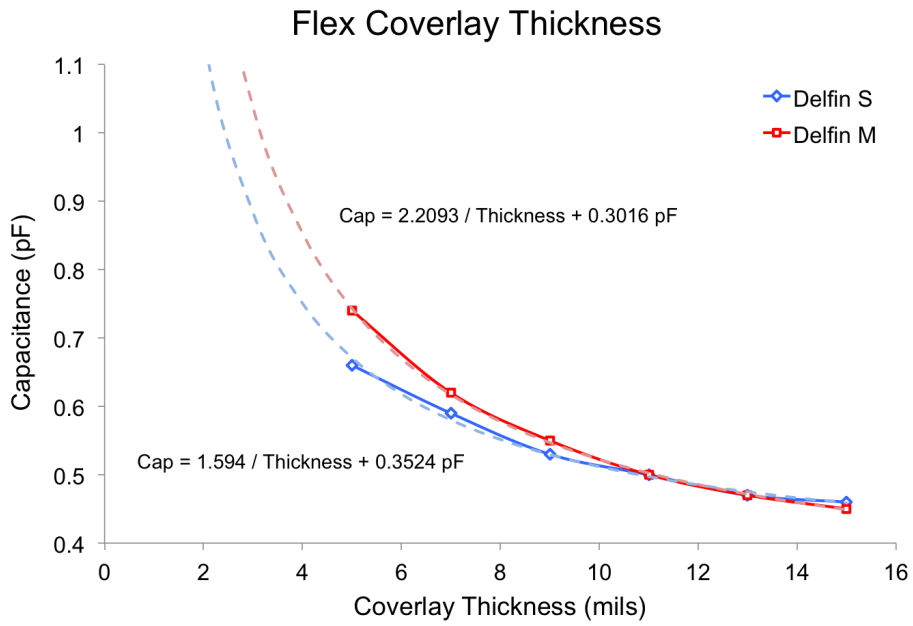

Figure 5.6: Effect of flex electrodes coverlay thickness on capacitance.

smaller static capacitance value. An experiment was performed to explore the effect by the coverlay thickness on the measured static capacitance. This experiment however did not address why the percentage change in capacitance was smaller than those seen in the rigid electrodes.

In this experiment, tape was added to both the Delfin M and S flex electrode, to simulate an increase in coverlay thickness. The sensor was then applied to the inner volar forearm, with the applied pressure maintained at 50kOhms. As expected, increasing the coverlay thickness resulted in a decrease in capacitance. The experimental data fitted nicely with the parallel plate capacitor model with an offset. Both the Delfin M and the Delfin S electrode had a R^2 value of 0.999.

$$C = \frac{\epsilon * A}{d} + offset$$

The sensitivity of the flex may be increased through minimizing the coverlay thickness to 2 mils, half of the current coverlay thickness. At 2 mils, the sensor will not saturate the input range of the CDC and would boost the static capacitance values into the pF range.

5.3.2 Effect of Ground Plane

Underneath the electrode is a hashed ground plane to isolate any stray capacitance originating from the backside of the electrode. The size of the ground plane will affect the measured static capacitance. To explore the effect between the size of the ground plane and the static capacitance, an experiment was performed where the ground plane of the Delfin S Flex sensor was cut consecutively smaller. For each radius, the capacitance was measured while maintaining a constant force at 50Kohms.

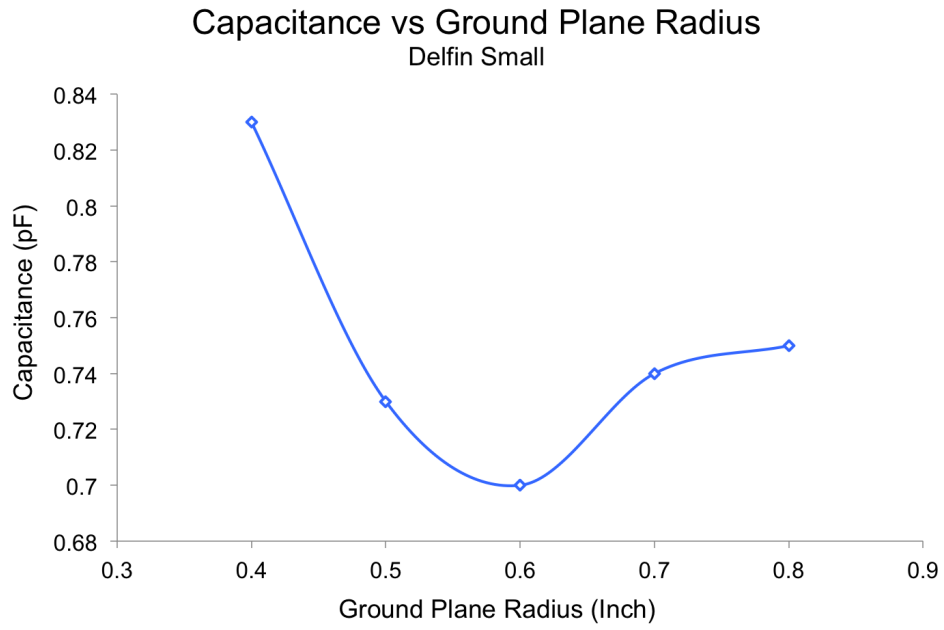

Figure 5.7: Effect of ground plane size on capacitance.

Figure 5.7 seems to suggest that as the radius was increased, the capacitance actually decreased, but after the radius was increased past a certain point, the capacitance increased. What the figure didn't convey was that although force was maintained to be constant, because of the consecutively smaller area, the applied pressure was increased. Taking into account the change in pressure with capacitance showed a much clearer picture of the situation as shown in Figure 5.8.

As shown in Figure 5.8, the dominant source of capacitance was from the fringe field of

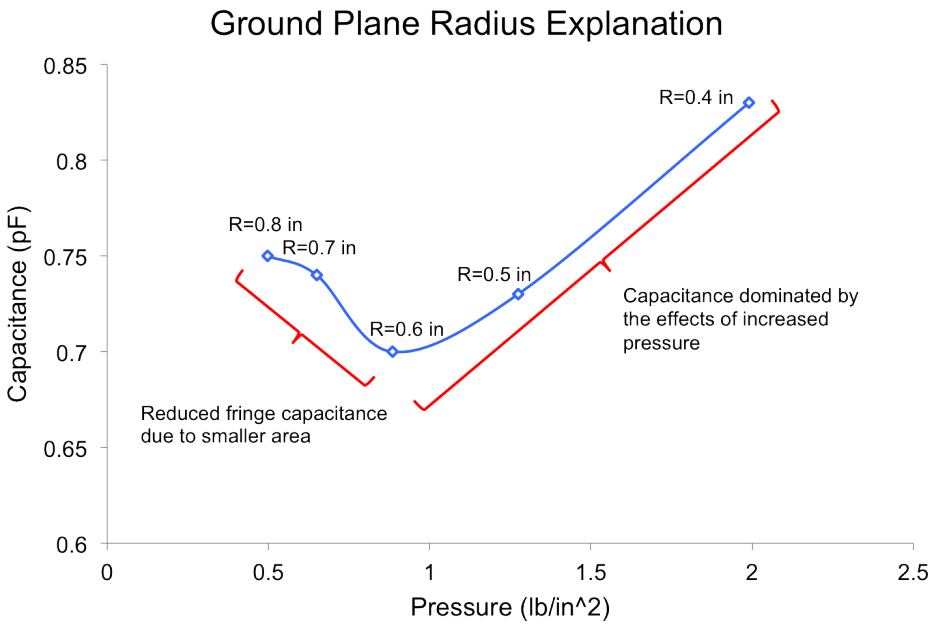

Figure 5.8: Effect of ground plane size while taking into account the increase in applied pressure on capacitance.

the electrode to the ground plane, where decreasing the radius resulted in smaller fringe capacitance. However, after reducing the radius past a certain point, the effect from the increase in applied pressure dominated the source of capacitance, thus resulted in the increase of capacitance. Since the two factors, reduced radius and increased pressure) were at play, it was hard to deduce an optimal pressure and radius from this experiment.

5.3.3 Revised Flex Stackup

The first version of the flex sensor suffered from diminished responsiveness in the dynamic performance when compared to the PCB electrode. Possible reasons were the distance from the electrode to the ground plane, the size of ground plane, and the thickness of the coverlay. It was determined that coverlay thickness affected the static capacitance but had little effect on the dynamic performance. Therefore, these issues were addressed in the next revision of the flex stackup, as shown in Figure 5.9. In the updated revision,

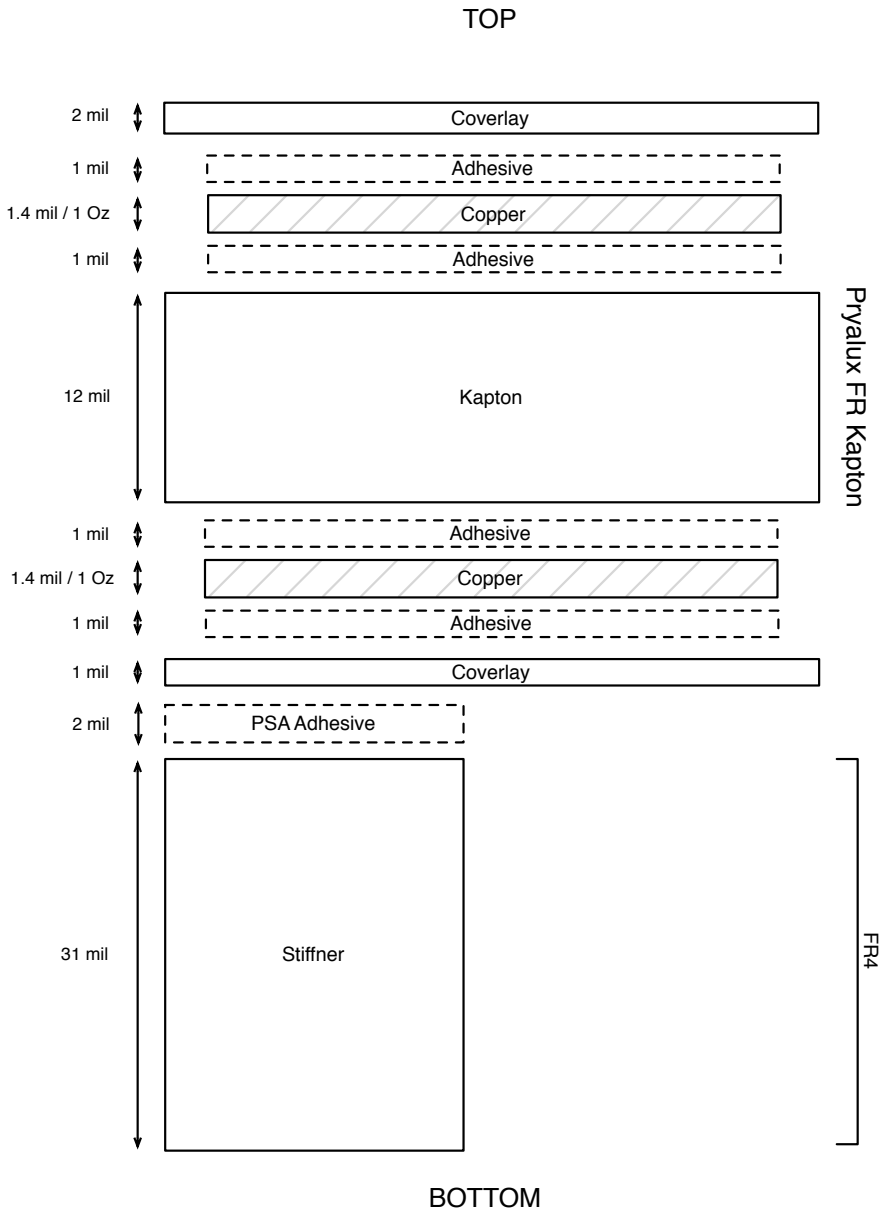

Figure 5.9: Revised flex stackup. The separation between the electrode and ground was increased and the coverlay thickness was decreased.

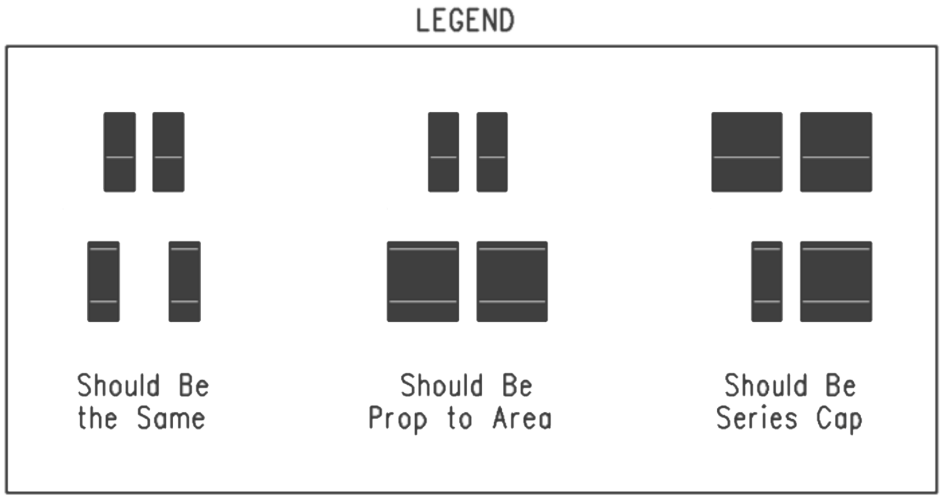

Figure 5.10: The capacitor test structure used for the optimization of the electrode.

the distance from the electrode to the ground plane was drastically increased to improve dynamic performance. Also, the coverlay thickness was now reduced to 2 mils to increase sensitivity.

5.4 Electrode Optimization

There were a few parameters that could be adjusted in optimizing the performance of the electrode: the lateral spacing between the two terminals, the area of the terminals, the distance from the terminals to the shield plane, and whether to ground the shield plane or leave it floating. A total combination of 63 test structures were designed and manufactured to be tested as shown in Figure 5.10. The three main tests were:

- Effect of the lateral spacing between the two terminal of the electrode
- Effect of the area of the electrode's terminals
- Effect of the vertical spacing between the electrode to the shield plane

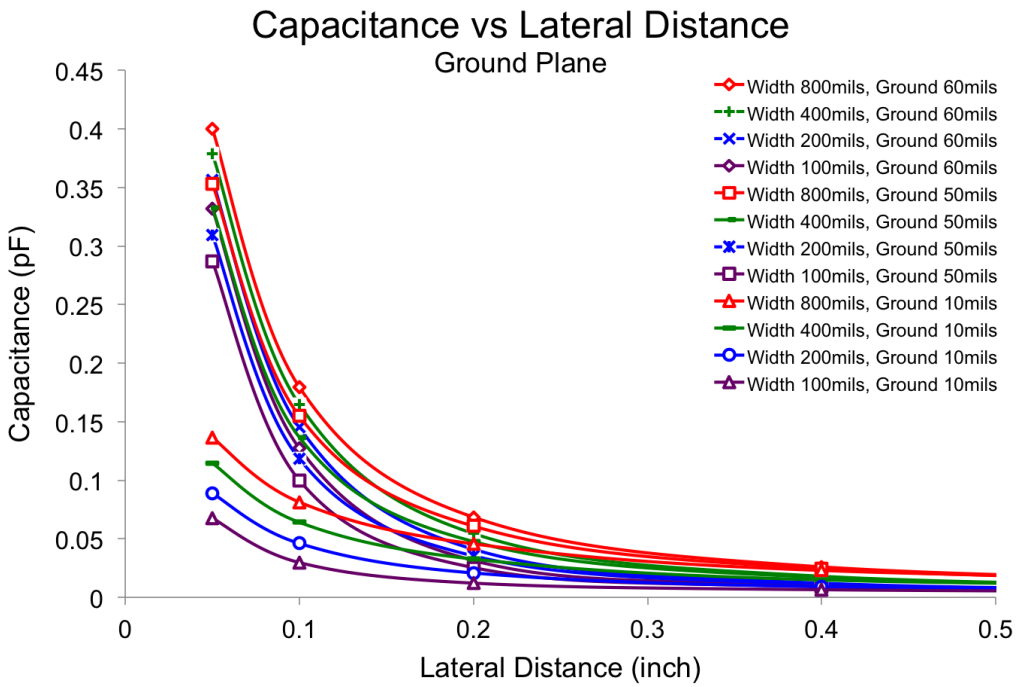

Figure 5.11: Capacitance vs Lateral Distance of an electrode with a ground plane underneath.

5.4.1 Electrode Geometry Parameters

The capacitor test structures were fabricated on a PCB which enabled the testing of any combination of the following parameters:

- Three lateral spacings of 0.1, 0.2 and 0.4 inches
- Three vertical distances (vertical spacing to the shield plane) of 10, 50 and 60 mils
- Three plate areas of 0.1, 0.2, 0.4, 0.8 square inches

5.4.1.1 Effect of Lateral Spacing on Capacitance

When the plane underneath the electrode was grounded, the majority of the capacitance was due to the fringe capacitance between the two terminals of the electrode. By separating the two terminals, the capacitance contributed by the fringe field becomes weaker, as shown in the Figure 5.11.

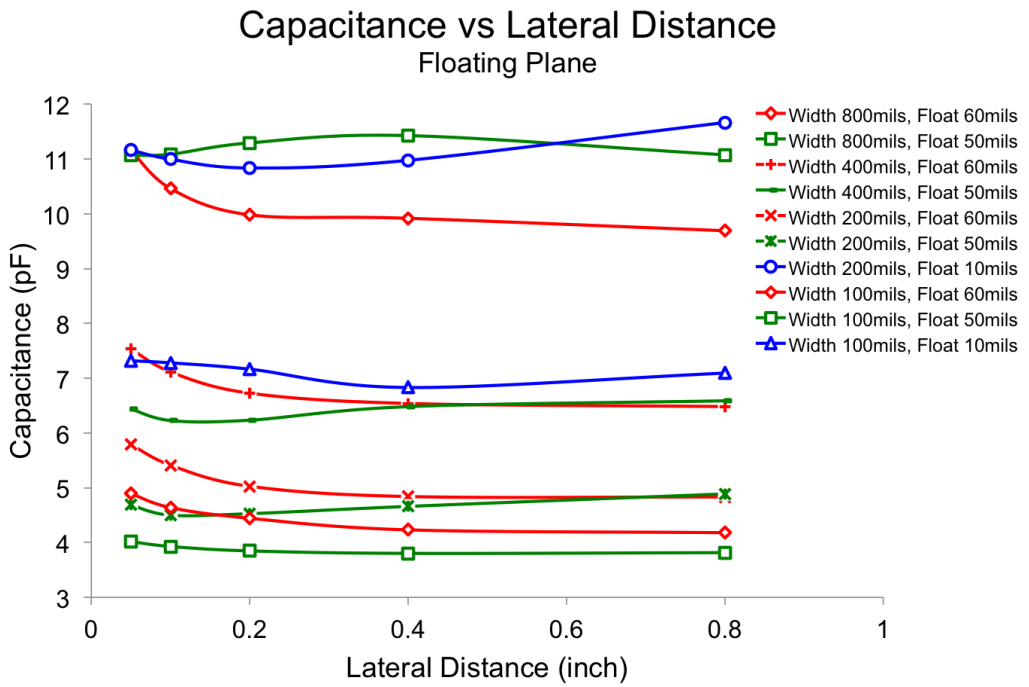

Figure 5.12: Capacitance vs Lateral Distance of an electrode with a floating plane underneath.

When the plane underneath the electrode was left floating, the electrode acted like a normal parallel plate capacitor. The lateral spacing between the two plates did not affect the capacitor, which was consistent with the area capacitor model.

5.4.1.2 Effect of Vertical Spacing on Capacitance

With the ground plane underneath the electrode, the main contribution to the measured capacitance was from the fringe capacitance between the two terminals. Due to the architecture of the capacitance to digital converter, the parasitic capacitance from the electrode to the ground plane was canceled out, as verified in this experiment. The farther away the terminal was to the ground plane, the weaker the fringe capacitance was shunted to ground, which resulted in a larger measured capacitance.

In the case where a floating plane was placed underneath the electrode, as the vertical distance between the electrode and the ground plane was increased, the capacitance

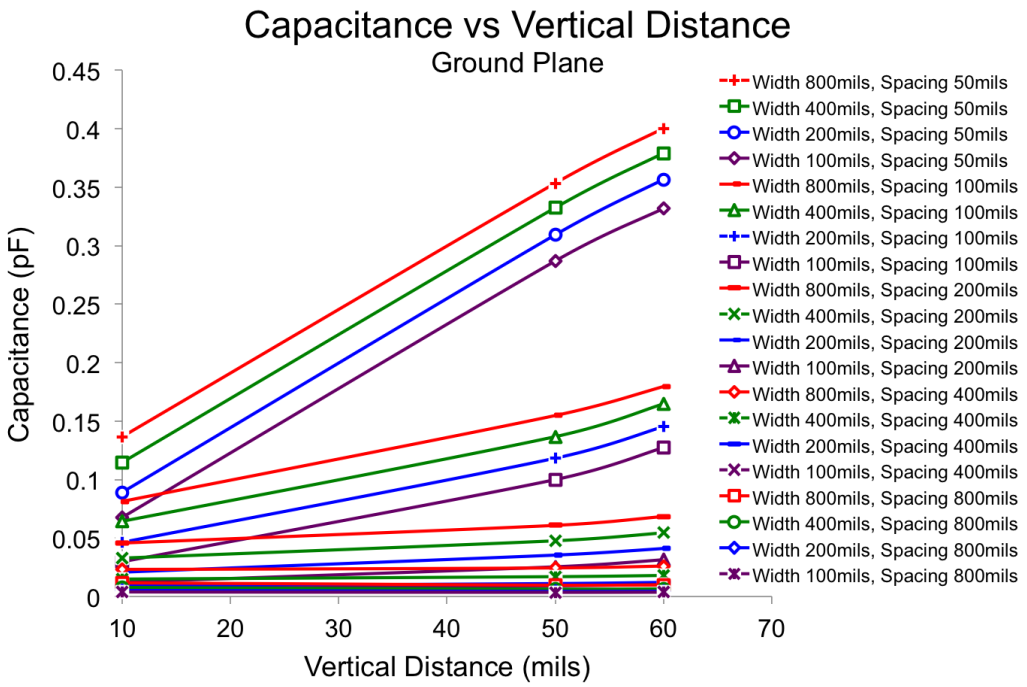

Figure 5.13: Capacitance vs Vertical Distance of an electrode to a ground plane.

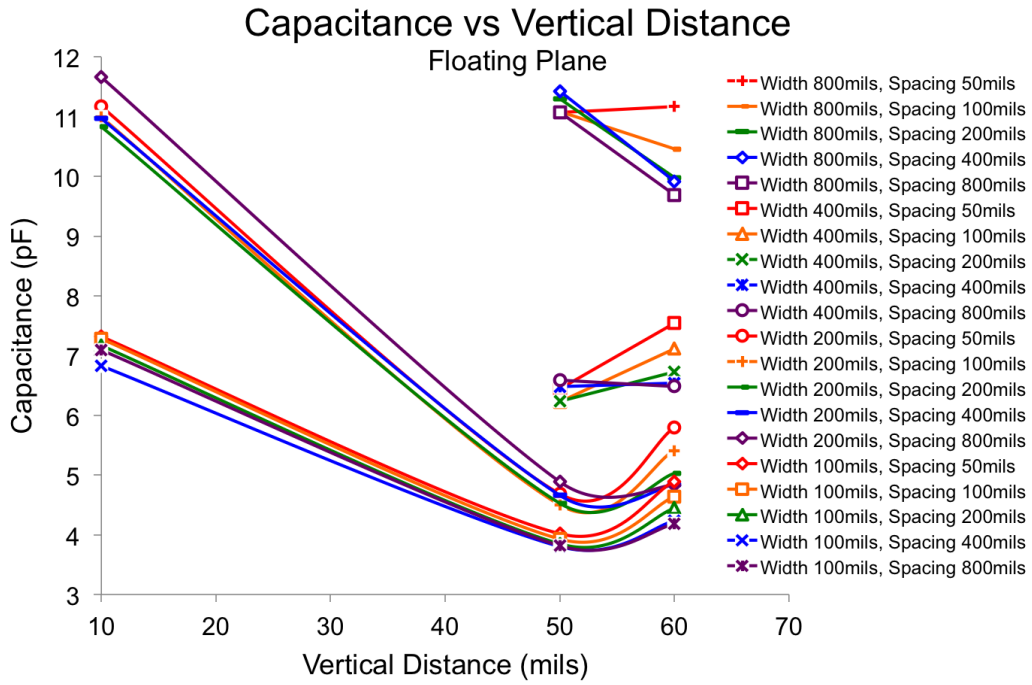

Figure 5.14: Capacitance vs Vertical Distance of an electrode to a floating plane.

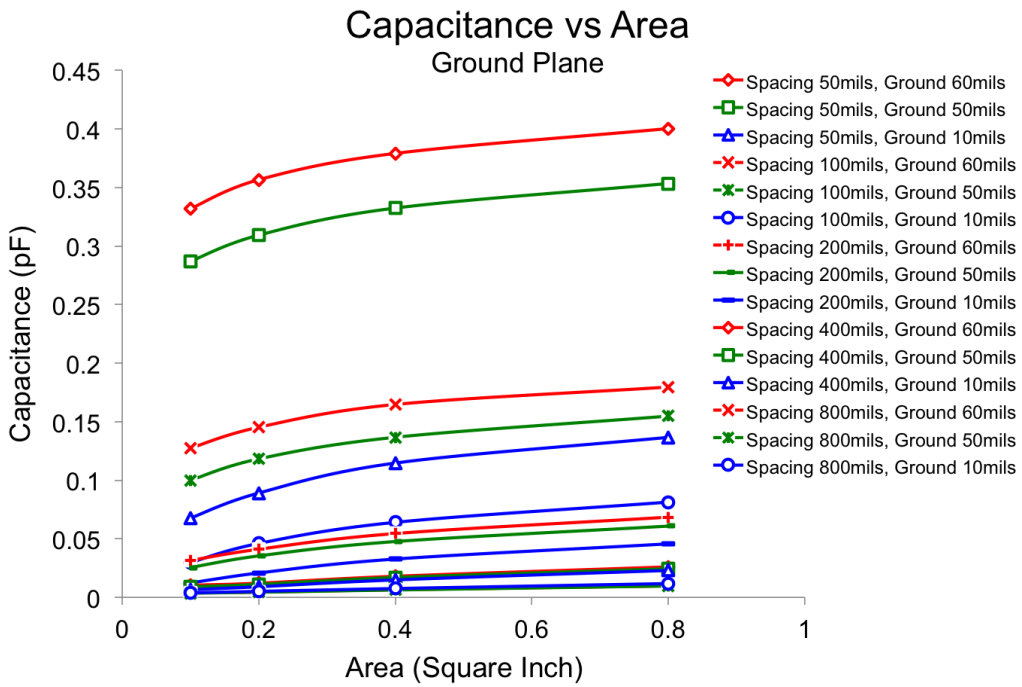

Figure 5.15: Capacitance vs Area of an electrode with a ground plane underneath.

decreased which was also consistent with the area capacitor model.

5.4.1.3 Effect of Plate Area on Capacitance

When a ground plane was placed underneath the electrode, as the area of the terminals were increased, the capacitance roughly stayed the same. As the area was increased, the parasitic capacitance from the electrode to the ground increased proportionally. However due to the architecture of the CDC, the parasitic capacitance to ground was canceled out, hence there was no measured increase in the capacitance. The slight increase in the measured capacitance, which was found to be proportional to the area as shown in Figure 5.15, might be attributed to the inherent limitations of the capacitance to digital converter architecture.

When the plane underneath the electrode was left floating, by increasing the area of the electrode it resulted in the increase of the measured capacitance, which was consistent

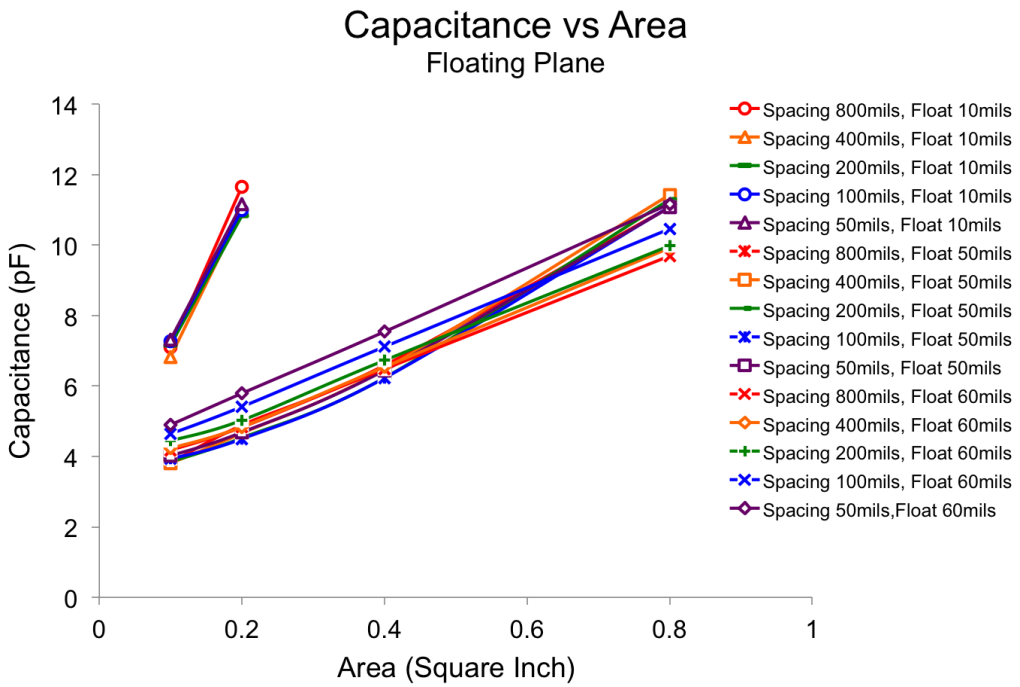

Figure 5.16: Capacitance vs Area of an electrode with a floating plane underneath.

with the area capacitor model.

5.4.1.4 Optimization of Electrode Parameters

Like any design problem, there were tradeoffs between each parameters. Using the test structures, insights were gained to what the tradeoffs were for each of those parameters. In the design of the electrode, the ground plane cannot be placed too close to the electrode, or else the fringe capacitance would be shunted to ground. However, the ground plane cannot be placed too far from the electrode, as that would result in a very stiff flex circuit. The spacing between the electrodes shouldn't be place too far apart as that decreases the fringe field. Also the electrodes cannot be placed too close together as the fringe field will not penetrate the desired depth. Lastly, the electrode area cannot be too large as the measured capacitance might exceed the limits of the capacitance to digital converter.

5.5 Electrode Penetration Depth

Analysis of the electrode's effective penetration depth in human tissue was performed using Ansys Maxwell EM simulation software. Using the human skin model proposed by Alanen [ALN99], the penetration depth of the small and medium electrodes were simulated in software. For this simulation, both the electrode and the human skin were modeled in software. A high dielectric point source was swept in both the lateral and vertical direction, and the capacitance measured by the electrode was then saved. Figure 5.17 shows the change in capacitance, or sensitivity to the dielectric point source as a function of depth.

The simulation showed that the penetration depth of both electrode has the same maximum depth sensitivity of 100 mils beneath the skin. However, the medium electrode, where the spacing between the outer and inner terminal was larger than in the small electrode, had a penetration depth sensitivity concentrated deeper into the tissue compared to that of the small electrode.

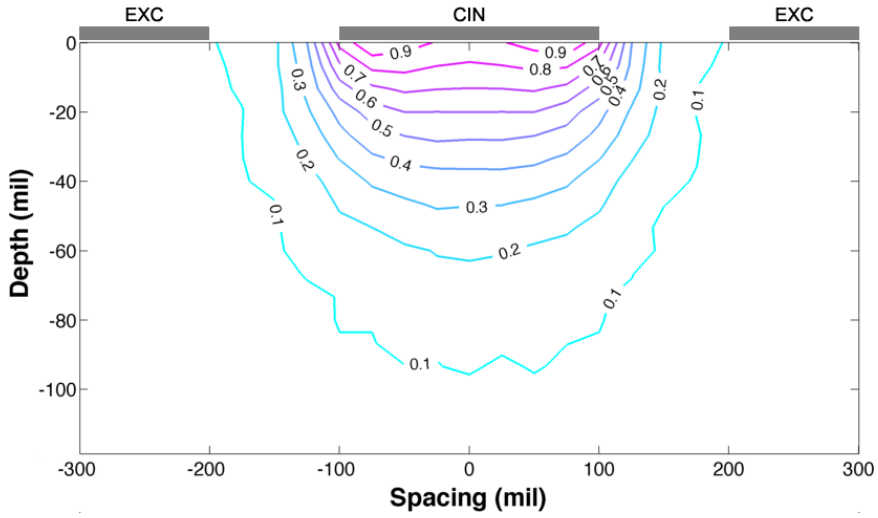

(a) Small Electrode

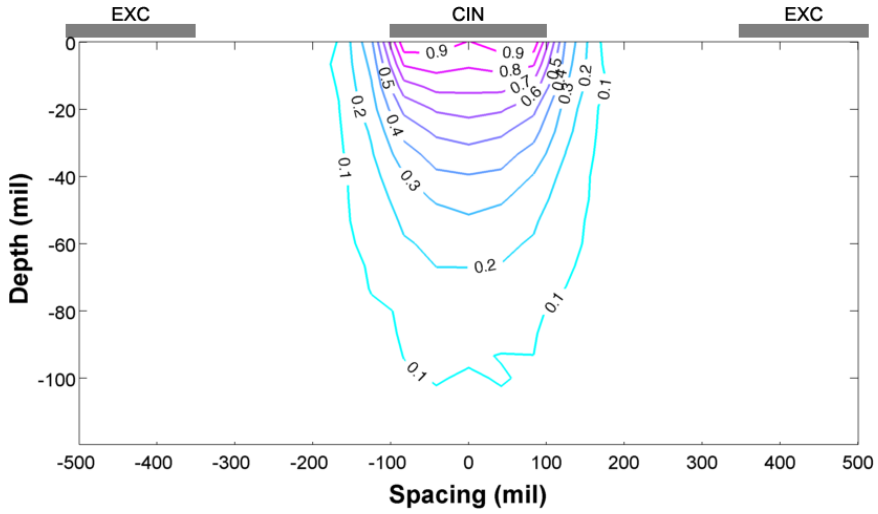

(b) Medium Electrode

Figure 5.17: Using Maxwell EM simulation software to simulate the effective penetration depth of the electrodes.

CHAPTER 6

SEM Scanner System

The SEM Scanner was a device designed to detect early stage pressure ulcers through the monitoring of sub-epidermal moisture (SEM). This device not only requires the integration of electrodes, capacitance measurement systems and pressure sensors but also requires a method of interacting with the user and the storage and communication of the measured data.

The initial prototype was targeted towards its use in an internal clinical trial, and not for commercial use. As such, the device was designed to capture additional factors that might influence SEM readings, such as a humidity, ambient room temperature, the patient's blood oxygenation level and pulse rate for further analysis.

6.1 Features

The SEM Scanner includes the following features:

- 2 electrodes to measure capacitance
- Pressure sensors to measure amount of applied pressure on each electrodes
- Records ambient room temp, relative humidity, heart rate, SpO2
- Buzzer for audible notifications
- Bright, OLED display

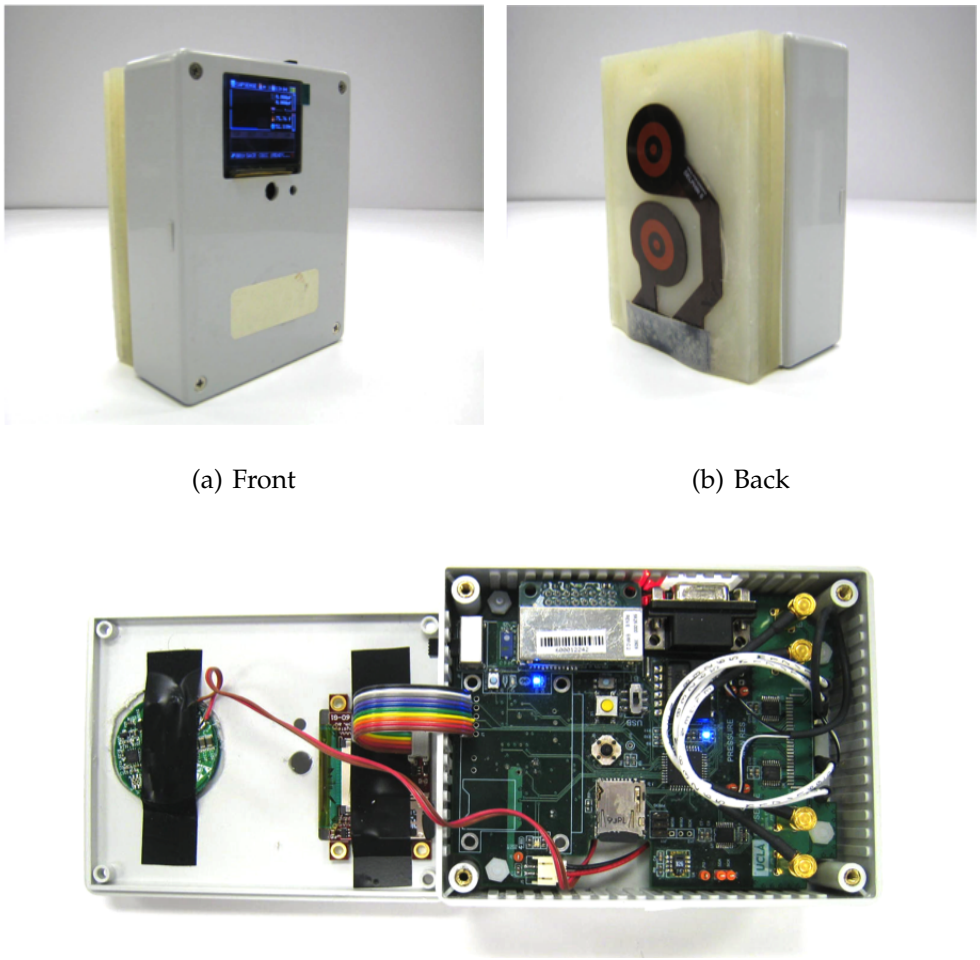

(a) Front (b) Back

(c) Inside

Figure 6.1: Prototype of the SEM Scanner.

- Wireless Bluetooth communication
- Wireless charging
- 2 Amp Hour battery allowing for 6 hours of continuous use
- Real-time Clock
- Local data logging onto microSD card in XML file format
- Fully enclosed design to facilitate easy sanitation

6.2 Architecture

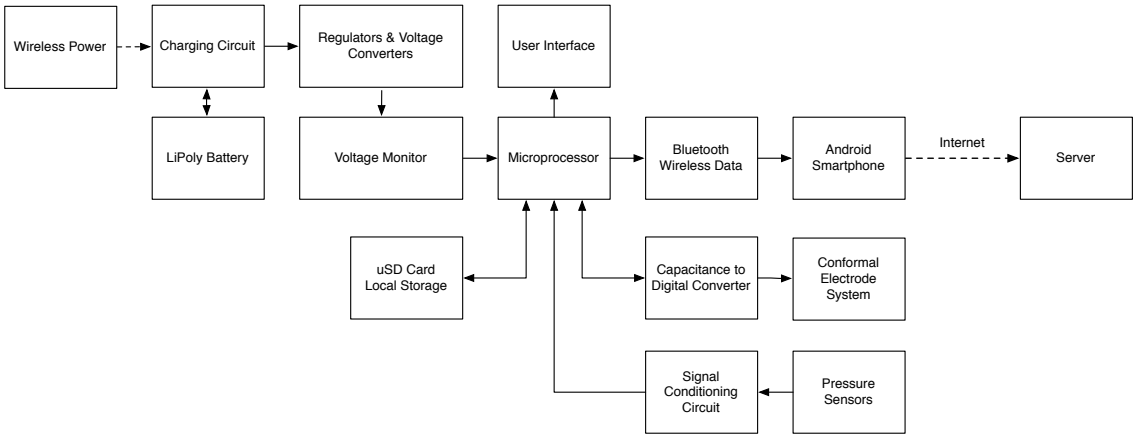

Figure 6.2: SEM Scanner System Architecture

At the heart of the SEM Scanner are two 24-bit capacitance-to-digital converter (CDC) from Analog Device. This allowed the design to support a total of four electrodes, however only two were used. A simple 8-bit microprocessor from Atmel was used to control the LCD and to acquire the data from the various sensors. The sensors all communicated over an I2C bus except the Nonin blood-oxymetry sensor. The Nonin OEM III blood-oxymetry solution was used to acquire the subjects heartrate and SpO2. Because this sensor was the only sensor that did not natively communicate over the I2C bus, another microprocessor was programmed to act as a translator between its native serial format and I2C.

A round-robin scheduler was implemented, to increase the data acquisition rate. Thus, when an individual sensor was acquiring data, instead of the microprocessor waiting for that sensor to finish acquisition, the next sensor would be initiated for measurement.

To enable Bluetooth communication, a Roving Networks RN-41 Serial to Bluetooth chip was used. Local storage of the data onto a micro-SD card was made possible by using open source FAT16 drivers from Electronic Lives Manufacturing.

Battery charging was implemented using a dedicated LiPoly charging integrated circuit from Maxim. In order for the microprocessor to monitor the current battery life, the battery

voltage was fed through a resistor divider which was then processed by microprocessor through an on-chip ADC. Wireless inductive charging was accomplished by incorporating a Powermat receiver into the SEM Scanner. The SEM Scanner can then be charged by placing the device onto a Powermat charger.

The firmware was written in C, without the use of an operating system.

6.3 Operation

The device can be used either in standalone mode or in conjunction with an Android smartphone which allowed the measured data to be relayed to a server in real-time. When the user first turned on the SEM Scanner, the device calibrated the electrode to subtract out the inherent parasitic capacitance due to the electrode geometry and humidity. The device was now ready to take measurements. Before initiating measurements on each patient, the operator needed to first scroll or type in the patient ID. The body location of the measurement also needed to be selected at the beginning of a new set of measurement. To initiate measurement, the operator placed the SEM Scanner with the top electrode over the area in question. The bottom electrode was placed over healthy skin to act as a local reference to what the baseline capacitance should be. The electrodes were designed on Kapton, which was a bio-inert flexible material. The electrodes rested on top of a stretchable silicone sheet, which allowed for the electrode to conform to various body locations. Underneath each electrode was a pressure sensor, which allowed for each capacitance measurement to be made with the same amount of applied pressure. This was important as the amount of pressure applied had a direct effect on the measured capacitance. The device displayed the applied pressure real-time in the form of two bar graphs on the OLED display. The operator then adjusted the applied pressure on both of the electrodes, such that the pressure on each electrode was within a predefined range. Once this condition was met, the device then took a measurement of skin capacitance, and also recorded other factors such

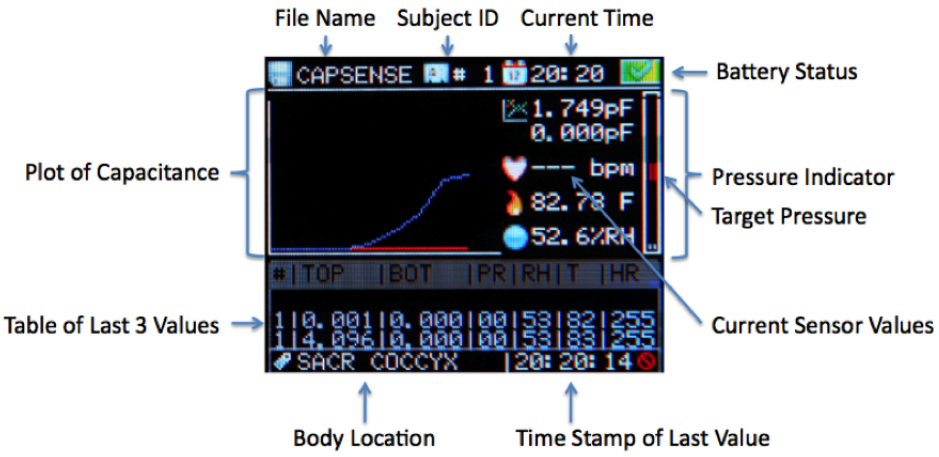

(a) Main Screen

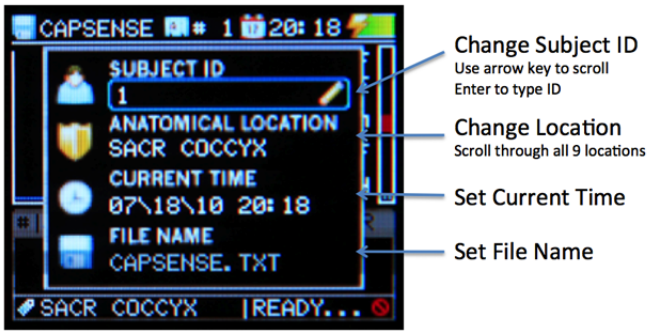

(b) Settings

Figure 6.3: The graphical user interface for the SEM Scanner.

as the ambient room temperature, relative humidity, heart-rate of subject. As an indication of a successful measurement, the device emitted an audible beep. The measurement result was appended on the OLED display, where it showed the last three measurements. The data was then stored onto a micro-SD card in an XML file format and if the SEM Scanner was connected wirelessly through Bluetooth to an Android smartphone, the data was then relayed to a central server where the measurement data can be viewed worldwide in near real-time.

Since the device was fully wireless, there were no wires present allowing the SEM Scanner to be fully enclosed. As such the device was easily sanitized in-between patient, by wiping down the entire surface with an alcohol wipe or an anti-microbial cleanser.

6.4 Electrodes

At the heart of the capacitance measurement system is the electrodes. By varying the size of the electrode, the penetration depth of the capacitance fringe field also varies. Thus different sized electrodes can target the sub-epidermal moisture at different depths. A ground plane was placed underneath the electrode to shield interference from the backside of the sensor, thus only allowing sensing from the front. The electrodes were carefully designed such that the parasitic capacitance does not overwhelm the input range of the CDC. The thickness of the substrate material was also calculated such that the skin capacitance does not dominate over the capacitance due to moisture, which is much smaller.

Since it was noted that other factors might affect the capacitance reading, and hence the affect the ability to measure the sub-epidermal moisture, the device also measured relative humidity, ambient room temp, and heart-rate for post data analysis to determine how each factor affected these readings.

In the prototype device, differential measurement between the two electrodes were used to cancel out the common effects from various factors. One electrode was placed

over the area in question, while the second electrode was placed over healthy skin which acted as a reference. Since the tissue underneath both electrodes experienced the same effect from the factors, by taking the difference in capacitance between the two electrodes, the capacitance due to the difference in sub-epidermal moisture between the two sites can be determined.

CHAPTER 7

Commercialization

The first generation of the SEM Scanner served as a useful starting point in developing the commercial SEM Scanner. To shorten the time to market, minor modifications were performed on the circuit side. In bringing the device to commercialization, most of the time was spent on the mechanical aspects of the design and also ensuring that the device would pass various safety standards. Also particular focus was placed on the user interaction with the SEM Scanner.

7.1 Enclosure Form Factor

The enclosure form factor was redesigned by Stellartech with a particular focus on ergonomics. The device needed to be small and easily hand-holdable for healthcare providers with smaller hands. The device also featured an angled display which allows for easy readability. The enclosure was fully-sealed, allowing the device to be easily cleaned after use and between patients.

7.2 Rigid Electrodes Molding

The electrode support structure, shown in Figure 7.3, was molded out of 2mm of medical-grade silicone. This silicone meets the biocompatible requirements of ISO10993 for surface devices in contact with skin for limited periods. The electrode support structure allowed for mechanical compliance, ensuring that the electrode had a good contact with the sur-

(a) Front (b) Back

Figure 7.1: SEM Scanner with a professionally designed enclosure and electrodes.

Figure 7.2: SEM Scanner features an ergonomic design.

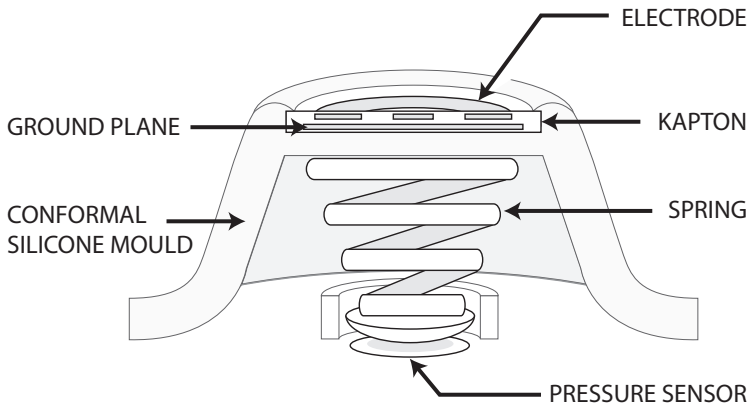

Figure 7.3: Cut-away view of the electrode design.

face of the patient's skin. The electrode was supported by a rigid printed circuit board to prevent the electrode from warping. Underneath each electrode was a small mechanical spring, with a nib that connected it to a pressure sensor. This allowed for the monitoring of the applied pressure from the electrode onto the surface of the skin.

7.3 Single Button Operation

The original user interaction method for the prototype SEM Scanner was considered to be too complicated. Since the SEM Scanner was to be used at the point of care, it needed to be simple and easy to use by the healthcare providers. As such, the operation of the device was greatly simplified to only provide the most pertinent information. The SEM Scanner was redesigned for a single button operation. The device would always be ready to acquire a sequence of measurements when the correct pressure was applied to the electrodes. Once the measurement has been completed, the mean and maximum values of the sequence of measurements were reported back to the user. Pressing the button started a new set of sequence, which reseted the mean and maximum value back to 0. Holding down the single button will allow the user to switch between the top (medium) and bottom (small) electrode. To power off the device, the button needed to be held down for a period of 2 seconds. This user interaction was greatly simplified, compared to the prior iteration

where a joystick was required to select through various options, such as the body location, patient ID, etc...

7.4 RFID

An enterprise version of the SEM Scanner was designed for streamlining its use within the hospital or nursing home environment, in particular to help track compliance of its use, and also to store the pressure ulcer assessment of each patient. In the enterprise solution of the SEM Scanner, an RFID reader was incorporated. It was envisioned that each patient would be given an RFID bracelet which would uniquely identify them. When the health-care provider performs the skin assessment, they will first scan the RFID of the patient with the SEM Scanner. The SEM Scanner will then store the date and timestamp along with the patient ID. This will serve as a record that the skin assessment was performed, helping with compliance verification.

It was also possible to use RFID tag as a method to interact with the SEM Scanner. Because of the single button on the SEM Scanner, it was particularly difficult to scroll through a list of items such as the body location. One possible solution was to use a set of RFID tags. Each RFID tag correspond to an action, such as measuring the heel, or to redo the last measurement.

The RFID read capability for the SEM Scanner was implemented using a chipset from ID Innovations. The RFID reader passed the information serially, however all the UARTS on the microprocessor were used. Instead, the RFID reader was connected to a spare UART on the OLED display. The OLED display firmware was modified to read the data from the RFID and to store each valid reading. Since the display was configured to act as a slave, the SEM Scanner microprocessor would continuously poll the OLED display for any new RFID readings. If a valid reading had occurred, the display then sent the ID tag information back to the main microprocessor.

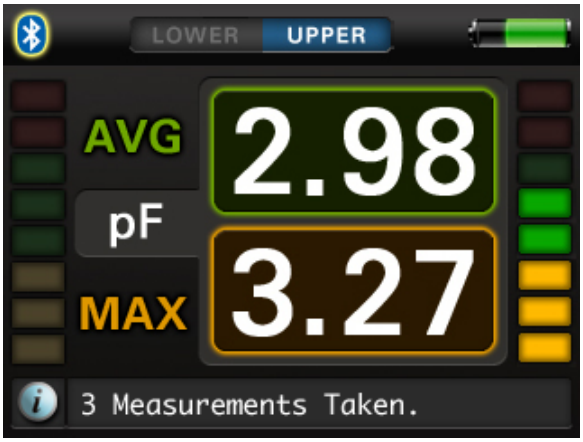

Figure 7.4: Refined GUI for the SEM Scanner.

7.5 GUI

Working with Stellartech, a much more polished GUI was designed. The display was simplified to only report the mean of all measurements, and also the maximum value. The display featured a pressure bar on each side of the screen; the left bar indicates the pressure on the top electrode, and the right bar indicates the pressure on the bottom electrode. Instead of using an analog pressure bar, the pressure bar was split into 9 segments. The pressure bar was also color coordinated to easily identify if the applied pressure was too large (identified by the color red) or too small (identified by the color yellow). If the pressure was within the target range, the color of the pressure bar turned green.

7.6 Data Transfer

In the enterprise version of the SEM Scanner, when the SEM Scanner is placed on the charging mat, it will transfer all internally stored data to a remote server via a bluetooth connection with an Android gateway.

Because the device was most likely off when placed onto the charging mat, the charging circuitry was responsible to monitor whether the device was placed on a charging mat.

If the charging mat was present, the charging circuit will power-on the microprocessor and the various internal power rails. Once the power-on sequence was complete, the microprocessor verified that indeed it was currently on the charger. The microprocessor will then attempt to communicate with the bluetooth host. If the communication was successful, the microprocessor will directly transfer the ASCII log file, byte by byte. The file transfer will terminate by sending a null character. The bluetooth host will return with a checksum, and if it matched the microprocessor checksum, the file transfer was finished.

7.7 Data Storage

As the enterprise version of the SEM Scanner required local data storage capabilities, the enterprise SEM Scanner supported the use of a microSD through the SPI interface. Since the device was implemented on a simple 8bit microprocessor, it did not have a full file system implementation. Working around this limitation, the device will open a log file, and store the changes sequentially. It does not attempt to open a file and modify existing data, for example in the case of redoing a measurement. The server will be required to parse the command logs in order to properly determine which capacitance measurement is associated with which patient.

The SEM Scanner logged all raw measurements, not just the mean and max. Each measurement was recorded with its timestamp. All command actions were also recorded, such as when the user started a new set of measurement, when the electrode was switched between the medium and small setting, when it was charged and when the device was powered on and off.

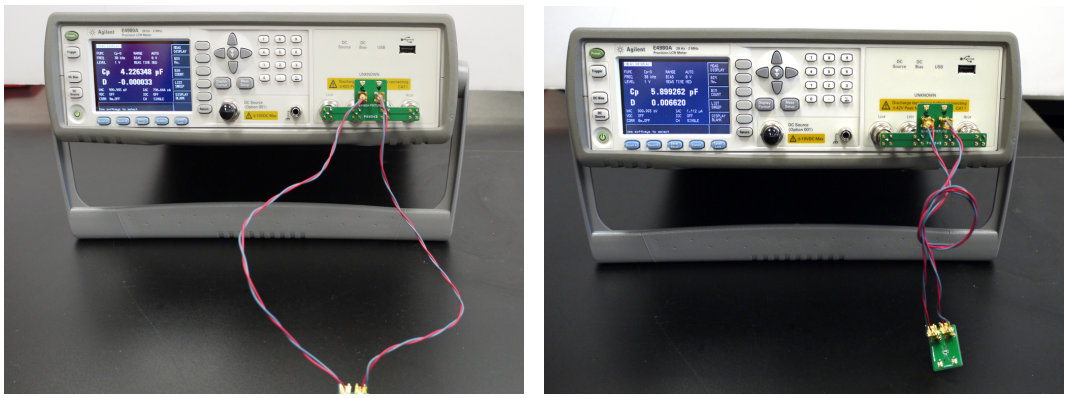

(a) Twisted Pair (4.22pF) (b) With Loop (5.89pF)

Figure 7.5: Twisted pair cabling has a large variation depending on orientation of cable.

7.8 Cabling

In the prototype version of the SEM Scanner, SMB shielded coaxial cables were used to connect the electrodes to the main circuit board. Each electrode required 2 cables, resulting in a total of 4 cables for the entire SEM Scanner. However, due to the expensive cost of each cable, replacements for the cables were evaluated. Also, the SMB cables were bulky and not very flexible.

An Agilent E4980A LCR meter was used to measure the performance of the alternate cable solution under various stress and conditions.

The first alternative solution to be evaluated was using normal wires for the excitation output and capacitance input wire. The two wires were twisted together, with the hope that it would cancel out common-mode interference. The main benefit of using normal wires was that it was cheap. However the performance was dismal. Connecting the normal wire to a 4pF load, the measured capacitance varied from 4.22pF for just a straight twisted pair to 5.89pF if the cable was routed with a loop. This was expected as the excitation output wire will interact with the capacitance input wire. The reason that the coaxial cable was not prone to this effect was that the coaxial contained a grounded shield which prevented outside signals from interfering with the shielded signal, but instead presented

the capacitance input wire with a constant parasitic capacitance to ground. The twisted pair also was affected by the number of turns, the length and how it is routed within the device, something that was not very easily controlled during manufacturing between devices. Also, in the prototype units, it was noted that if the SEM scanner was dropped, the capacitance value would drift. This was later attributed to the fact that the wire would shift its position internally, varying the parasitic capacitance.

The second cable to be evaluated was a ribbon cable. The ribbon cable was organized such that the capacitance input wire was surrounded by grounded wires to act as a ground shield. The 4 wire ribbon cable was arranged in the following order: excitation output, ground, capacitance input, ground. Without any bends, the cable measured 5.1pF when connected to a 4pF load. However when the cable was bent and twisted, the measured load capacitance increased to 5.6pF. The ribbon cable, compared to the twisted pair, performed much better. The length between devices can also be better controlled with the ribbon, and without the need to worry about the number of turns. If during manufacturing the cable can be organized in such a way that it is consistent among all devices, this might be a viable alternative to the twisted pair.

Lastly, a micro-coaxial cable was evaluated. Compared to the performance of the twisted pair and ribbon cable, the micro-coaxial cable performed solidly. Regardless how the cable was bent, routed, and intertwined with each other, the measured capacitance was always measured at 4.09pF for the 4pF load. The downside to this solution was its cost.

7.9 End of Line Calibration and Testing

Each device that came off the manufacturing line needed to be calibrated and tested. To facilitate this process, a SEM Calibrator stand was designed to consistently calibrate the measured capacitance and pressure of each device.

Figure 7.6 shows a cut-away view of the SEM Calibrator stand. The SEM Calibrator

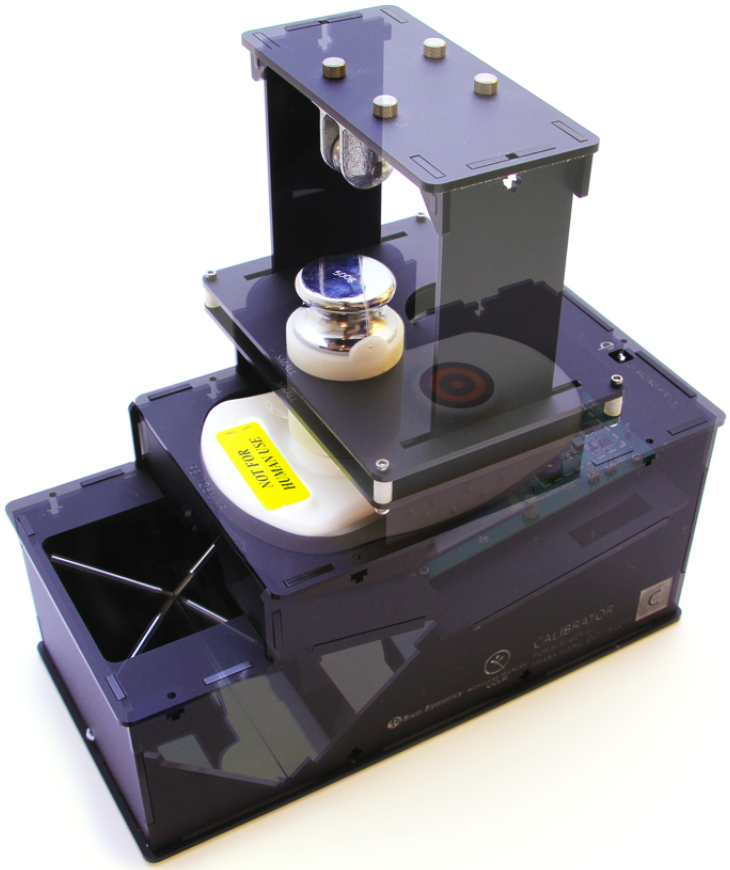

Figure 7.6: Cut-away diagram of the calibrator stand for the SEM Scanner.

stand featured a pulley system and a weight guide for the pressure calibration, three different dielectric materials to calibrate the electrodes, two mirrors to reflect the SEM display to the operator, and also a built-in charger to test the charging functionality.

For the pressure calibration, a precise method of applying a known and repeatable pressure was required. The SEM Calibrator stand was designed to satisfy this need. To apply a known pressure, a known weight was applied to the surface of the electrode. Since the surface area of the weight was also known, the applied pressure could be calculated.

In order to have an accurate and repeatable measurement, the weight must apply a force perpendicular to the surface of the electrode. However, as the electrode was supported by a flexible membrane, applying the weight perpendicular to the surface of the

electrode was quite difficult. Direct application of the weight onto the electrode will result in the weight tilting unpredictably in one direction or the other, ie unstable.

To help stabilize the weight, a mechanical weight guide was used. This ensured that the tilting of the weight was minimized, and guaranteed that the applied pressure was perpendicular to the surface of the electrode.

Standard weights are only available in 50g, 100g, 250g, 500g, and 600g. To apply a pressure other than what the standard weights can provide required a combination of weights, such as two weights attached to each other. This however was undesirable as the combined weight will now have a higher center of mass, which will lead to increased instability.

The calibrator stand instead used a solution based on pulleys. In this solution, the SEM scanner pressure sensors were calibrated to the pressure applied by the 500g weight and the 600g weight. For verification of successful calibration, the SEM Scanner was then tested at 550g. For the 550g verification pressure, the 600g weight was attached to one side of the pulley, with a 50g weight hanging on the other side. This not only resulted in the 550g target calibration weight, it also better stabilized the 600g weight from tilting.

Due to the size of the weights, inserting and removing the weights was difficult. To help facilitate the operator in easily removing and replacing the weights, the weight guide can be tilted to either the small electrode side or the medium electrode side. With the tilt, the weight can be easily inserted without obstructions from the pulleys.

7.9.1 Fabrication of Calibration Stand

The calibration stand was designed using AutoCAD. The target material for this design was black, acrylic with a matte finish. The thickness for this plastic was 118 mils with a tolerance of +/- 15%. To account for this tolerance in AutoCAD, the wall thickness in the design was set to 130mils. During the laser cutting process, an additional 3 mils will be

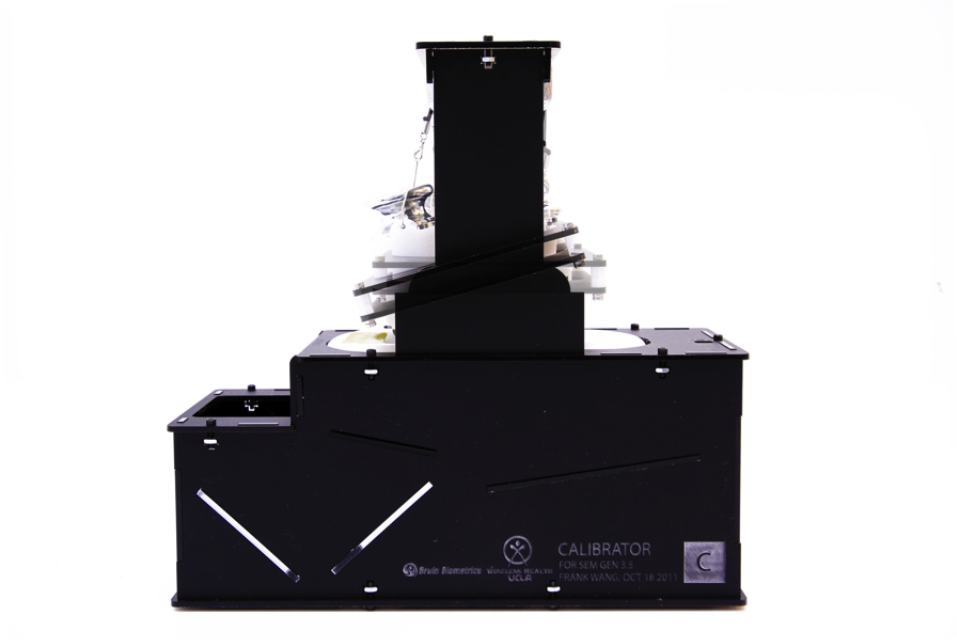

Figure 7.7: Weight guide can be tilted to either direction to facilitate the insertion and removal of weights.

removed from each side from a cutout. Therefore a cutout designed for 130 mils will result in 136mils, which is larger than the 118*1.15=135 mils.

Once the charger calibration was designed, each piece was individually isolated and projected onto the X-Y plane.

The design was then exported from AutoCAD to Illustrator where it was arranged, and final touches were applied, such as logos and text. This design was then sent to Ponoko for fabrication.

7.9.2 Calibration and Testing Procedure

The SEM Scanner employs a two-point linear calibration for both the pressure sensor and capacitance sensor.

For the pressure calibration the following weights were used:

Figure 7.8: Weight holder to attach weight to pulley.

Manufacturer:	American Weight Scales
Distributor:	Sharp Gear, through Amazon
Included Weights:	500g, 200g, 100g, 50g.
Accuracy:	OIML Class M2

Manufacturer:	WeighGold
Distributor:	PuriTest, through Amazon
Included Weights:	600g.

The SEM Scanner was calibrated to 500g and 600g. This required the use of the 600g, 500g and the 50g standard weight.

To attach the weight to the pulley system, a plastic holder was designed and manufactured using 3D printing through Ponoko.com. The diameter of the 500g and 600g weights were the same at 1.53 inch.

With the addition of the weight holder, the combined weight are listed below:

Weight	Combined Weight with Holder
500g	522g
600g	622g
50g	54.3g

Table 7.1: Combined weight of the metal weight and the plastic holder.

For the capacitance calibration, three different targets consisting of various dielectric constant were used. When these targets were measured using the SEM Scanner, their measured capacitance values were 0.5pF, 1pF and 2pF.

2.0 pF Target Capacitance	
Description:	Electrostatic Foam (supplied with RFID Reader ID-20)
Distributor:	Sparkfun
Part Number:	SEN-08626

1.0 pF Target Capacitance	
Description:	Custom 2 Layer PCB disk with 1.5 diameter
Manufacturer:	Advanced Circuits
PCB Stackup:	1.5solid 1oz copper circle on top most layer. Copper is covered by a 2mil soldermask. Substrate is FR-4, with a total stackup height of 65 mils.

0.5 pF Target Capacitance	
Description:	1oz Copper foil tape cutout to a 1.5 diameter circle attached to bottom of the weight holder.
Part Number:	JVCC CFL-5CA
Distributor:	FindTape, through Amazon.

Figure 7.9: SEM Scanner GUI guiding the operator through the calibration procedure.

The complete calibration routine for both the small and medium electrode consisted of 6 steps. The average time to complete the calibration was 3 minutes.

To initiate the calibration sequence, the SEM Scanner was first placed in calibration mode. This was accomplished by first placing the SEM Scanner in the calibration stand, then turning on the power while holding down the small electrode. To prevent normal users from accessing this calibration mode, the SEM Scanner can only be placed in calibration mode from the calibration stand.

The next step was for the SEM Scanner to remove the static parasitic capacitance due to the structure of the electrode, the internal wiring and parasitic capacitance from the PCB. During the internal calibration, the operator ensured that the electrode was not in contact with anything, as that will introduce a systematic offset in future readings.

The operator was now greeted by a GUI with instructions on how to perform the calibration. The next step was to calibrate the small electrode to the 500g pressure and the 0.5pF capacitance. The 500g weight, with the target capacitance of 0.5pF was placed on the small electrode. Once the SEM Scanner detected the application of the weight, it began the measurement sequence. It continuously took an running average of 100 pressure samples, and 25 capacitance samples which it used to determine when the weight has stabilized. Once stabilized, the SEM Scanner set the lower bound of the calibration.

The SEM Scanner then proceeded to calibrate for the 600g pressure and the 2pF target capacitance. The GUI then instructed the user to remove the 500g weight and to apply the 600g weight to the small electrode. The 600g weight has an electrostatic foam attached on the bottom, with a target capacitance of 2pF. Once the weight settled, the SEM took the measurement for this calibration point.

The procedure was then repeated for the medium electrode.

Once the calibration procedure was complete, the SEM Scanner verified that the calibration constants seemed reasonable, ie it checked that the second weight applied was both heavier and had a larger capacitance than the first weight applied. If an error was found, the GUI will ask the operator to re-perform the calibration. If no error was detected, the SEM scanner proceeded back to normal operation. The test operator then manually verified the calibration by placing the 600g weight on the electrode with a 50g weight attached to the pulley and checked that the electrode registered a mid-level pressure and also that it reported a capacitance of 1.0pF +/- 0.2pF. This check was then repeated for the other electrode.

7.9.3 Operator Guidance in the Calibration Process

The SEM Scanner provided the operator guidance in performing the calibration. However, due to the structure of the calibration stand, the LCD display was facing down, which hindered the operator's ability to view the display. This problem was rectified by using a series of mirrors to reflect the display with the correct orientation back to the operator.

Figure 7.10 shows the ray diagram of the two mirrors used in the calibrator stand. It reflected the image of the LCD screen such that it appeared parallel to, but below the surface of the SEM Calibrator stand.

To reduce the glare from the internal reflections from the LCD screen on the SEM Scanner, a polarizer film was placed in front of the LCD on the calibration stand. The polarizer

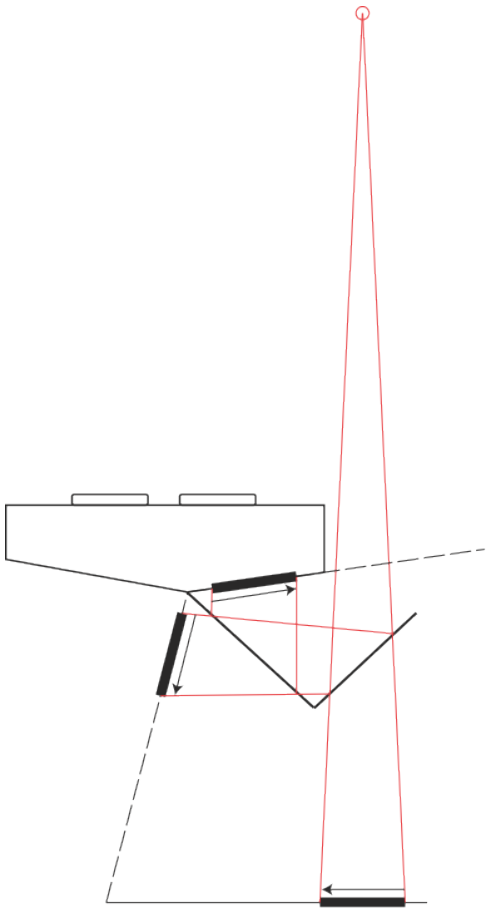

Figure 7.10: Ray diagram for the two internal mirrors.

film was oriented at 0 degrees, which provided a significant reduction in the glare.

7.9.4 Verification of Wireless Charging

The SEM Calibration stand featured a built-in charger. This allowed the test operator to verify the charging functionality of the SEM device. The charger was from an off-the-shelf TI Wireless Qi Development Kit.

The SEM charging verification consisted of two steps. The first step was looking at the status LED of the wireless charger. A cutout in the SEM Calibration stand facilitated easy viewing of the LED indicator. If any error was detected by the charger, the LED will turn red. During normal, charging operation, the LED will flash green.

Figure 7.11: Large reduction in glare with the application of a polarizer film.

After the calibration was complete, the SEM Scanner will return back to normal operation. The GUI display on the SEM Scanner will also indicate the current charging status. While the SEM Scanner is on the calibration stand, the GUI should indicate that the device is being charged.

7.10 Standards and Approvals

The device is currently undergoing tests to obtain the necessary regulatory approvals in order to be sold in the US and the European Union. The device has already obtained CE certification for sale in the European Union, and is currently waiting for FDA 501(k) approval. The SEM scanner also complies with the EN 60601 standard, which regulates medical electrical equipment for safety and electromagnetic compatibility and also the ISO 10993 standard for biological evaluation of medical devices. The device has been tested to be fully operational in the temperature range of 15-30C, and can survive a minimum of 22,000 cleaning/disinfecting cycles.

CHAPTER 8

Clinical Trials

To validate the efficacy of the SEM Scanner, clinical trials using this device were performed at multiple nursing homes and intensive care units in the greater Los Angeles area. The clinical trials were all IRB approved by the University of California, Los Angeles, Human Subject Protection Committee.

8.1 Internal Healthy Subject Trial

For the first validation of the SEM Scanner, a healthy subject trial was performed. 30 volunteers participated in this trial, where the efficacy of the SEM Scanner was tested in response to a simulated pressure ulcer through the application of moisturizer to skin.

For each subject, measurements were first taken with the Delfin device followed by the SEM Scanner. Measurements were taken at two locations: the right Volar forearm and the back of the right heel. The volar forearm was selected due to the similarity in tissue structure to the buttocks and trochanter where pressure ulcer commonly occurs. The heel was also selected due to high occurrence of pressure ulcer on the heel.

All measurements from the Delfin consisted of three measurements taken at each location. SEM scanner measurements consisted of three to five measurements on the heel and three to five differential measurements on the right Volar forearm. Differential measurements were taken simultaneously from each of the two electrodes on the SEM scanner.

An initial measurement was taken at each location to establish a baseline skin moisture

(a) SEM Scanner (b) Deflin

Figure 8.1: Internal trial with 30 subjects comparing the efficacy of the SEM Scanner to the Delfin.

level. The measurement locations on the skin were marked with a non-permanent pen in order for subsequent measurements to be taken as close as possible to this original location. After the initial measurement, a uniform amount of Novolan Emollient cream applied to a plastic film, which was then placed on the skin and affixed with tape. This application of emollient cream was left on the skin for a period of thirty minutes. After this period, the film was removed and any remaining emollient cream was wiped off. For each subject, measurements were taken with each device at 10 minute intervals for a period of an hour.

The response of all the subjects, overlaid on top of each other, are shown in Figures 8.2 and 8.3. These plots showed the overall trend after the moisturizer was applied. In the plots, the solid black line represented the mean of all samples, and the dashed dot represented the 1 standard deviation range.

For the measurements performed on the inner volar forearm, the SEM differential measurement was able to detect on average a 30% increase in moisture compared to the 10% increase, as detected by the Delfin device. The SEM Scanner, over time, was also able to detect a clear trend in the decreasing level of moisturizer, as the moisturizer was being absorbed by the surrounding tissue. The Delfin device does not establish that trend clearly.

Comparison between the SEM single and differential showed a very close correlation between the mean responses of all the subjects, as shown in Figure 8.2(d). However the

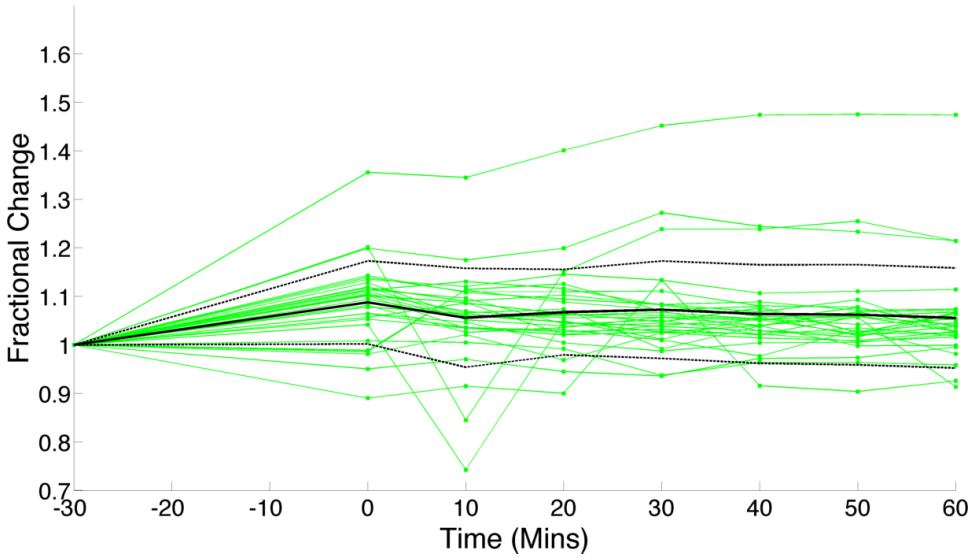

(a) Delfin

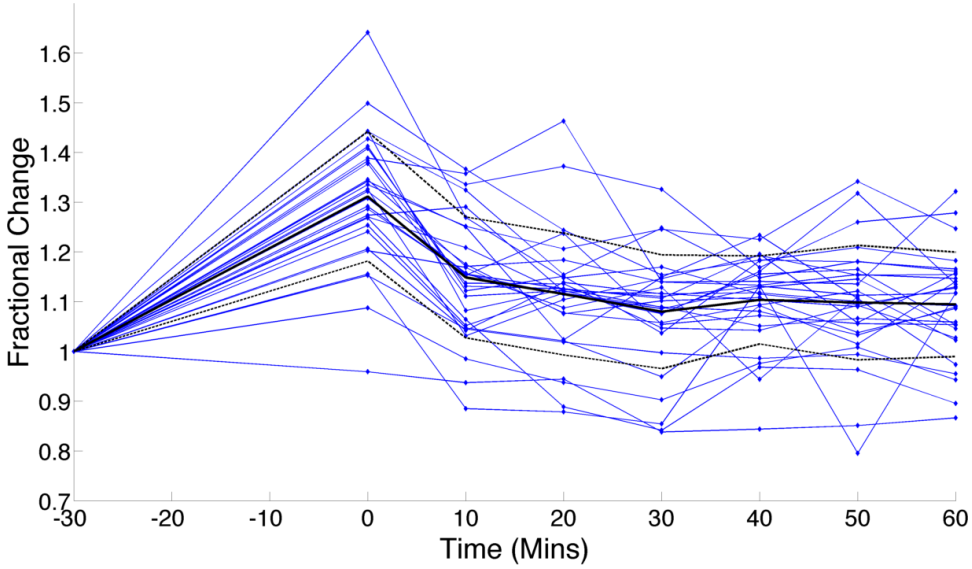

(b) SEM Single

Figure 8.2: Forearm measurement result for all 30 subjects with the Delfin, the SEM single and differential.

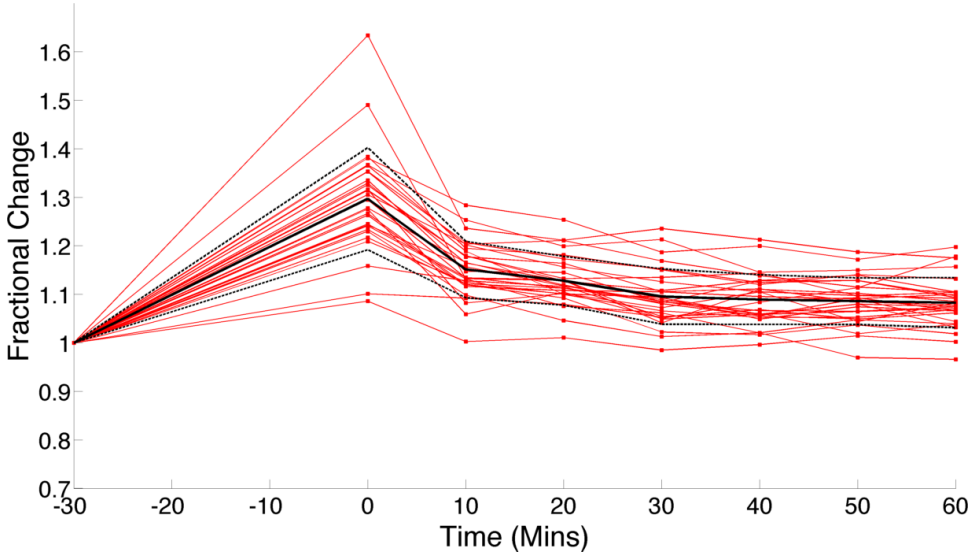

(c) SEM Differential

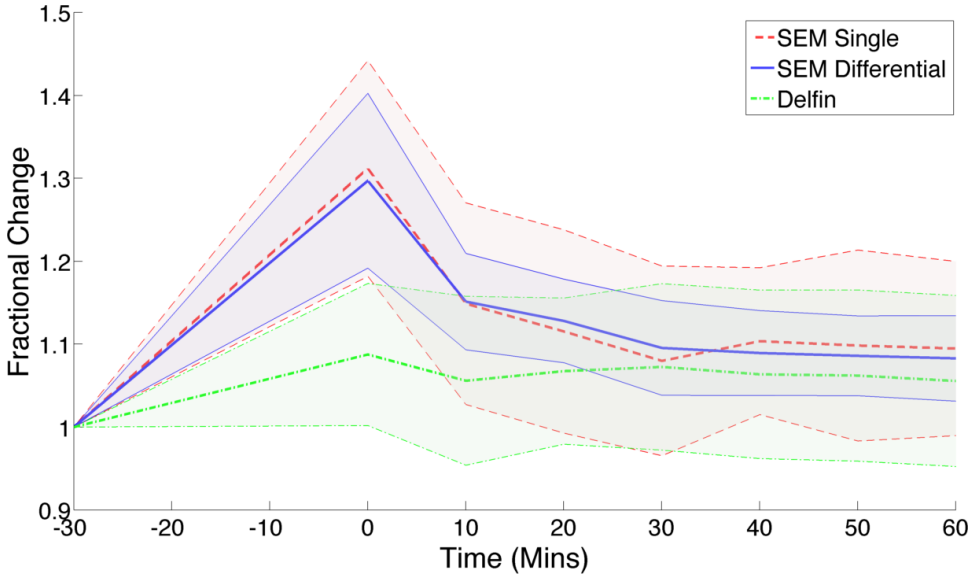

(d) Comparison

Figure 8.2: Forearm measurement result for all 30 subjects with the Delfin, the SEM single and differential. (Continued)

differential measurement resulted in a much smaller standard deviation than that of the single-ended measurement. The performance improvement in the differential measurement was attributed to the fact that each measurement on the tissue in question was compared to the surrounding reference tissue.

For the measurements performed on the heel, the SEM Scanner had a slightly better sensitivity response to the application of moisturizer while surprisingly, the Delfin device had less variance between subjects as shown in Figure 8.3. The smaller variation between measurements from the Delfin device might be attributed to the fact that the Delfin wand allows for easier consistent positioning between measurements compared to the prototype SEM device used.

From the data analysis on the 30 subjects, it was shown that the SEM differential device was able to clearly detect a change in skin moisture, at an increased sensitivity compared to the Delfin device. The fact that the SEM Scanner was able to measure a change in skin capacitance with a small standard deviation among all 30 subjects, validated the SEM Scanner architecture.

8.2 Nursing Home Trial

A clinical trial using the SEM Scanner prototype was conducted at four nursing homes within the greater Los Angeles area. This clinical trial was approved by the UCLA Office for Protection of Research Subjects [Bat10]. 59 residents were monitored weekly over a period of 16 weeks. The research team visited each resident in the early morning prior to the resident getting out of the bed. If any incontinence was discovered on the patient, the patient was first cleaned and the skin patted dry prior to performing any measurement. Measurements were taken at the following 9 body locations: the left and right buttocks, trochanters, ischiums, heels and the sacrum. These locations were selected due to the high incidence rate of pressure ulcer occurrence in these locations. Four measurements

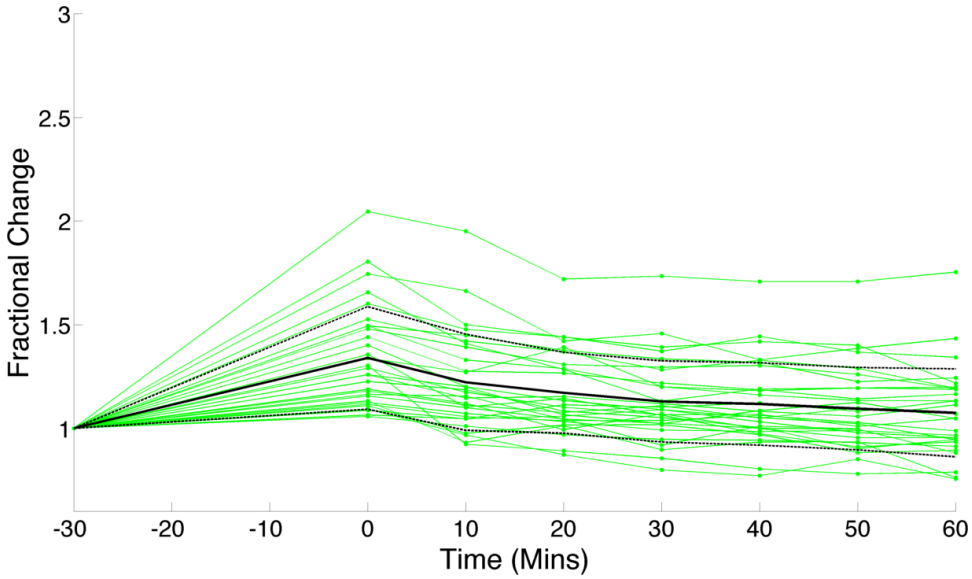

(a) Delfin

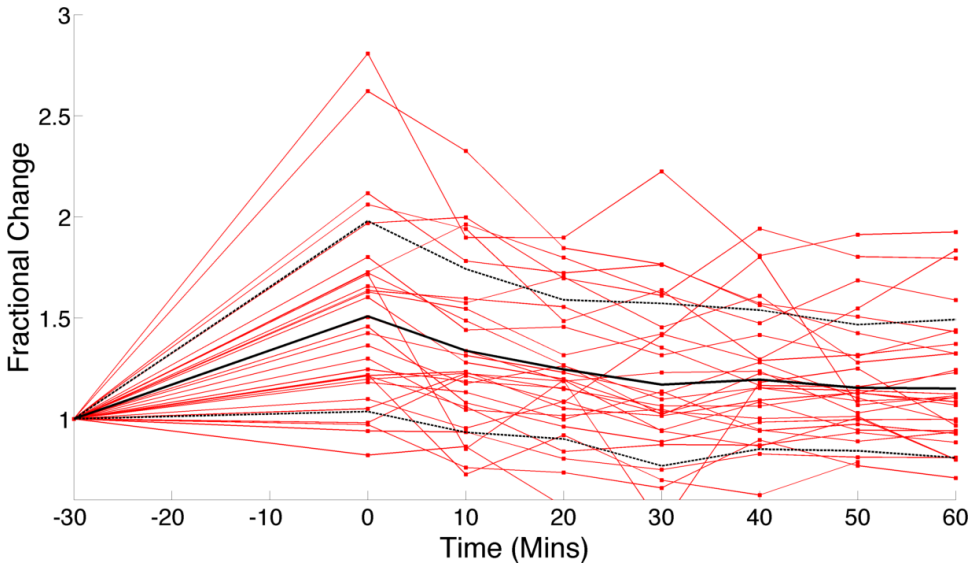

(b) SEM Single

Figure 8.3: Heel measurement result for all 30 subjects with the Delfin and the SEM single.

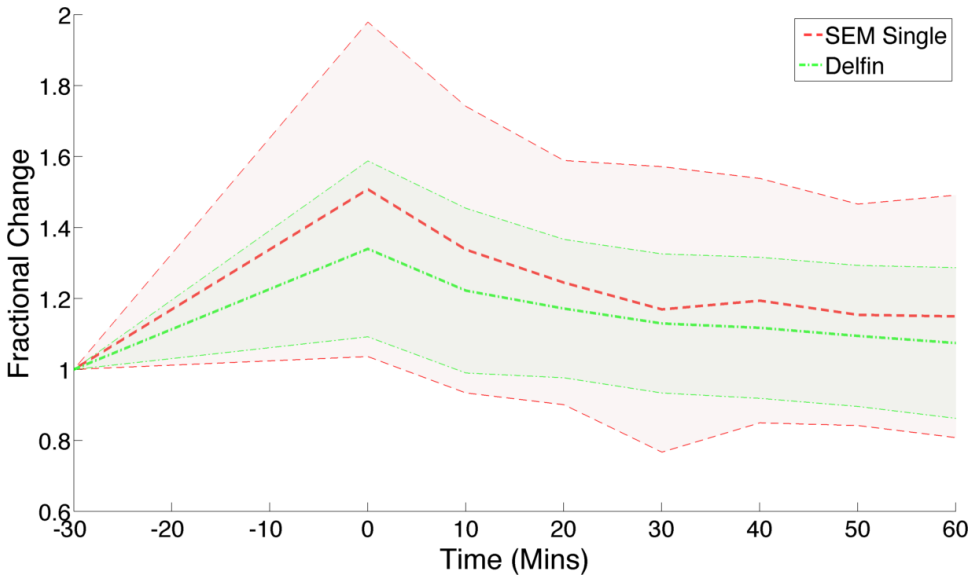

(c) Comparison

Figure 8.3: Heel measurement result for all 30 subjects with the Delfin and the SEM single. (Continued)

were taken at each location, one using the Delfin MoistureMeter-D Medium Probe, one using the Delfin MoistureMeter-D Small Probe, and two from the SEM Scanner where the small and medium electrode were measured simultaneously. Visual inspections were also performed by trained research staff to assess the skin condition for each of those nine body locations.

The results from this trial were plotted with patient ID on the x-axis, and each of their weekly measurements plotted on the y-axis as shown in Figures 8.5 and 8.6. The week of the trial for each data point was labeled using hexadecimal format. For patients with over 5 data points, the standard deviation from the patient's weekly measurements were calculated and was represented by the green bar. The red bar represented the standard deviation from measurements across all samples for all patients. For the weeks where a pressure ulcer was detected, the SEM Scanner data point was colored pink, whereas the measurement associated with the week prior to a pressure ulcer being detected was colored red.

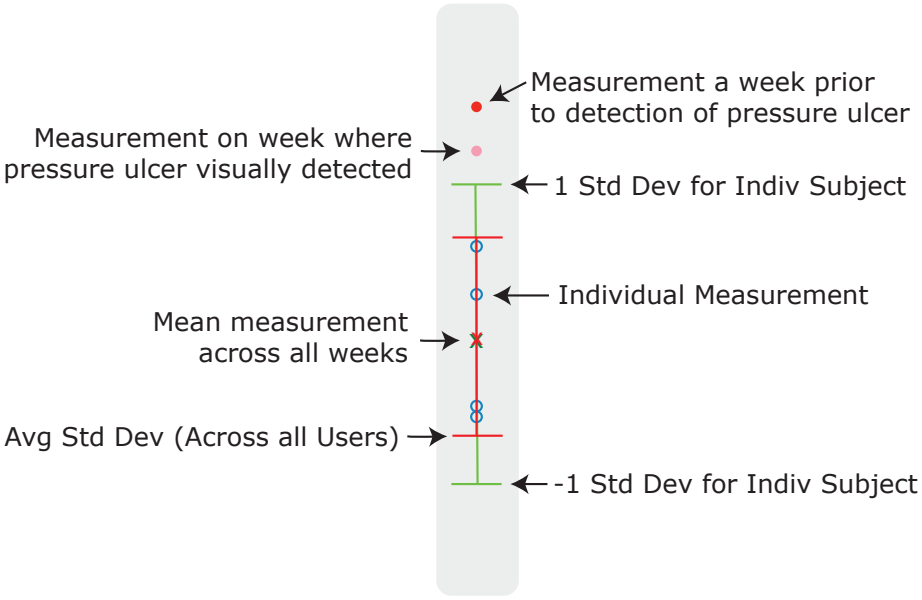

Figure 8.4: Legend for the clinical trail result plots.

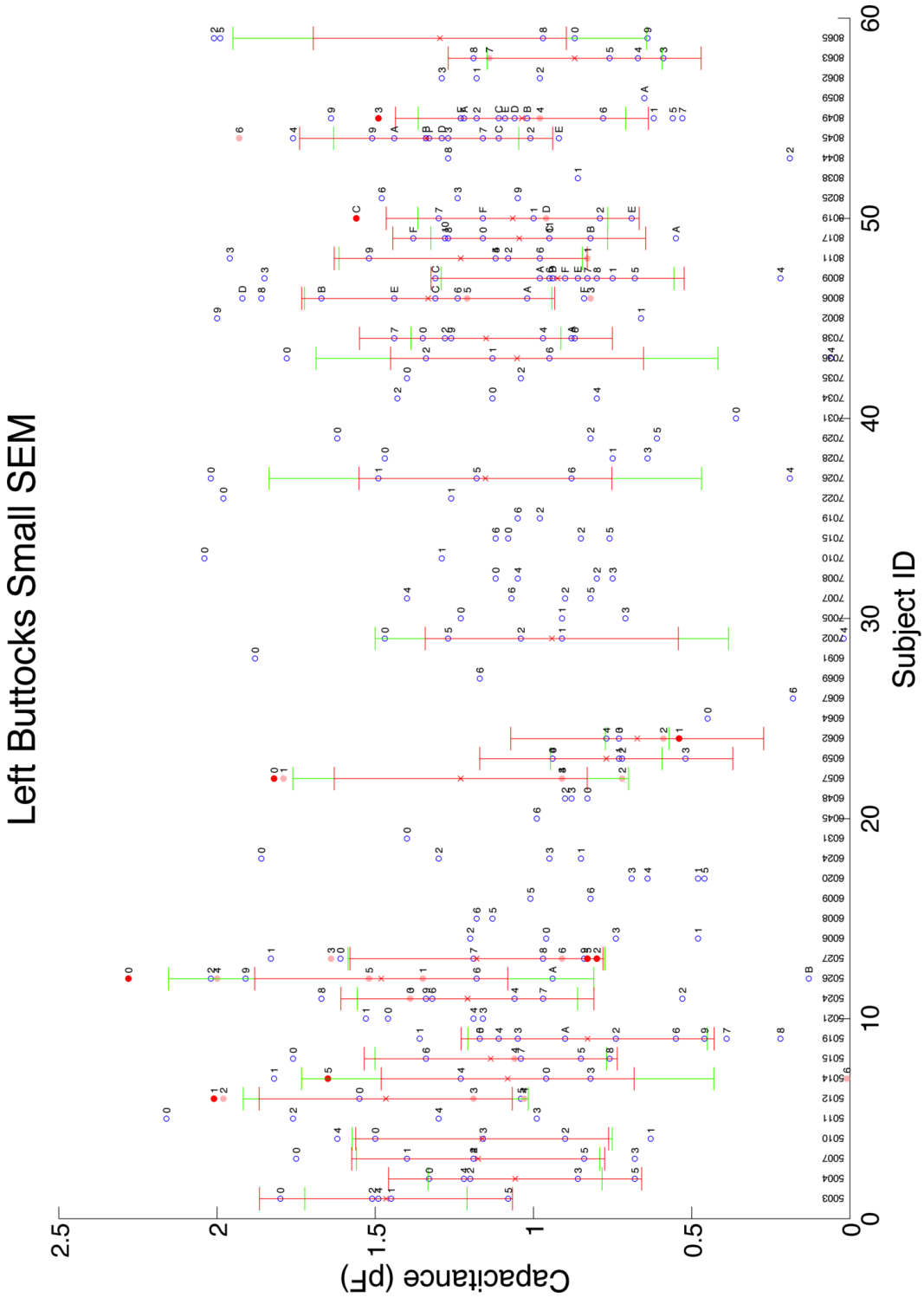

Figure 8.5: Clinical trial results for the left buttocks using the SEM Scanner small electrode.

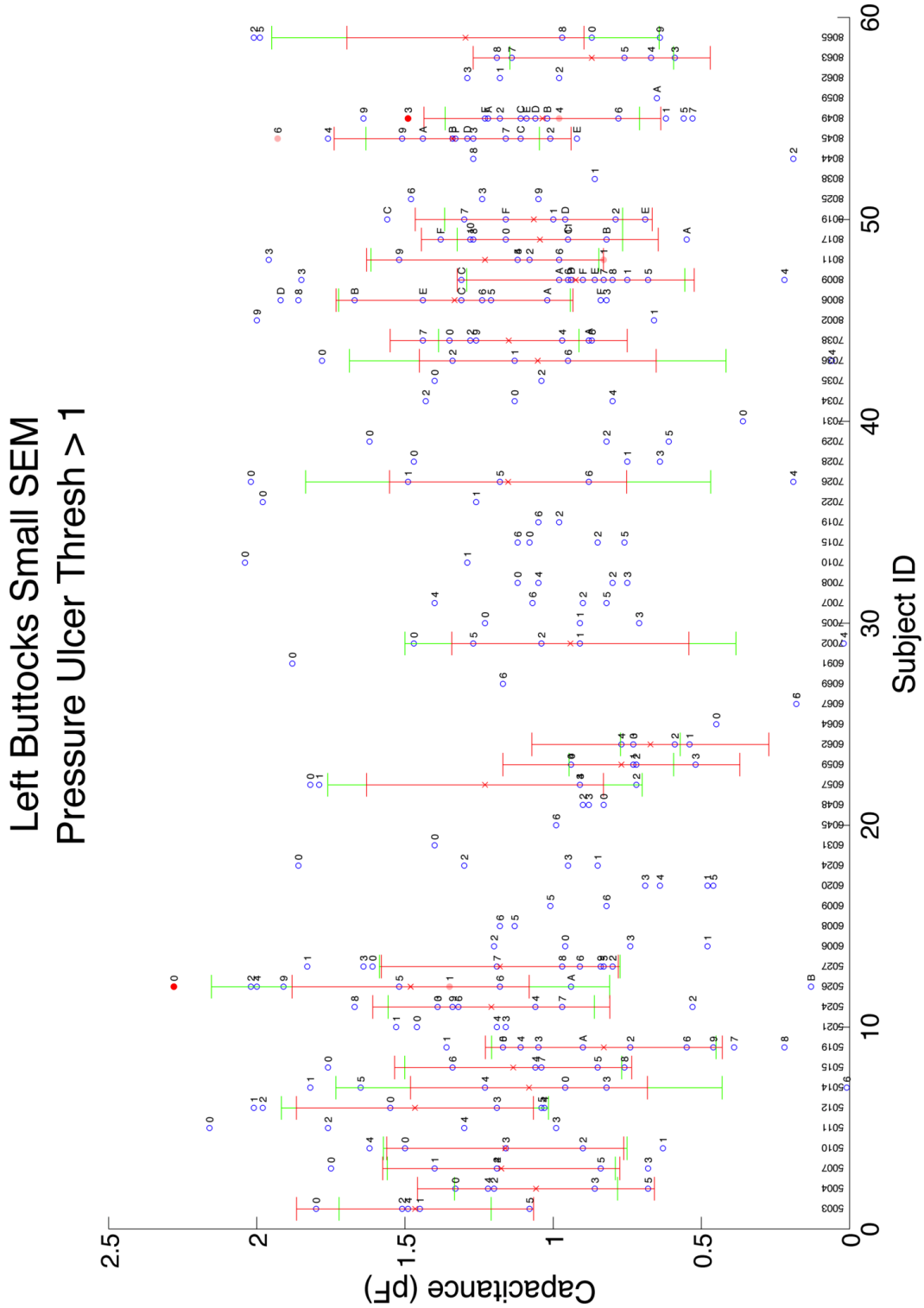

Figure 8.6: Clinical trial results for the left buttocks using the SEM Scanner small electrode, where incidence of pressure ulcer was classified as a stage 2 or greater PU.

In the nursing home trial, the majority of patients who developed a pressure ulcer developed it on the left buttocks. As such, the results from the small electrode on the left buttocks measurements were analyzed in detail. In Figure 8.5, which represented the measurements from the small electrode, 9 patients over the course of 16 weeks developed a pressure ulcer stage 1 or greater. 1 of the 9 patients had incomplete data, as the measurement was not performed the week prior to the visual detection of the pressure ulcer. In the remaining 6 out of the 8 patients, the measured capacitance for the week prior to the visual detection of the pressure ulcer was greater than 1 standard deviation from the patient's mean capacitance reading over the 16 week trial.

Next, patients who developed a stage 2 or greater pressure ulcer over the trial period were analyzed in Figure 8.6. Three patients developed a stage 2 or greater pressure ulcer. One patient had incomplete data. In the remaining two cases, the capacitance reading for the week prior to the visual detection of the stage 2 or greater pressure ulcer was larger than 1 standard deviation from the patient's mean capacitance reading.

One might have noticed that the capacitance reading for the patients with pressure ulcer was actually lower than the week prior to the detection of the pressure ulcer. This was because if the patient had developed an ulcer, the SEM Scanner was used on the surrounding tissue, and not on top of the ulcer itself.

In Figure 8.6, patient 8049 had a reading on the 9th week that was larger than 1 standard deviation from his/her mean. However in the following week, no pressure ulcer was observed. This might not be a true false positive, as pressure ulcers can develop in a short amount of time, as short as a day. Measurements were only taken weekly, and preventive actions might have occurred in the days between measurement.

For patients who did not develop pressure ulcers, the false positive rate was quite high. From the internal healthy subject trial, the use of a differential measurement was able to remove common-mode noise from the signal. However in this clinical trial, no differential measurements were performed. Differential signal would have been particularly useful

to compare the area in question to surrounding tissues, by minimizing factors such as humidity, temperature and skin moisture.

8.3 Intensive Care Unit Trial

A third clinical trial was performed using the production-ready SEM Scanner. The third clinical trial was performed at the intensive care unit at the UCLA Santa Monica hospital where 38 patients were monitored every 12 hours for a period of 7 days. Unlike the nursing home trial, this trial monitored the patients at a much shorter time interval of 12 hours. This change was in response to the fact that a pressure ulcer can develop within a day, and the prior time interval of 7 days would not provide the temporal resolution needed to determine how far in advance the SEM Scanner can detect the onset of a pressure ulcer. Twice a day, trained research staff used the SEM Scanner to measure the patient's SEM at the following 5 locations: both the left and right buttocks, both the left and right heels and the sacrum. A visual inspection for pressure ulcers at those locations were also performed to serve as the ground truth. A SEM measurement was also performed on the inner volar forearm to act as a reference measurement for healthy tissue.

In the days leading up to the visual detection of the pressure ulcer, an increase of the SEM values was observed. The SEM measurements performed within 1.5 days of the visual detection of the pressure ulcer showed a distinct difference in distribution compared to the distribution of the SEM measurements on healthy tissue, as shown in Figure 8.7. A receiver operating characteristic (ROC) curve was used to determine the most optimal binary threshold for the SEM capacitance value in determining the presence of pressure ulcer prior to the visual detection. The most optimal point on the ROC curve would be the point closest to the upper left hand corner, representing 100% accuracy.

As more subjects were added to the analysis, the Receiver Operating Characteristic became increasingly stable and unaffected by the incremental addition of new subjects, as

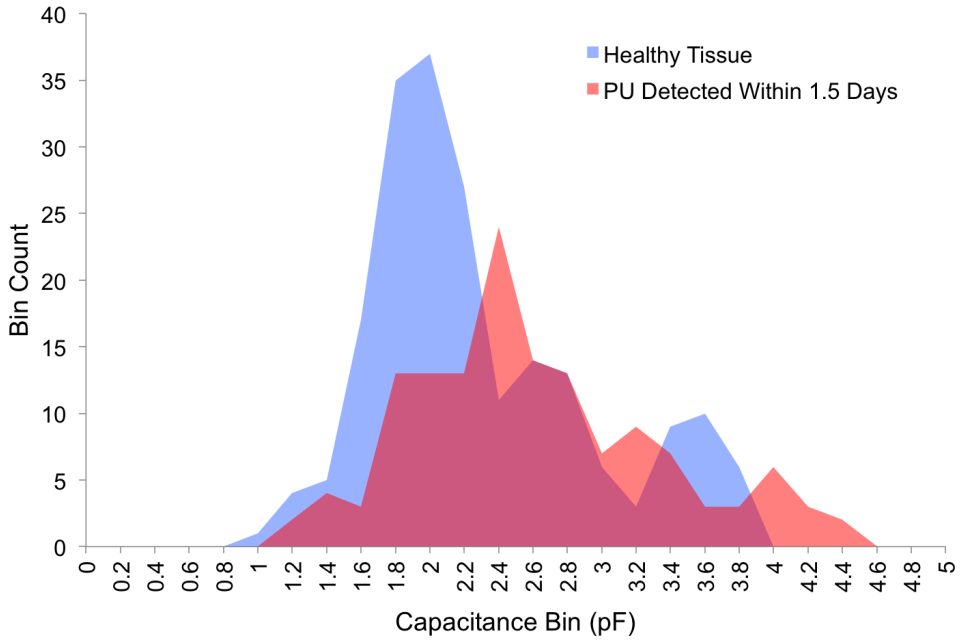

Figure 8.7: Distribution of SEM values across all body location for measurements within 1.5 days of developing a PU and measurements of healthy tissue.

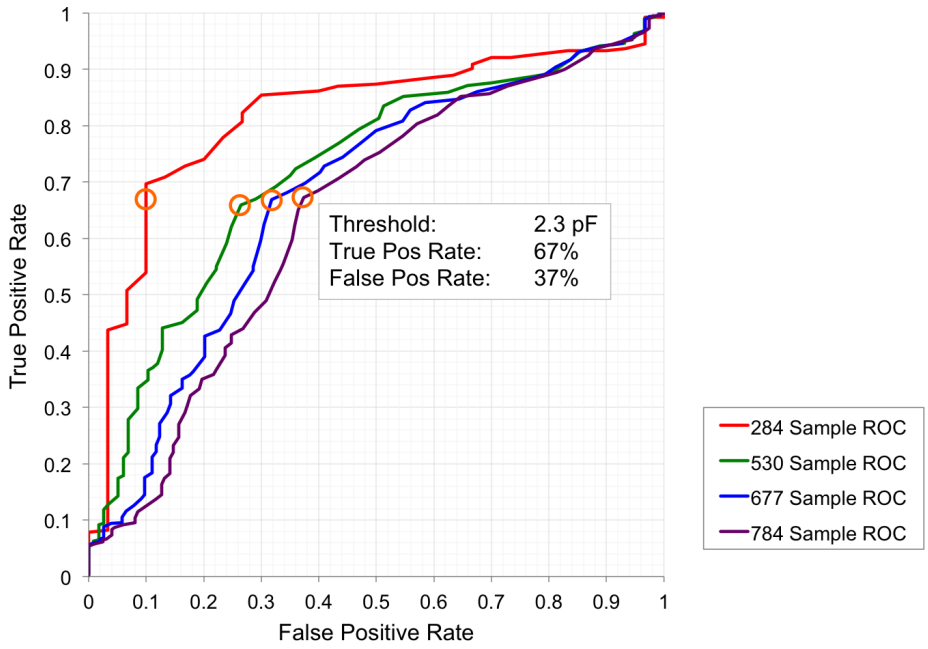

Figure 8.8: The receiver operating characteristic curve of SEM Scanner Index Values for increasing subjects, with the optimal threshold of 2.3pF highlighted, using a 1.5 day precursor and 1.5 day postcursor window.

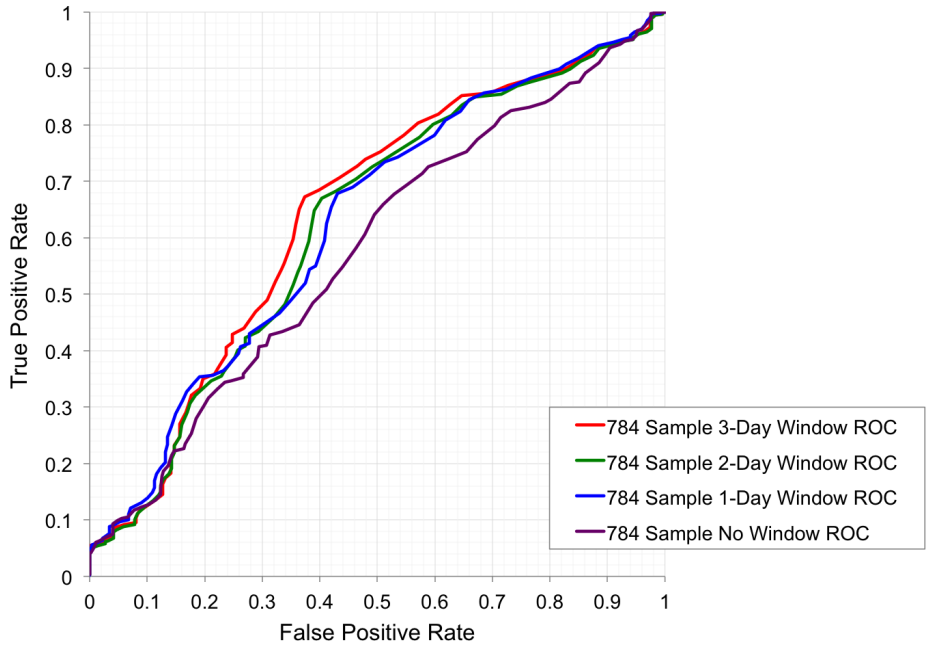

Figure 8.9: The receiver operating characteristic curve of SEM Scanner Index Values for 16 subjects and 784 samples with varying pre and postcursor window widths.

shown in Figure 8.8. For this analysis, only patients with light colored skin were included, since only the visual inspections on light colored skin were reliable to serve as the ground truth.

Total Sample Count	Subject Count
284	4
530	8
677	12
784	16

Table 8.1: Receiver Operating Characteristics computed for the following instances.

The Receiver Operating Characteristics were also computed for varying precursor and postcursor windows as shown in Figure 8.9. The motivation behind this window, was that the tissue damage associated with early stage PU occurred before it was visually detected.

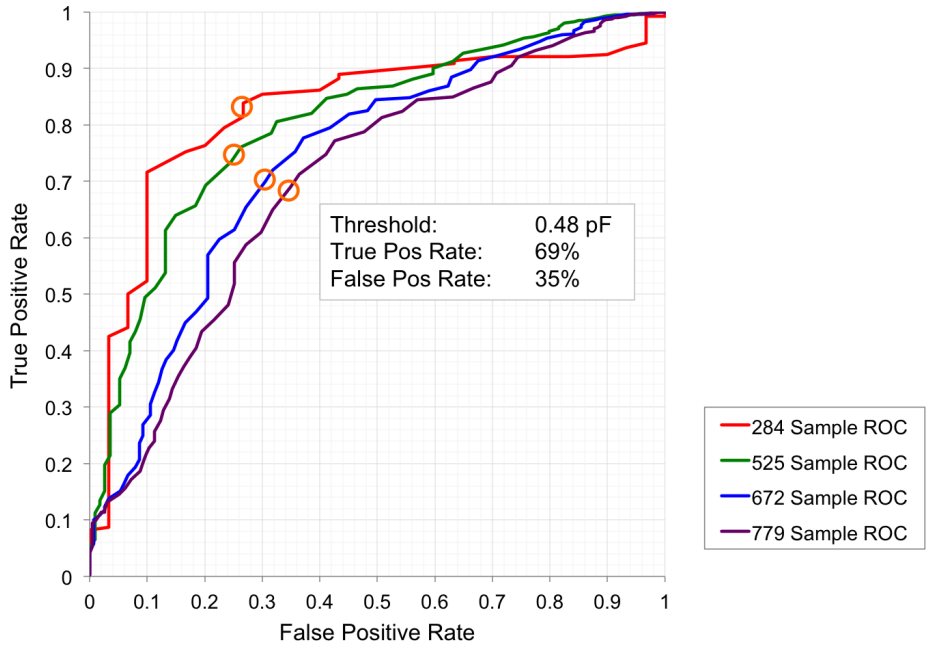

Figure 8.10: The receiver operating characteristic curve of SEM Scanner Index Values when referenced with the inner volar forearm for increasing subjects, with the optimal threshold of 0.48pF highlighted, using a 1.5 day precursor and 1.5 day postcursor window.

With the 1.5 day pre and postcursor window, it declared that the skin was pressure ulcer positive on 1.5 days prior and 1.5 days after any observation of positive pressure ulcers. By increasing the pre and post cursor days, the ROC performed better, converging at pre and postcursor of 1.5 days. With the incorporation of the pre/postcursor window, it prevented the SEM measurement values associated with the damaged tissue from being misclassified as healthy.

From the ROC curve of the clinical trial, the most optimal point was selected to be a threshold of 2.3pF. If a patient does have a pressure ulcer or will develop one within 1.5 days, 67% of the time the SEM Scanner will report a reading larger than 2.3pF, correctly identifying the condition. If the patient does not have a pressure ulcer and will not develop one within 1.5 days, 37% of the time the SEM Scanner will report a reading larger than 2.3pF, falsely stating that the patient will develop a pressure ulcer.

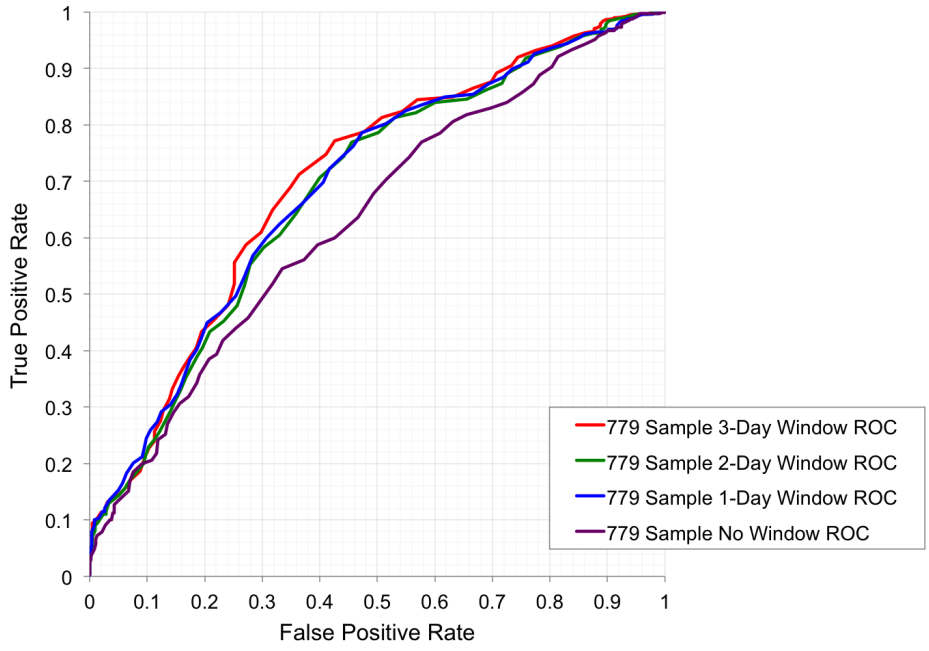

Figure 8.11: The receiver operating characteristic curve of SEM Scanner Index Values when referenced with the inner volar forearm for 16 subjects and 784 samples with varying pre and postcursor window widths.

It was observed that the SEM value of healthy tissue varied among subjects. Instead of having a set threshold applicable to all patients, a threshold should be set specific to the individual patient. The average SEM reading of healthy tissue was calculated for each patient using readings from the inner volar forearm. This served as a reference SEM value for healthy tissue for that individual patient. The reference SEM value were then subtracted from the SEM readings from the other body locations. The resulting values represented the deviation of the SEM value from the tissue in question to the healthy tissue. The receiver operating characteristic of the deviation in SEM values is shown in Figure 8.10.

Using this new analysis, if the patient will develop a pressure ulcer, 69% of the time, the SEM Scanner will report a SEM reading greater than 0.48 pF from the reference SEM value for the individual patient, correctly identifying the presence of a pressure ulcer. However if the patient will not develop a pressure ulcer, 35% of the time, the SEM Scanner will still report a SEM reading greater than 0.48 pF from the reference SEM value for that patient, incorrectly identifying that the patient will develop a pressure ulcer. By basing the SEM reading off the individual patient, the true positive rate increased by 2% while the false positive rate decreased by 2%. The area under the ROC curve was used to compare the ROC performance for the normal measurements to the ROC performance for the referenced measurement. The larger the area under the ROC curve, the better average performance of the classifier. From Figure 8.12, the ROC curve for the referenced measurement was shown to be superior to the ROC curve for the normal measurements.

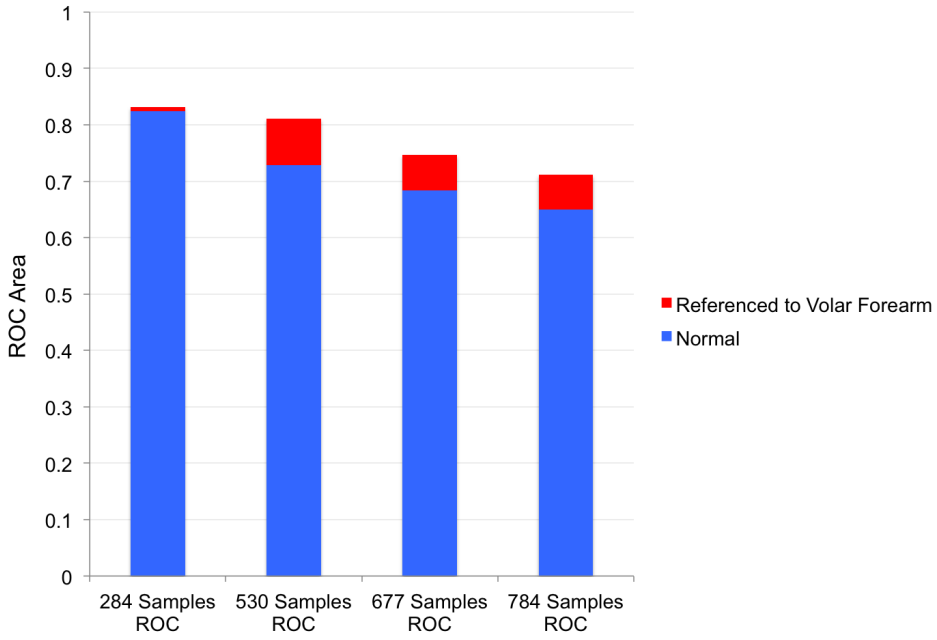

Figure 8.12: The area under the curve (AUC) was computed using a 1.5 day pre/post cursor as subjects were added to the analysis. The AUC increased when the SEM values were referenced with the inner volar forearm reading.

CHAPTER 9

Imaging Sub-Epidermal Moisture

Through the three clinical trials, the SEM Scanner has shown significant promise in detecting the early onset of pressure ulcers. However, there were a few limitations to the SEM Scanner that needed to be addressed, in particular, the SEM Scanner was a single point measurement, which imposed difficulty on the clinician's part to pinpoint the location of the pressure ulcer. It was also discovered that classification of the pressure ulcer improved when the SEM reading was compared to the SEM reading of the patient's healthy tissue. By using an imaging solution, it would resolve both these issues, allowing the clinician to probe in the vicinity of the ulcer and allowing the clinician to compare the SEM of the tissue in question with the healthy tissues surrounding it.

A possible imaging solution is to measure multiple locations simultaneously by using an array of electrodes, so that clinicians only needs to probe in the general vicinity of the ulcer. However these were still just point measurements. For the actual imaging of pressure ulcers, an innovative solution was required. The SEM Imager was based on the breakthrough insight that the electrode could be emulated by breaking the outer ring into multiple pieces. This allowed the formation of multiple overlapping electrodes within the same area. Since this new architecture can support any arbitrary electrode shape, an anisotropic electrode was used to further increase the resolution.

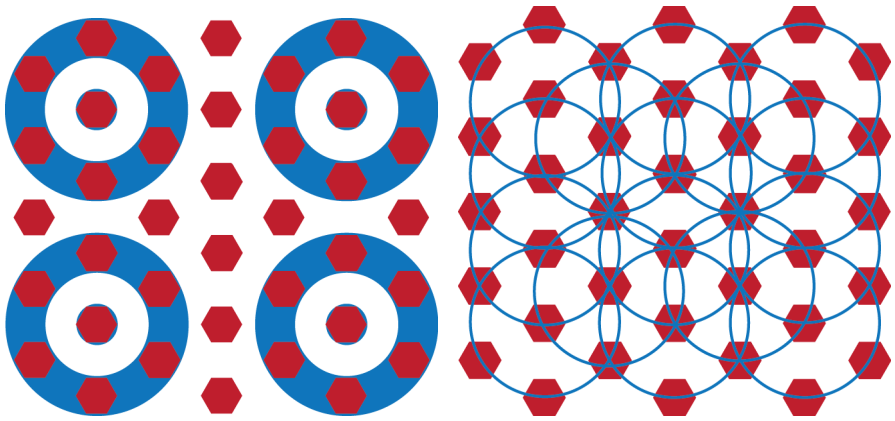

(a) Concentric Ring Array (b) Hexagon Array

Figure 9.1: Resolution can be increased by a factor of 4.5x if concentric ring electrode is approximated by the reconfigurable electrode blocks.

9.1 Reconfigurable Electrode Array

In the current SEM scanner, the electrode structure is a concentric ring, where the outer ring is the excitation node, while the inner circle is the capacitive input node. Expanding this to a 2-D array, the logical next step would be creating a 2-D array of concentric rings, as shown in Figure 9.1(a). For a 2 by 2 array, there will only be 4 data-points in this image. It was noted that the voltage potential on the outer ring is the same across all points on the ring. Therefore the solid electrode ring was approximated by 6 conductive hexagon pads spaced evenly around the ring and electrically connected to each other through an analog switch. Each hexagon pad was digitally controlled to be either connected to the excitation output or the capacitance input node. To emulate the electrode, the 6 outer hexagon pads were connected to the excitation node, while the center hexagon was connected to the capacitance input node. Using digital control, all combinations of the ring were swept. This resulted in an increase in resolution from 4 to 18 data-points from the same area as shown in 9.1(b).

To further increase the resolution, the programmable electrode was reconfigured with different geometries. One example is shown in Figure 9.2. The anisotropic electrode can

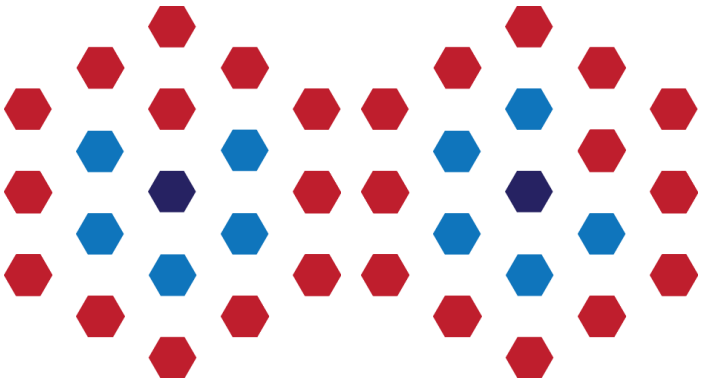

(a) 0 Degree Polarization (b) 60 Degree Polarization

Figure 9.2: Resolution can be increased by another factor of 6x if the electrode can incorporate angle information.

infer angular information, allowing additional data to be captured for a total of 126 data points in the same area. Using the anisotropic electrode increased the resolution by a factor of 31.5 times when compared to the original 2x2 concentric ring array.

This flexible, programmable electrode array allows for many different types of electrode geometries to be explored.

9.1.1 Targeting Different Penetration Depth

The depth sensitivity of the electrode depends on the spacing between the excitation and the input nodes, as shown in Figure 9.4 [SM08]. Using the reconfigurable electrode array previously presented, the distance between the excitation ring and input can be swept programmatically. This will allow for 2-D images to be generated at a different depth slice. However, as the penetration depth is increased, the resolution will decrease due to area constraint of the electrode array.

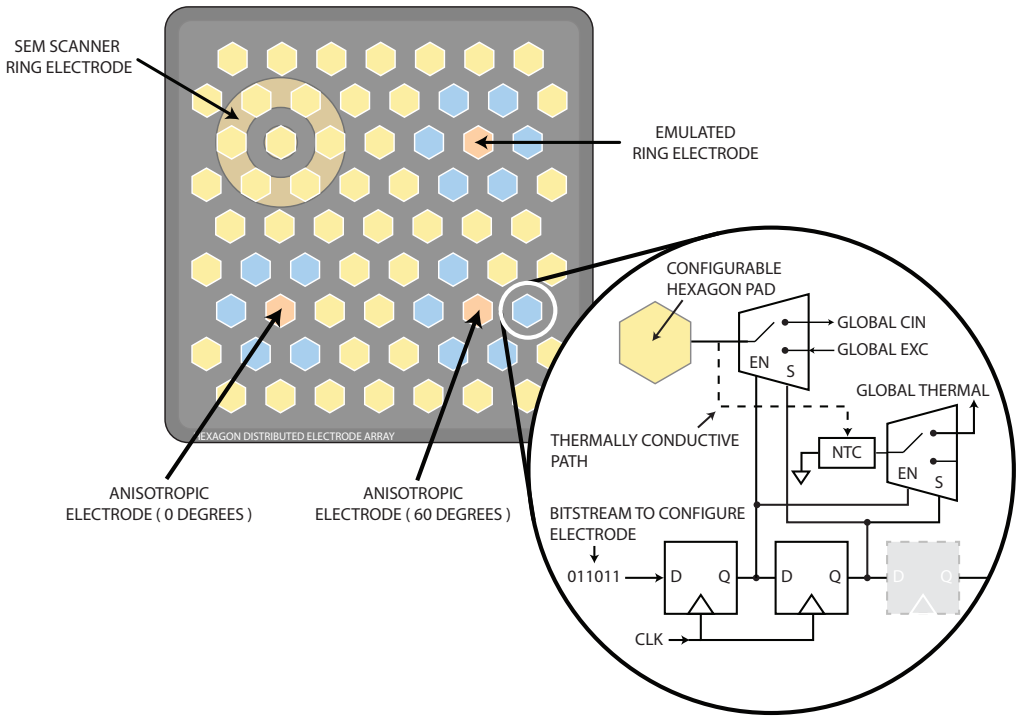

Figure 9.3: The reconfigurable electrode architecture behind the SEM Imager.

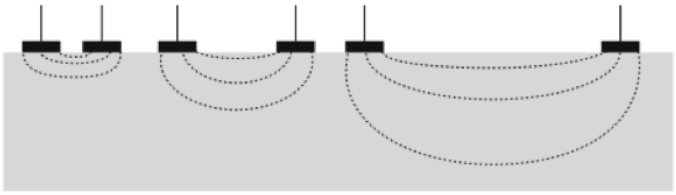

Figure 9.4: The penetration depth of an electrode depends on the spacing between the two nodes.

9.2 Image Reconstruction

The most ideal anisotropic electrode, in terms of image reconstruction ease, would be an electrode with one excitation output terminal and one capacitance input terminal. As the excitation terminal is swept around the capacitance input terminal, each individual measurement will reveal if the point source is or is not at that particular location. However,

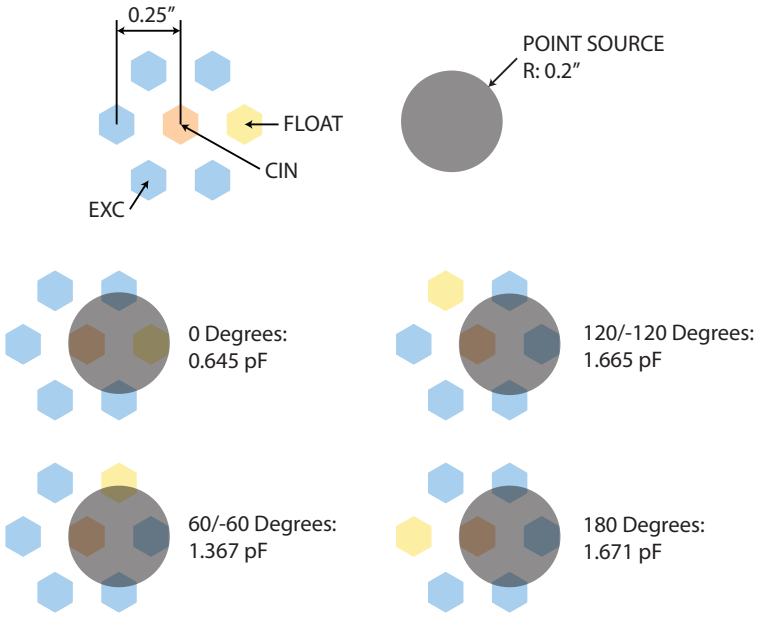

Figure 9.5: Example demonstrating the angular selectivity of the anisotropic electrode.

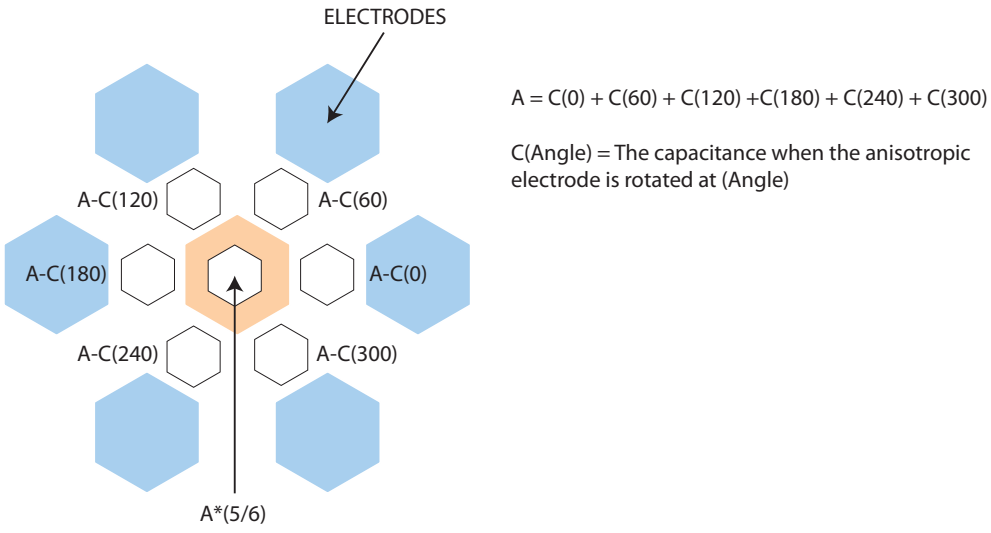

Figure 9.6: Algorithm for reconstructing the image from the anisotropic electrode.

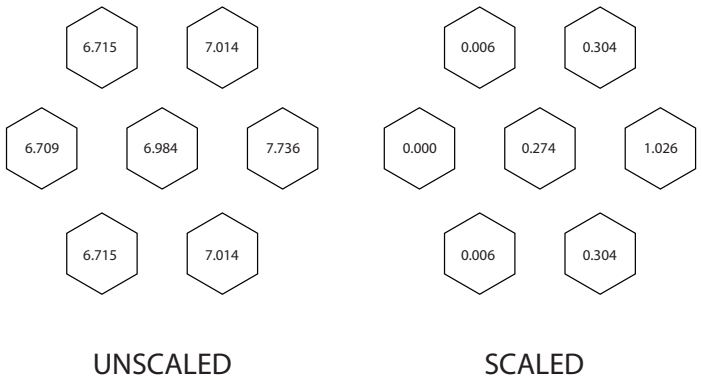

Figure 9.7: Reconstruction example using a point source and anisotropic electrodes. Notice, after scaling, the position of the point source is clearly visible.

in terms of the electrode's sensing capability, the capacitance to digital converter was not able to distinguish the SEM capacitance from the noise.

In order for the capacitance to digital converter to detect the desired signal, an electrode with a larger excitation terminal area was needed. This revised anisotropic electrode consisted of 5 hexagon excitation terminals and one floating terminal while surrounding the central capacitance input terminal. This electrode was also swept radially. However, each individual measurement in the sweep will not pinpoint the exact location of the point source, but instead provided a broad location of where the point source lies, as shown in Figure 9.5. For this electrode geometry, if an increase of capacitance was detected, the point source is known to lie within the area defined by the 5 hexagon excitation terminals.

By combining the data from all the sweeps, the location of the point source can be easily determined. This is accomplished using the algorithm as shown in Figure 9.6. In the example from Figure 9.5, at 0°, the 0.645 pF capacitance was the cumulative contributions of capacitance from the point source being detected at angle 60°, 120°, 180°, 240° and 300°. As a result, the 0.645 pF capacitance was added to the pixels representing those five locations. As the electrode was then swept to 60°, it measured a capacitance of 1.367 pF. This represented the cumulative contributions of capacitance from the point source being detected

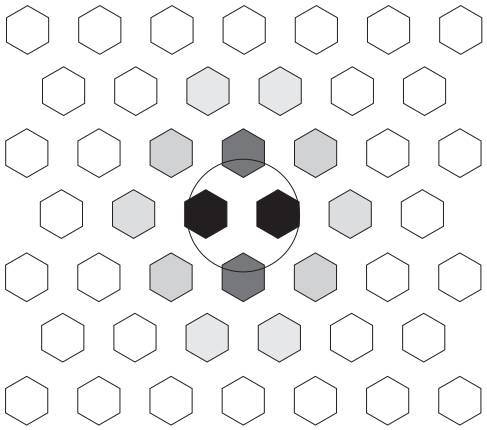

(a) Low Resolution, Isotropic Electrode

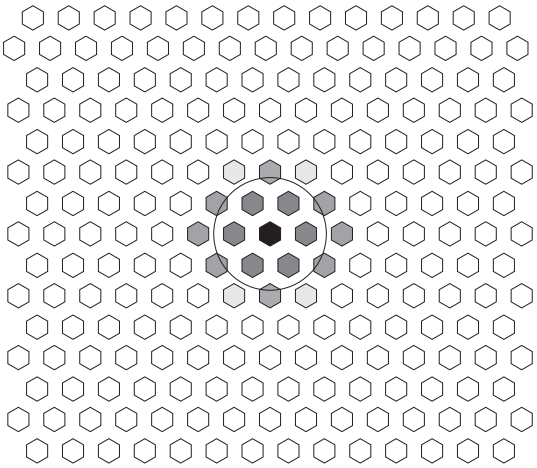

(b) High Resolution, Anisotropic Electrode

Figure 9.8: Reconstruction of a point source extrapolated to the entire array for both the isotropic and anisotropic electrode. The point source is indicated by the circle. Notice, the anisotropic electrode has higher resolution.

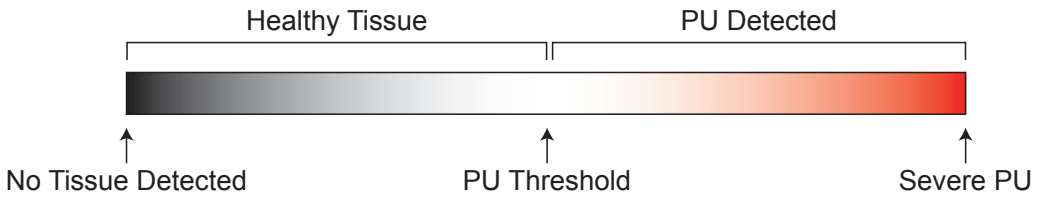

Figure 9.9: The use of a two tone colormap allows clinicians to easily distinguish between healthy tissues and damaged tissues.

at at angle 0°, 120°, 180°, 240° and 300°. The 1.367 pF was added to the pixels representing those locations. After a complete sweep, Figure 9.7 shows the accumulated capacitance in each of the pixel location. Because of this cumulative addition, the DC was systematically being offset. To help increase contrast, the output was rescaled. The pixel with the smallest capacitance was set to zero, by shifting every pixel down by that capacitance value.

This technique was then extrapolated over the entire array area. This allowed for the reconstruction of a high resolution image, compared to what could be achieved from the isotropic electrode as shown in Figure 9.8. Since the usefulness of this architecture is that it allows the clinician to compare surrounding healthy tissue with the inflicted tissue, image processing algorithms can be used to further increase the contrast of the image. Image interpolation techniques were employed to interpolate the pixels between the measured pixels thereby increasing the smoothness of the generated image, while rescaling the pixel intensities was used to increase contrast. To help easily distinguish the healthy tissue from the damaged tissue, a two-tone color map was used, as shown in Figure 9.9. As pressure ulcers are typically associated with high capacitance values, pixels associated with a capacitance below a certain threshold had a linear grayscale color map where the colors ranges from black to white, while pixels associated with a capacitance higher than that threshold had a linear red color map, where the colors ranges from white to dark red. The severity of the pressure ulcer can then be represented by the darkness of the red, while healthy tissue are indicated by shades of gray.

Figure 9.10: The SEM Imager, front view.

9.3 SEM Imager

The SEM Imager allows for the generation of a 2-D image of sub-epidermal moisture which can show the contrast between healthy and damaged tissues. The SEM Imager acquires 273 individual SEM measurements across a 2 inch x 2 inch area thus allowing the formation of an image representing the sub-epidermal moisture. The SEM Imager is fully wireless, sporting a battery life of 16 hours. The device, through a wireless 802.11b connection, transmits the sub-epidermal moisture imaging data to a laptop running a custom software for storage and analysis. The custom software, shown in Figure 9.11 was written in Objective C for the Mac OSX. It has the ability to manage multiple clinical trials sites and allows for researchers to manage and monitor patient's sub-epidermal images over time.

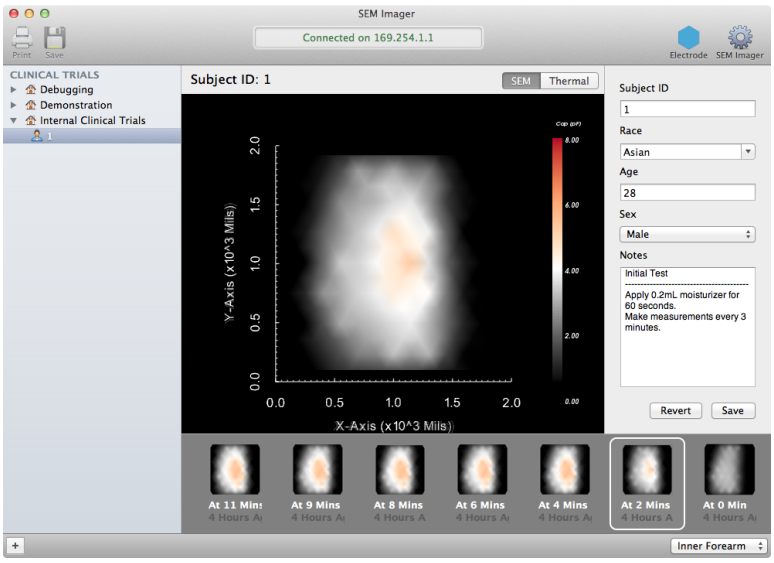

Figure 9.11: The patient record management software written in Objective C for the Mac OSX.

9.4 Healthcare Impact

The SEM Imager has received IRB approval to begin human trials. The device is currently being evaluated in a healthy-subject trial, where a pressure ulcer is simulated by a 60 second application of 0.2mL moisturizer on the subjects inner forearm. An SEM image is taken of the inner forearm prior to and immediately after the application of the moisturizer, and subsequently every 10 minutes for a period 2 hours (Figure 9.12). Phase 2 of the clinical trial will test the efficacy of the SEM Imager in the clinical environment on actual vulnerable patients. We expect to commence phase 2 trial in mid 2013.

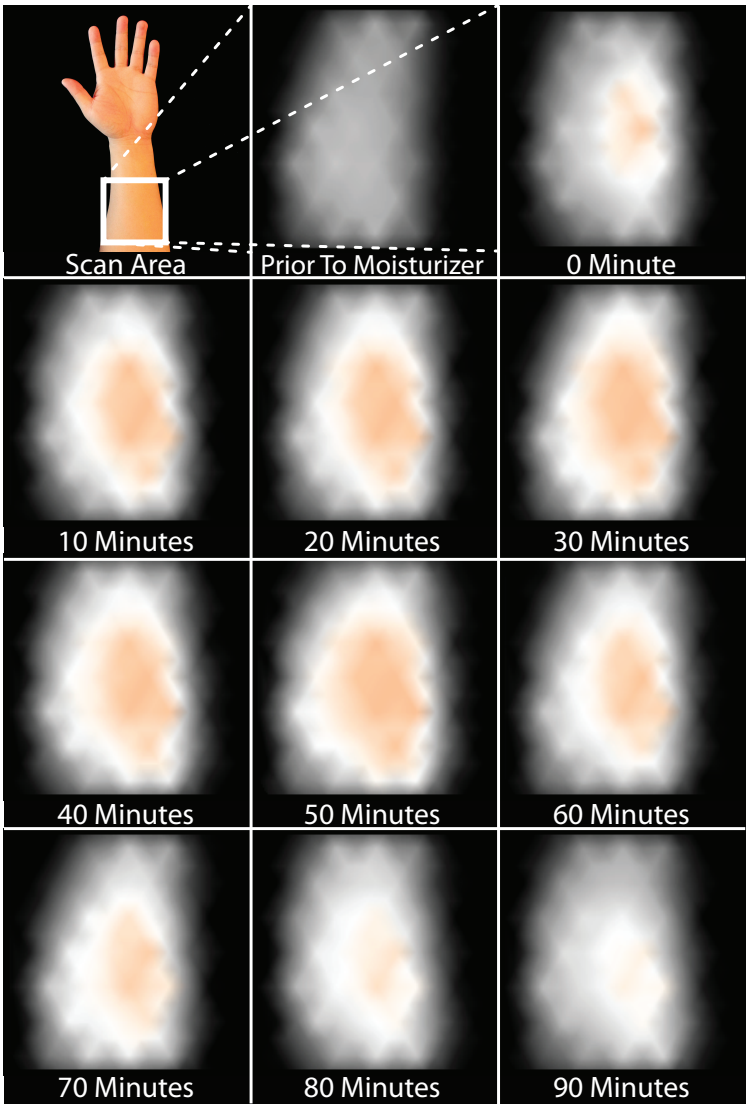

Figure 9.12: A sequence of SEM images over time for a healthy subject where a pressure ulcer was simulated using moisturizer.

CHAPTER 10

Conclusion and Alternate Applications

Both the SEM Scanner and the SEM Imager has made considerable progress in the detection of early stage pressure ulcers, and through commercialization has had a direct impact on improving health care. Despite these advances, there are still quite a large number of research directions in this field that are worthy to be pursued. Two future research directions were evaluated. One potential research topic that was evaluated was to expand the SEM Imager to become a broadly applicable platform to analyze a variety of skin conditions, besides just pressure ulcers. The other research topic that was evaluated was to reduce the cost and complexity of the SEM Imager for mass adoption in the clinical environment.

10.1 Impedance Tomography System

The foundation for the SEM Scanner and the SEM Imager were based on the research performed by Dr. Barbara Bates-Jensen. In her research, the interrogation device (Delfin) measured the dielectric constant at 300 MHz. The SEM Scanner and the SEM Imager relied on an off the shelf Capacitance to Digital Converter which only operated at 30KHz. Because of this, the SEM Scanner targeted the α dispersion range while the Delfin meter targeted the γ dispersion range. It was proposed that in the future, the system will allow researchers to analyze not only the α dispersion range, but also both the β and γ dispersion range. A preliminary study was performed on the feasibility of implementing such a system.

10.1.1 System Overview

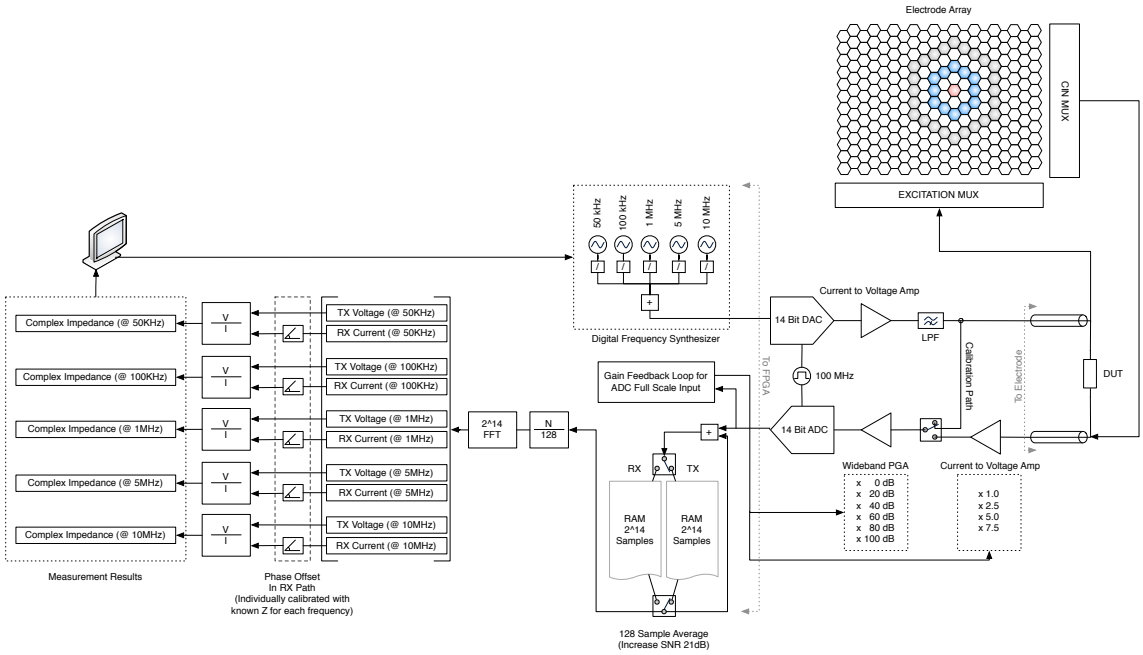

Figure 10.1: System architecture for the impedance tomography system.

To enable the probing of sub-epidermal moisture level with a wide range of frequencies will require the design of the capacitance to digital converter. There is currently no known off-the-shelf component that can achieve the desired frequency range. The desired system has a target frequency range from 50KHz to 10MHz, and will require the simultaneous acquisition of both the imaginary and real impedance.

At the heart of the proposed system is the digital frequency synthesizer. The digital frequency synthesizer will be implemented on the FPGA. It will allow for generating arbitrary frequency waveforms. In the system, to minimize the data acquisition time, the excitation signal will be the linear combination of multiple frequencies. The frequency are chosen such that for a single excitation, measurements can be made across all dispersion range from 50KHz to 10MHz. The frequency must be carefully chosen such that the harmonics of the chosen frequencies will not overlap with each other. The frequencies can be chosen by selecting the frequency closest to a prime multiple of the unit frequency. The

unit frequency is determined by the ADC sampling frequency divided by the number of FFT points to be performed.

This digital excitation signal is then converted to a current signal through the use of a high-speed 14 bit DAC. Since high speed DAC are usually current output, a current to voltage amplifier is used to convert the signal to a voltage signal. The signal is then fed through a low-pass reconstruction filter before being used to excite the electrode. On the receive side, the input is held at a virtual ground, allowing the input amplifier to convert the current received back into a voltage. Due to the wide range of possible current input, the current to voltage amp will feature a programable gain. This stage is then followed by a wideband programable gain amplifier. Through a feedback loop, the gain will be set such that signal occupies the entire full-scale input of the 14-bit ADC.

To increase the Signal to Noise ratio of the received signal, the FPGA will take a 128 sample average. The data output stream from the ADC will be stored on the FPGA on-board RAM. To be able to perform the calculation for the real and imaginary impedance, the system needs to be able to measure the transmitted excitation voltage. Prior to each measurement, the transmit excitation current is measured and stored. The next step is for the system to take the FFT. By dividing the transmitted voltage with the received current (taking account into phase offset for each electrode), both the real and imaginary impedance for all the excitation frequencies can be calculated.

10.1.2 MATLAB Model

The system was simulated and verified using MATLAB. The MATLAB model is shown in Figure 10.2. The system model allows each of the component specification to be defined. The ADC and DAC needs a minimum of 12 effective bits, with a sampling rate of 100MHz. Since the frequency range spans 4 decades from 50KHz to 10MHz, the variable gain amplifier in the receive chain needs a minimum of 60dB in programable gain. The number of points for the FFT is set to be 2^{14} points.

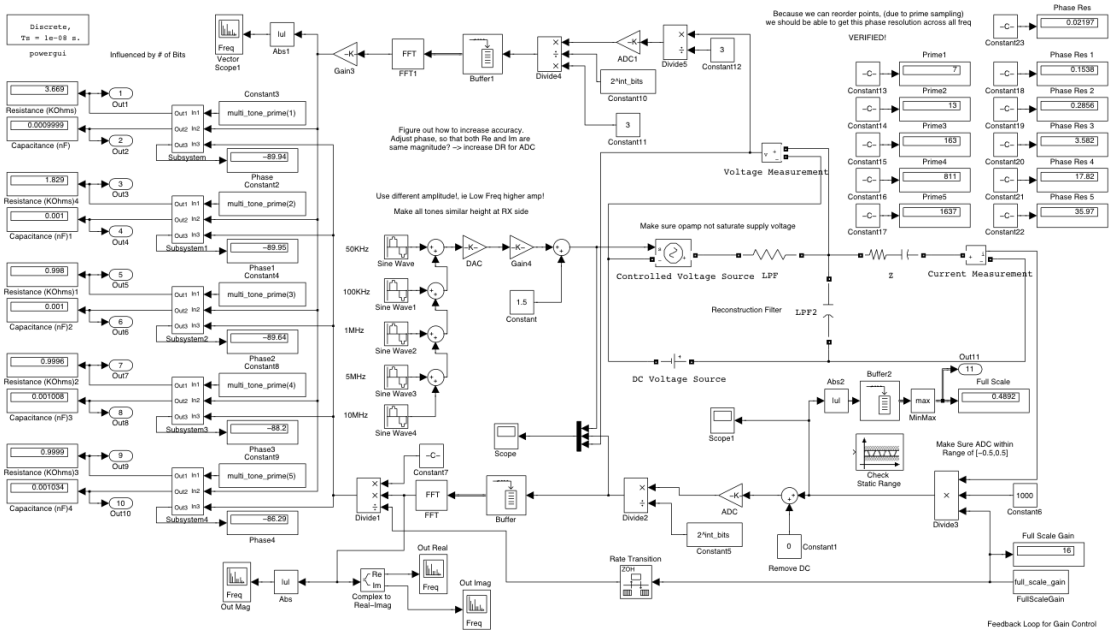

Figure 10.2: System architecture simulated in MATLAB.

10.1.3 Analog Signal Conditioning

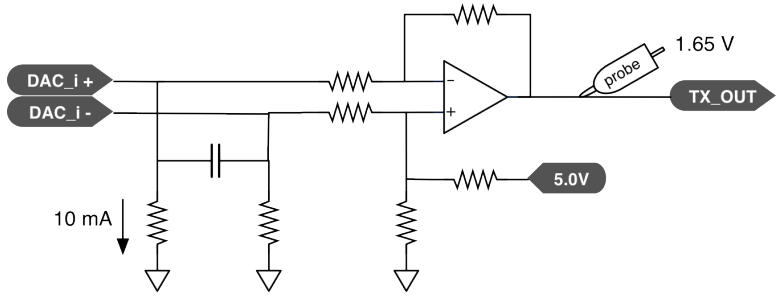

Figure 10.3: Proposed transmit architecture.

The transmit architecture is quite simple as shown in Figure 10.3. The differential current output of the DAC is converted to a single voltage output with the common-mode level set at 1.65V. The opamp selected for this is a wide-bandwidth, high speed, rail-to-rail amplifier from Analog Devices AD8041.

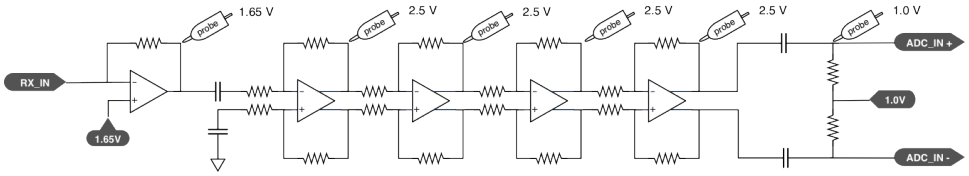

Figure 10.4: Proposed receive architecture.

For the receive side, due to the requirement of achieving a minimum of 60dB in programable gain, a distributed cascaded amplifier topology was used. The single-ended current input is first converted to a voltage output, using a ADA4817 which is a low noise, 1GHz Bandwidth amplifier. This stage also provides a transimpedance gain of 5000. The single ended voltage is then capacitively coupled into the next stage. The next stage consists of 4 fully differential opamps each with 6 programmable gain resistors. In each stage, the gain can be selected to be 1, 1.8, 3.2, 5.6, 10 and 18. The fully differential opamp selected is the ADA4937 which is a low noise, ultralow distortion high speed differential amplifier. The common-mode level for this stage is set at 2.5V. At the end of this cascaded stage, the output voltage is once again coupled capacitively with the common-mode level set to 1V which is the required ADC input common-mode voltage.

The entire analog circuit was simulated in Cadence. The Spice models for the opamps chosen were used to evaluate the entire analog chain performance. Using this topology, it should be able to achieve 80dB in programable gain across 4 decades spanning from 1KHz to 10MHz as shown in Figure 10.6.

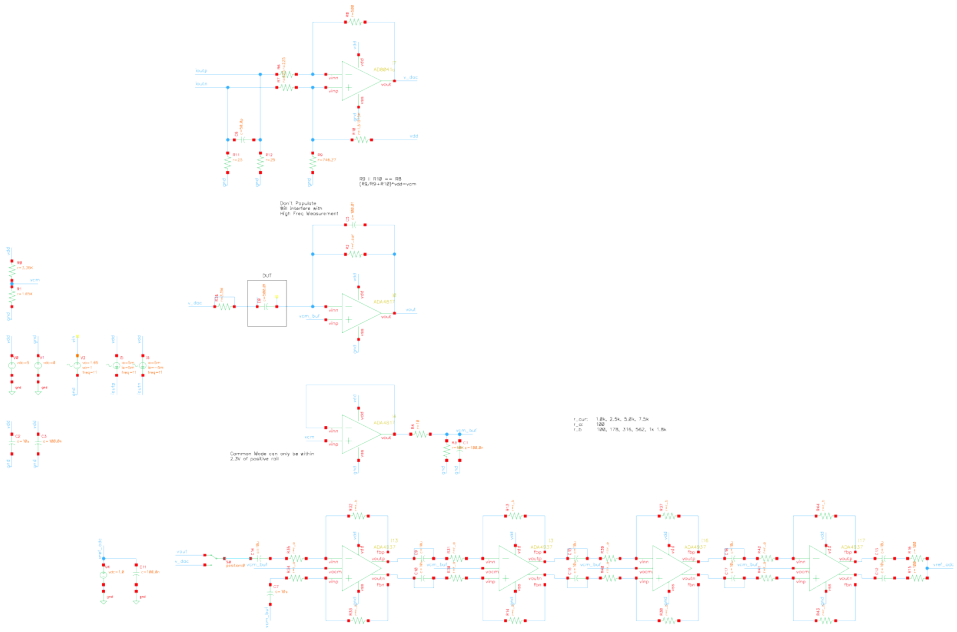

Figure 10.5: Cadence schematics with all op-amps identified and simulated.

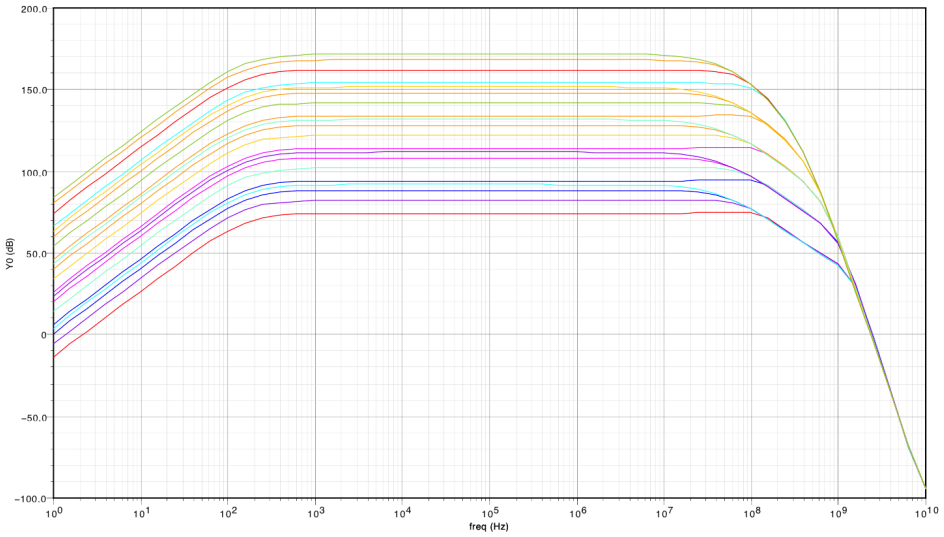

Figure 10.6: Simulated bandwidth of the transmit and receive chain.

10.2 SEM Disposable Array

One of the downsides to the SEM Imager is the complexity in fabrication. Due to the sheer number of electronics required to control each of the hexagon pad, it was quite difficult

to migrate the design from a rigid PCB to a flex PCB. As a result, the SEM Imager cannot conform to the contours of the patient's skin, but instead has a flat rigid sensing area.

Early discussions with clinicians has concluded that the actual imaging of sub-epidermal moisture is not critical for the detection of the onset of a pressure ulcer. Instead, it is the ability to reference the SEM values of surrounding healthy tissue that is important. Also due to concerns for sanitation, there is a growing trend for medical device manufacturers to create one time use, disposable sensors. Guided by this insight, a cost-down version of the SEM Imager was designed, called the SEM Disposable Array.

The SEM Disposable Array consists of an array of concentric ring electrodes, connected by flexible kapton ribbon cable. The kapton was designed in a way to allow for each of the electrode to conform to the patient's skin.

It is envisioned that each patient will have their own SEM Disposable Array, with a lifespan of a week. When the patient is given a pressure ulcer assessment, the clinician will slide the SEM Disposable Array underneath the patient to record the trochanters, buttocks and the sacrum. The clinician will then have the patient roll on their side, lying on-top of the SEM Disposable Array to perform the pressure ulcer assessment on the ischials.

To increase the resolution of this array, analysis was performed on minimizing the electrode area in-order to increase density, while maintaining similar performance as the SEM Scanner.

With this envisioned use case, the entire system was designed to be disposable after 1 week of use by an individual patient. The system is powered by a Zn-Air disposable battery, which will power the device for a minimum of 3 weeks. The SEM Disposable Array will communicate the result of the scan through Bluetooth to a iOS/Android smartphone or tablet computer.

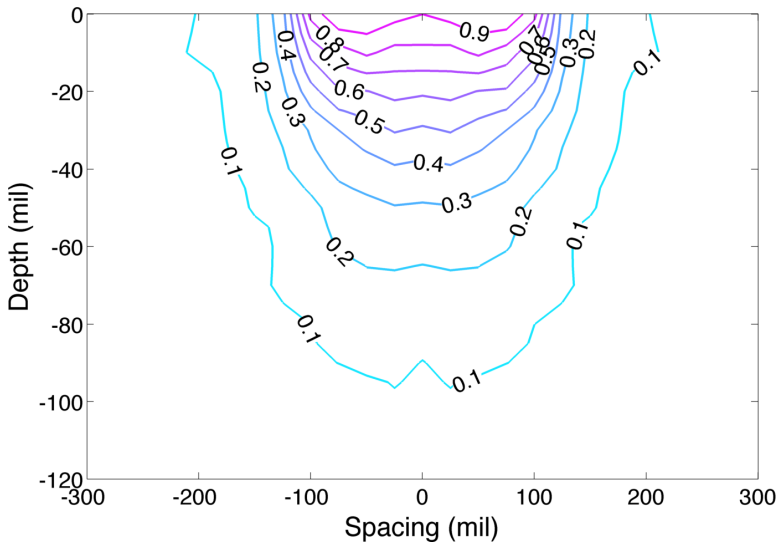

(a) Original Electrode Profile

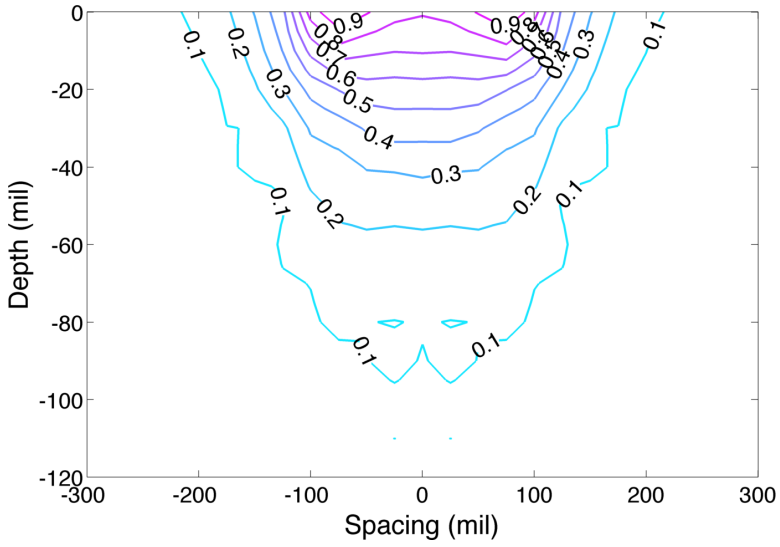

(b) Miniaturized Electrode Profile

Figure 10.7: The optimized electrode geometry results in a 55% reduction in area.

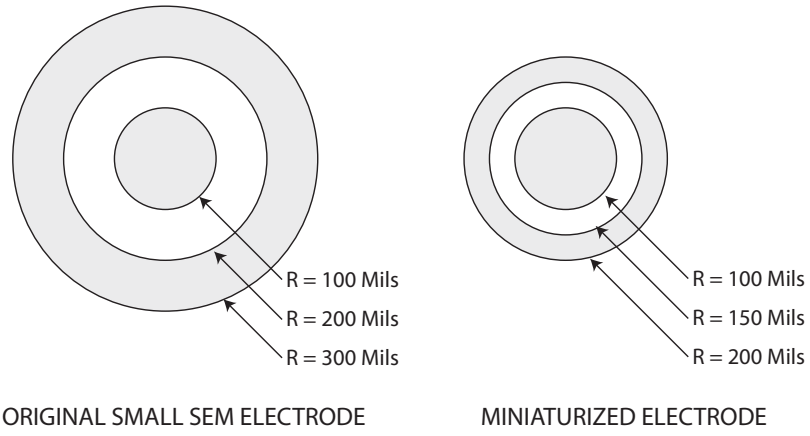

Figure 10.8: Optimized electrode geometry to maximize electrode density in array.

10.3 Conclusion

Four years of extensive research and testing have culminated in the work presented in this thesis. The SEM Scanner has gone through an extraordinary refinement process, beginning as a prototype made with off the shelf components and manual assembly, and resulting in a commercially produced, clinically viable device that can be mass produced. The detection capabilities of the SEM Scanner were verified in three large scale, strictly controlled clinical trials at a number of nursing homes and hospitals, which resulted in proof of the device's effectiveness. The SEM Scanner has passed several milestone regulatory approvals, including CE certification and FDA approval, as well as being the subject of an international patent, allowing it to be deployed directly to patients and care providers across the country. Also a new method for visualizing sub-epidermal moisture was developed during this program, and has shown promise as a new evidence based method for pressure ulcer detection with the goal of enabling significantly improved patient care.

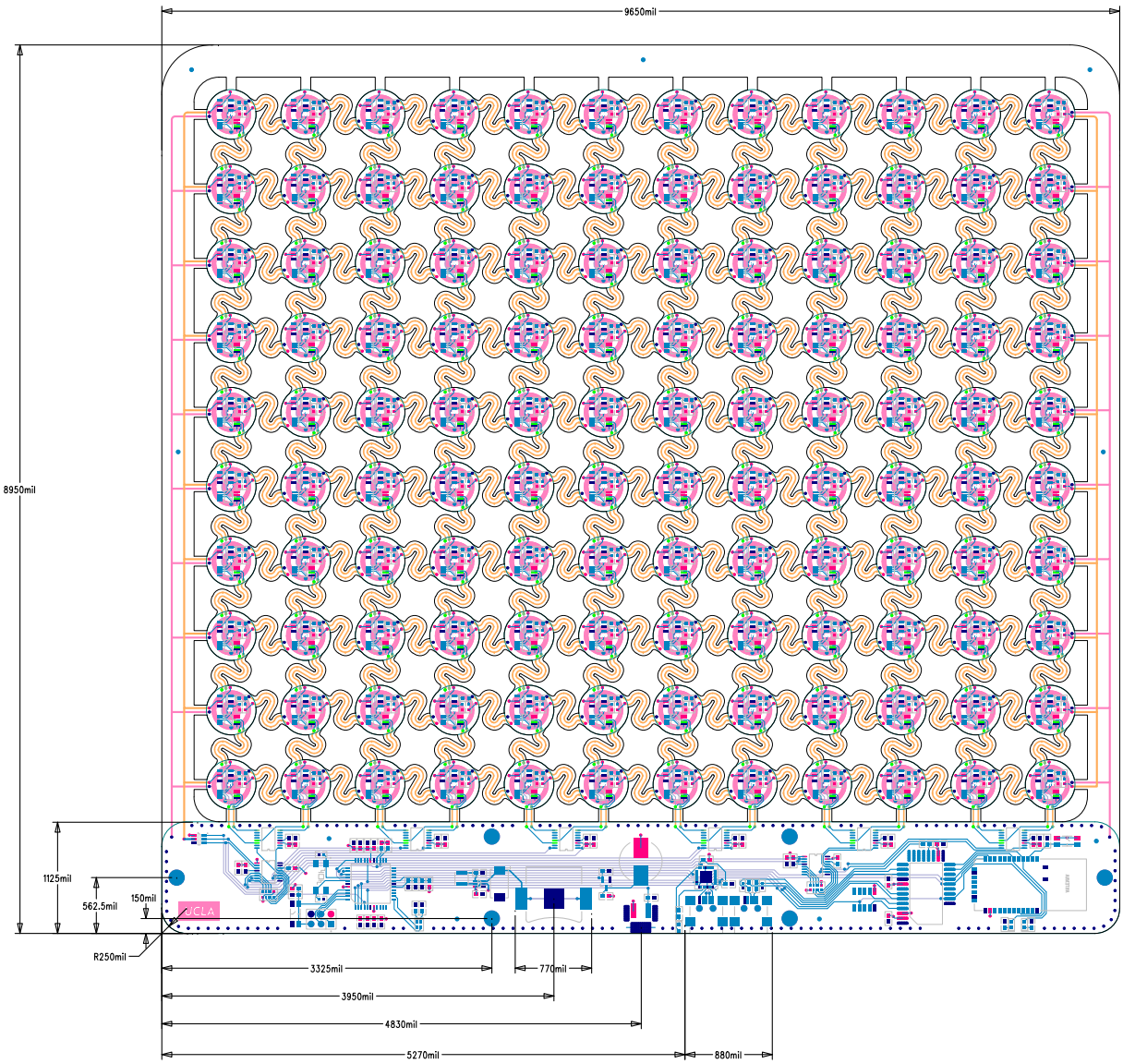

Figure 10.9: SEM Disposable Array design and layout.

REFERENCES

[ALN99] E. Alanen, T. Lahtinen, and J. Nuutinen. "Penetration of electromagnetic fields of an open-ended coaxial probe between 1 MHz and 1 GHz in dielectric skin measurements." *Phys. Med. Biol*, **44**:N169–N176, 1999.

[ANN04] E. Alanen, J. Nuutinen, K. Nicklen, T. Lahtinen, and J. Monkkonen. "Measurement of hydration in the stratum corneum with the MoistureMeter and comparison with the Corneometer." *Skin Research and Technology*, **10**:32–37, 2004.

[B 09] D. Thomas B. Dorner, M. Posthauer. "The Role of Nutrition in Pressure Ulcer Prevention and Treatment." *National Pressure Ulcer Advisory Panel White Paper*, 2009.

[Bat10] B. Bates-Jensen. "Biophysical Measure to Predict Pressure Ulcers in Nursing Home Residents." *UCLA Office for Protection of Research Subjects, IRB Application*, 2010.

[BMK07] B. Bates-Jensen, H. McCreath, and A. Kono. "Subepidermal Moisture Predicts Erythema and Stage 1 Pressure Ulcers in Nursing Home Residents: A Pilot Study." *The American Geriatrics Society*, **55**:1199–1205, 2007.

[BMP08] B. Bates-Jensen, H. McCreath, and V. Pongquan. "Subepidermal moisture differentiates erythema and stage 1 pressure ulcers in nursing home residents." *Wound Repair and Regeneration*, **16**:189–197, 2008.

[Bro03] G. Brown. "Long-term outcomes of full-thickness pressure ulcers: healing and mortality." *Ostomy Wound Manage*, pp. 42–50, October 2003.

[Bry05] M. Brychta. "Measure Capacitive Sensors With A Sigma-Delta Modulator." *Electronic Design*, 2005.

[Gab96a] C. Gabriel et al. "The dielectric properties of biological tissues: I. Literature survey." *Phys. Med. Biol*, **41**:2231–2249, 1996.

[Gab96b] S. Gabriel et al. "The dielectric properties of biological tissues: II. Measurements in the frequency range of 10 Hz to 20 GHz." *Phys. Med. Biol*, **41**:2251–2269, 1996.

[Gab97] C. Gabriel. "Comments on 'Dielectric properties of the skin'." *Phys. Med. Biol*, **42**:1671–1674, 1997.

[Gab06] C. Gabriel. *Dielectric Properties of Biological Materials*. Taylor Francis Group, Boca Raton, FL, 2006.

[Int06] Longport International. "Episcan I-200 Dermal Ultrasound Scanner.", 2006.

[LNA97] T. Lahtinen, J. Nuutinen., and E. Alanen. "Dielectric properties of the skin." *Phys. Med. Biol*, **42**:1471–1472, 1997.

[May12] Mayo Clinc. "Bedsores (Pressure Sores).", 2012.

[Nat07] National Pressure Ulcer Advisory Panel. "NPUAP Pressure Ulcer Stages/Categories.", 2007.

[NPU01] "Pressure ulcers in America: prevalence, incidence, and implications for the future. An executive summary of the National Pressure Ulcer Advisory Panel monograph." *Advance Skin Wound Care*, 2001.

[Og07] S. O'goshi. "Skin conductance; validation of Skicon-200EX compared to the original model, Skicon-100." *Skin Research and Technology*, 2007.

[RKI00] V. Raicu, N. Kitagawa, and A. Irimajiri. "A quantitative approach to the dielectric properties of the skin." *Phys. Med. Biol*, **45**:L1–L4, 2000.

[SA00] B. Scholz and R. Anderson. "On Electrical Impedance Scanning - Principles and Simulations." *Electromedica*, 2000.

[SM08] S.Grimnes and O. Martinsen. *Bioimpedance and Bioelectricity Basics*. Elsevier, Oxford, UK, 2008.